The Dissertation Committee for Jacob Spencer Anderson Certifies that this is the approved version of the following dissertation:

Compositional Changes of Light Hydrocarbons during Migration through Overburden: Proxy for Assessing Potential Leakage from Geological Carbon Storage

Committee:

Michael Young, Supervisor

Marc Hesse

Luc Lavier

Daniel Breecker

David DiCarlo

Compositional Changes of Light Hydrocarbons during Migration through Overburden: Proxy for Assessing Potential Leakage from Geological Carbon Storage

by

Jacob Spencer Anderson

Dissertation

Presented to the Faculty of the Graduate School of

The University of Texas at Austin

in Partial Fulfillment

of the Requirements

for the Degree of

Doctor of Philosophy

The University of Texas at Austin

December 2017

Dedication

To Cinthia

"It is reassuring that we will all be buried in the same, very thin layer of rock."

-Terrance Hayes

Acknowledgements

This research was a collaborative effort that would not have been possible without many people. I would first like to thank Sue Hovorka and Michael Young for their mentorship and patience. It was appreciated! Thanks to my committee (Dan Breecker, David DiCarlo, Marc Hesse, and Luc Lavier) for their constructive feedback. The people of the Gulf Coast Carbon Center at the Texas Bureau of Economic Geology were incredibly supportive. Thank you to Jiemin Lu and Katherine Romanak for their willingness to collaborate and provide feedback. Patrick Mickler generously helped with field work and made it enjoyable. Thanks to Tip Meckel for sharing data and his time reviewing. JP Nicot, Changbing Yang, and Seyyed Hosseini provided technical discussions that improved this research. Rebecca Smyth helped in the field and by organizing funding. Thanks to Toti Larson and Roxana Darvari for lab analysis. I would like to thank friends and colleagues that made my time at UT memorable, including Mike Patson, Logan West, Ramon Gil, Emmanuel Bolostrino, Sean Porse, and Jonathon Osmond.

I would like to acknowledge funding sources including the U.S. Department of Energy's National Energy Technology Laboratory (DOE-NETL, DE-FC26-05NT42590, DE-FE000194, DE-FE-0002381, & DE-FE-0003311) and UT Graduate School Dissertation Writing Fellowship.

Finally, I would like to thank my wife Cinthia, sisters Adelle and Laura, and parents for their support.

Light Hydrocarbon Geochemical Changes during Migration through Overburden: Proxy for Assessing Potential Geological Carbon Storage Leakage

Jacob Spencer Anderson, Ph.D

The University of Texas at Austin, 2017

Supervisor: Michael Young

Light hydrocarbon compositions evolve during migration through geologic media, but our understanding of geochemical alteration is limited because of the challenges with analyzing fluids in the sedimentary column. Understanding fluid evolution is timely because of the possibility of upward fluid migration from Geologic Carbon Storage (GCS) operations.

The first goal of this research is to identify to what extent hydrocarbons migrate to shallower intervals. Addressing this goal is challenging because microbial hydrocarbon production commonly occurs in the near-surface. Light hydrocarbon compositions are investigated in soil gas above a hydrocarbon system and in offshore sediment above a gas chimney. In both cases, the fluid sources are interpreted as microbial in origin. However, these geochemical datasets are relevant to attributing future light hydrocarbon seeps and anomalies above GCS sites.

The second goal is to quantify alteration processes when migration has occurred. I hypothesize that phase changes and sorption are the primary alteration processes. To test this hypothesis, I numerical simulation these processes to compare with field datasets that are interpreted as migration. The models indicate that sorption has the most

significant influence on light hydrocarbons, although more lab work is warranted to improve these models. Forward models of CO_2 migration show that phase changes are important in attenuating CO_2 and can be identified with noble gas compositions. This conclusion may be valuable to determining the source of CO_2 anomalies above GCS sites.

Table of Contents

List of Tables

List of Figures

Chapter 1: Introduction

1.1 OVERVIEW

Geologic Carbon Storage (GCS), whereby CO_2 is captured from point sources and stored in deep geologic formations, is considered to be a key technology to mitigate greenhouse gas emissions to the atmosphere (Stocker, 2014). Significant CO_2 volumes, stored underground, are not expected to migrate upward into groundwater, the vadose zone, or the atmosphere because of multiple trapping mechanisms (Gilfillan et al., 2009; Juanes et al., 2006). Even so, monitoring systems will be important to satisfy expected regulation requirements, address stakeholder concerns, verify carbon credits, and, detect potentially anomalous signals. In these scenarios, further geochemical assessment is necessary to attribute the source of a potential fluid anomaly. In the context of this research, a fluid anomaly is defined as elevated concentrations of CO_2 or light hydrocarbons (methane, ethane, and propane) in the vadose zone, groundwater, or seafloor sediments. Fluid source attribution is important for leakage interpretations that may require environmental assessments, costly remediation, and carbon credit adjustments while non-leakage would require no further action. This research studies fluid alteration by considering hydrocarbon systems as an analog for CO_2 because (1) natural light hydrocarbon seepage is common on the Gulf Coast, and (2) field operations allow for sampling at multiple zones in the sedimentary column.

Fluid source attribution is an inverse problem, because causal processes must be interpreted from observations in the near-surface. To date, examples of attribution have been rare, partly because of a paucity of disposal projects and partly because monitoring systems at the few operational scale projects that do exist, have not detected upward fluid

migration (Eiken et al., 2011; Hovorka et al., 2013). Yet at the Weyburn CO_2 enhanced oil recovery site in Canada, nearby landowners interpreted dead animals and CO_2 in soil gas as fluid leakage. Further investigation contradicted the leakage claim because geochemical measurements indicated a natural near-surface origin of the fluid anomaly (Romanak et al., 2013; Gilfillan et al., 2017). Other notable fluid anomalies occurred at the Illinois Basin Decatur project and the Pump Canyon Pilot project. In both of these cases, attribution was straightforward after identifying faulty equipment near the anomaly (Wimmer et al., 2011; Wells et al., 2013). At future GCS sites, industrial operations, natural hydrocarbon migration, and diverse near-surface environments may create fluid anomalies that are not clearly interpreted with the current geochemical toolset. To complicate matters further, the investigation of anomalies themselves cannot fully address the attribution inverse problem. Observations in the near-surface environment may have evolved away from their original compositions from alteration processes during upward migration. The second chapter of this dissertation rigorously evaluates a fluid anomaly in the vadose zone and presents a thorough comparison of geochemical tools that attribute gas fluid sources.

The ECO_2 research consortium recently identified gas chimneys or pipes as a potential leakage concern because of the possibility of near-vertical fluid migration (Jones et al., 2015). The third chapter investigated fluid compositions above a gas chimney within 3 m of the sediment–water interface. The results of this study were negative because light hydrocarbon concentrations were consistent with typical background values. Yet this dataset and interpretation are a novel contribution for two reasons: (1) the lack of hydrocarbons is consistent with episodic fluid migration between

dormant periods of ~10,000a (Roberts and Carney, 1997) and, therefore, gas chimneys are not necessarily a CO_2 leakage concern; and (2) typical background concentrations may be misinterpreted as seepage using the Bernard plot technique.

Previous compilations of light hydrocarbon seepage measurements revealed consistent alteration patterns at field sites across the globe. Lighter components by weight (methane, helium, neon) were enriched in shallower zones relative to heavier components (ethane, propane, krypton, xenon) (Ballentine et al., 1991; Etiope et al., 2009; Ma et al., 2009). The consistent patterns indicate that similar processes are causing alteration, yet these processes remain poorly understood. Differential solubility and sorption have been qualitatively proposed as the cause of alteration but few studies have investigated these processes at the field scale. Klusman (2003) modeled microseepage volumes and fluxes from a natural seep in Rangely Field, Colorado, but did not consider phase changes and sorption effects. Ma et al. (2012) modeled diffusion and differential solubility of noble gases, which showed that alteration effects aligned with field data.

The fourth chapter of this study offers a unique quantification of light hydrocarbon alteration from solubility and sorption. These results show that solubility causes relatively small compositional changes. In contrast, our sorption model is consistent with alteration observed in field data. The fourth chapter presents a novel tool for tracking potential CO_2 leakage. The interactions between CO_2, noble gases, and water have been documented within natural accumulations (Gilfillan et al., 2009) and CO_2-EOR reservoirs (Gyore and Gilfillan, 2016). We build on these results by simulating compositional changes as a hypothetical plume migrates to shallower depth intervals.

These results show increases in noble gas concentrations that would distinguish fugitive CO_2 from natural values.

This introductory chapter provides a brief overview of fluid flow and geochemistry concepts relevant to chapters three, four, and five.

1.2 LIGHT HYDROCARBON SOURCES

The two broad categories of light hydrocarbon formation pathways are thermal degradation of organic matter (thermogenic) or microbially-mediated anaerobic reactions (biogenic). Thermogenic light hydrocarbons are formed by cracking oil at 150-180 °C to produce methane, ethane, propane, butane, and pentane (C1 – C5) or by cracking kerogen at 150-220 °C to produce primarily methane (Allen and Allen, 2013). Within the category of biogenic hydrocarbons, the two dominant methanogenic reactions are methyl group fermentation and CO_2 reduction.

These formation pathways (thermogenic, biogenic – methyl fermentation, biogenic – CO_2 reduction) are commonly interpreted from two geochemical plots. The Schoell plot uses stable carbon and hydrogen isotopes of methane to distinguish between all three formation pathways (Schoell, 1983). The Bernard plot compares stable carbon isotopes of methane to the "Bernard Ratio" (concentrations of CH_4 / (C_2H_6 + C_3H_8)) (Bernard, 1978). The Bernard plot assumes that biogenic methane originates from CO_2 reduction, which is typical in offshore environments.

Radiocarbon (carbon-14) dates the age of carbon in light hydrocarbons or CO_2 from modern up to approximately 50,000 years. This measurement can identify carbon originating from recent organic matter decomposition, regardless of the microbial

formation pathway. Thermogenic hydrocarbons that have been trapped in the subsurface for >>50,000 years would no longer contain radiocarbon.

Geochemical measurements of CO_2 have limited value in attributing its source. Stable carbon isotopes of CO_2 captured from power plants are within the range of typical biogenic CO_2 (O'Leary, 1988). The oxygen isotopes of CO_2 do not maintain their original values because of exchange with oxygen in water (Germery et al., 1996). However, radiocarbon is most valuable CO_2 attribution tool because its presence can distinguish modern biogenic CO_2 from radiocarbon-free captured CO_2 (Flude et al., 2016).

1.3 SEEPAGE AND POTENTIAL ALTERATION

The term *seepage* refers to natural vertical migration of buoyant fluids. Gas migration occurs as continuous or episodic events when gas hydraulic head from buoyancy forces exceeds the capillary entry pressure of faults, natural fractures, or pores (Hunt, 1990). Hunt (1990) described typical events as gas periodically “burping” up to shallower layers and migrating laterally. The actual flowpaths are often complex and depend on pore to meso-scale heterogeneity (Trevisan et al., 2015). At the surface, gas can terminate at pock marks, mud volcanoes, or as diffuse micro-seepage that does not have a surface signature.

1.3 SEEPAGE AND POTENTIAL ALTERATION

The term seepage refers to natural vertical migration of buoyant fluids. Gas migration occurs as continuous or episodic events when gas hydraulic head from buoyancy forces exceeds the capillary entry pressure of faults, natural fractures, or pores (Hunt, 1990). Hunt (1990) described typical events as gas periodically “burping” up to

shallower layers and migrating laterally. The actual flowpaths are often complex and depend on pore to meso-scale heterogeneity (Trevisan et al., 2015). At the surface, gas can terminate at pock marks, mud volcanoes, or as diffuse micro-seepage that does not have a surface signature.

1.4 BROADER IMPACTS OF THIS RESEARCH

Buoyancy-driven fluid migration through water-wet earth materials is relevant to numerous applied disciplines. This research focuses on light hydrocarbons, given extensive natural seepage and the feasibility of sampling from oil and gas infrastructure. However, the significance of this work goes beyond hydrocarbon migration and CO_2 storage—the same alteration processes could influence other buoyant fluids as well. Consequently, numerical models and fluid source attribution methods proposed in this research can be adapted to other environmental and industrial problems.

For example, the generalized fluid source framework can be applied to at least three contexts. First, this framework could be implemented to support GCS monitoring systems to detect fluid anomalies or to resolve landowner concerns (e.g., Romanak et al., 2013). Second, the source of groundwater methane near hydraulic fracturing operations is still debated near the Marcellus shale (Osburn et al., 2011). While this research cannot distinguish shale gas leakage from natural seepage, it can identify thermogenic methane from biological processes. Third, uncertainties in the atmospheric methane budget make it difficult to predict its role in future climate change (Walter et al., 2006). Rising global temperatures may initiate a positive feedback loop with biogenic methanogenesis, but the Intergovernmental Panel on Climate Change recently increased the contribution of *thermogenic* methane in the overall atmospheric budget from ~20% to ~30% (Stocker et

al., 2014). This framework could improve atmospheric methane budgets by identifying source(s) in future field studies documenting methane emissions compositions.

Numerical models proposed in this research could add value to three practical applications. First, one implication of this research is that an unreported process may decrease CO_2 contamination risks after potential GCS leakage. By assessing the role of sorption in buoyant hydrocarbons, models adapted from this research may show that CO_2 is sequestered at the water-grain interface. While previous modeling studies have predicted capillary (Juanes et al., 2010) and solubility trapping (Gilfilan, 2008), this research and future work could theoretically show CO_2 'sorption trapping.' Additionally, these forward models could show changes in the relative amounts of CO_2 and C1-C3 to assess pathways and timescales of migration from CO_2-EOR reservoirs or infrastructure.

Second, oil explorationists create petroleum system models by comparing reservoir and source rock compositions. While this research focused on gas migration, oil compositional changes during migration indicate the importance of sorption as an alteration process (Leythaeuser et al., 1984). Consequently, reactive transport algorithms adapted from this research could advance future basin models used by the oil and gas industry. Third, radon produced from radioactive decay in earth materials is a serious human health risk when it accumulates indoors. Considering that radon is relatively soluble and differences in sorption properties between its stable isotopes (Wong et al., 1992), reactive transport models from this research could be adapted to understand radon migration. Given the wide range of applications that are intertwined with fluid migration, the products of this research may have practical outcomes far beyond hydrocarbon migration.

1.5 REFERENCES

Allen, P. A., & Allen, J. R. (2013). Basin analysis: principles and application to petroleum play assessment. Oxford, UK: John Wiley & Sons. 632.

Ballentine, C. J., O'nions, R. K., Oxburgh, E. R., Horvath, F., & Deak, J. (1991). Rare gas constraints on hydrocarbon accumulation, crustal degassing and groundwater flow in the Pannonian Basin. *Earth and Planetary Science Letters*, *105*(1–3), 229–246.

Benson, B. B., & Krause Jr, D. (1976). Empirical laws for dilute aqueous solutions of nonpolar gases. *The Journal of Chemical Physics*, *64*(2), 689–709.

Bernard, B. B. (1978). *Light hydrocarbons in marine sediments* (Doctoral dissertation, Texas A&M University.).

Eiken, O., Ringrose, P., Hermanrud, C., Nazarian, B., Torp, T. A., & Høier, L. (2011). Lessons learned from 14 years of CCS operations: Sleipner, In Salah and Snøhvit. *Energy Procedia*, *4*, 5541–5548.

Etiope, G., Feyzullayev, A., & Baciu, C. L. (2009). Terrestrial methane seeps and mud volcanoes: a global perspective of gas origin. *Marine and Petroleum Geology*, *26*(3), 333–344.

Flude, S., Gilfillan, S., Johnston, G., Stuart, F., & Haszeldine, S. (2016, April). Fingerprinting captured CO_2 using natural tracers: Determining CO_2 fate and proving ownership. In: *EGU General Assembly Conference Abstracts,* v. *18*, 6819.

Gemery, P. A., Trolier, M., & White, J. W. (1996). Oxygen isotope exchange between carbon dioxide and water following atmospheric sampling using glass flasks. *Journal of Geophysical Research: Atmospheres*, *101*(D9), 14415–14420.

Gilfillan, S. M., Lollar, B. S., Holland, G., Blagburn, D., Stevens, S., Schoell, M., Cassidy, M., Ding, Z., Zhou, Z., Lacrampe-Couloume, G., & Ballentine, C. J. (2009). Solubility trapping in formation water as dominant CO_2 sink in natural gas fields. *Nature*, *458*(7238), 614–618.

Gilfillan, S. M., Sherk, G. W., Poreda, R. J., & Haszeldine, R. S. (2017). Using noble gas fingerprints at the Kerr Farm to assess CO_2 leakage allegations linked to the Weyburn-Midale CO_2 monitoring and storage project. *International Journal of Greenhouse Gas Control*, *63*, 215–225.

Gyore, D., Stuart, F., & Gilfillan, S. (2016). Understanding the interaction of injected CO_2 and reservoir fluids in the Cranfield enhanced oil recovery (EOR) field (MS, USA) by non-radiogenic noble gas isotopes. In *EGU General Assembly Conference Abstracts* (v. 18, p. 15910).

Hovorka, S. D., Meckel, T. A., & Trevino, R. H. (2013). Monitoring a large-volume injection at Cranfield, Mississippi—Project design and recommendations. *International Journal of Greenhouse Gas Control*, *18*, 345–360.

Hunt, J. M. (1990). Generation and migration of petroleum from abnormally pressured fluid compartments (1). *AAPG Bulletin*, *74*(1), 1–12.

Jones, D. G., Beaubien, S. E., Blackford, J. C., Foekema, E. M., Lions, J., De Vittor, C., West, J. M., Widdicombe, S., Hauton, C., & Queirós, A. M. (2015). Developments since 2005 in understanding potential environmental impacts of CO_2 leakage from geological storage. *International Journal of Greenhouse Gas Control*. DOI:10.1016/j.ijggc.2015.05.032.

Juanes, R., Spiteri, E. J., Orr, F. M., & Blunt, M. J. (2006). Impact of relative permeability hysteresis on geological CO_2 storage. *Water Resources Research*, *42*(12). W12418, doi:10.1029/2005WR004806.

Juanes, R., MacMinn, C. W., & Szulczewski, M. L. (2010). The footprint of the CO_2 plume during carbon dioxide storage in saline aquifers: storage efficiency for capillary trapping at the basin scale. *Transport in porous media*, *82*(1), 19–30. 1573–1634. https://doi.org/10.1007/s11242-009-9420-3

Klusman, R. W. (2003). A geochemical perspective and assessment of leakage potential for a mature carbon dioxide enhanced oil recovery project and as a prototype for carbon dioxide sequestration; Rangely field, Colorado. *AAPG bulletin*, *87*(9), 1485–1507.

Leythaeuser, D., Mackenzie, A., Schaefer, R. G., & Bjoroy, M. (1984). A novel approach for recognition and quantification of hydrocarbon migration effects in shale-sandstone sequences. *AAPG Bulletin*, *68*(2), 196–219.

Ma, L., Castro, M. C., & Hall, C. M. (2009). Crustal noble gases in deep brines as natural tracers of vertical transport processes in the Michigan Basin. *Geochemistry, Geophysics, Geosystems*, *10*(6). Q06001, doi:10.1029/2009GC002475.

O'Leary, M. H. (1988). Carbon isotopes in photosynthesis. *Bioscience*, *38*(5), 328–336.

Osborn, S. G., Vengosh, A., Warner, N. R., & Jackson, R. B. (2011). Methane contamination of drinking water accompanying gas-well drilling and hydraulic fracturing. *Proceedings of the National Academy of Sciences*, *108*(20), 8172–8176.

Ozima, M., and Podosek, F.A. 2002. *Noble Gas Geochemistry*. Cambridge, UK: Cambridge University Press. 286.

Roberts, H. H., & Carney, R. S. (1997). Evidence of episodic fluid, gas, and sediment venting on the northern Gulf of Mexico continental slope. *Economic Geology*, *92*(7–8), 863–879.

Romanak, K., Sherk, G. W., Hovorka, S., & Yang, C. (2013). Assessment of alleged CO_2 leakage at the Kerr farm using a simple process-based soil gas technique: Implications for carbon capture, utilization, and storage (CCUS) monitoring. *Energy Procedia*, *37*, 4242–4248.

Schoell, M. (1983). Genetic characterization of natural gases. *AAPG bulletin*, *67*(12), 2225–2238.

Stocker, T. (Ed.). (2014). *Climate change 2013: the physical science basis: Working Group I contribution to the Fifth assessment report of the Intergovernmental Panel on Climate Change*. Cambridge, UK: Cambridge University Press. 1535.

Trevisan, L., Pini, R., Cihan, A., Birkholzer, J. T., Zhou, Q., & Illangasekare, T. H. (2015). Experimental analysis of spatial correlation effects on capillary trapping of supercritical CO_2 at the intermediate laboratory scale in heterogeneous porous media. *Water Resources Research*, *51*(11), 8791–8805.

Warr, O., Rochelle, C.A., Masters, A. & Ballentine, C.J. (2015) Determining noble gas partitioning within a CO_2–H_2O system at elevated temperatures and pressures. *Geochimica et Cosmochimica Acta* 159, 112–125.

Wells, A.W., Diehl, J.R., Strazisar, B.R., Wilson, T.H., & Stanko, D.C., 2013. Atmospheric and soil-gas monitoring for surface leakage at the San Juan Basin CO_2 pilot test site at Pump Canyon New Mexico, using perfluorocarbon tracers, CO_2 soil-gas flux and soil-gas hydrocarbons. *International Journal of Greenhouse Gas Control* 14, 227–238.

Wimmer, B.T., Krapac, I.G., Locke, R., & Iranmanesh, A., 2011. Applying monitoring, verification, and accounting techniques to a real-world, enhanced oil recovery operational CO_2 leak. *Energy Proceedings* 4, 3330–3337.

Wong, C. S., Chin, Y. P., & Gschwend, P. M. (1992). Sorption of radon-222 to natural sediments. *Geochimica et cosmochimica acta*, *56*(11), 3923–3932.

Chapter 2: Gas Source Attribution Techniques for Assessing Leakage at Geologic CO_2 Storage Sites: Evaluating a CO_2 and CH_4 Soil Gas Anomaly at the Cranfield CO_2-EOR Site[1]

Abstract

At the Cranfield CO_2 enhanced oil recovery (CO_2-EOR) site, a localized area of high concentrations of CO_2 (up to 44%) and CH_4 (up to 47%) in soil gas was detected near a plugged and abandoned well. The complexity of attributing this anomaly, especially in a CO_2-EOR setting, underscores the need for careful attribution techniques and provides rare and valuable experiential knowledge on attributing blind anomalies. An extensive geochemical monitoring program utilizing process-based soil gas ratios, stable and radioactive isotopes of CO_2 and CH_4, light hydrocarbon concentrations, noble gases, and perfluorocarbon and sulfur hexafluoride tracers was undertaken from 2009 through 2014. The goals were to attribute source, assess the usefulness of various attribution techniques, and begin to develop a framework for attribution in complex CO_2-EOR settings. Initial process-based assessment indicated an "exogenous" source meaning that it was not the result of natural in-situ processes (Romanak et al., 2012). We report on the additional analyses used to determine the degree to which the anomaly was related to CO_2 injection. This work included characterization of potential non-reservoir gas sources within the overburden using mud-gas samples collected during a new drill and downhole

[1] A version of this chapter is published as Anderson, J. S., Romanak, K. D., Yang, C., Lu, J., Hovorka, S. D., & Young, M. H. (2017). Gas source attribution techniques for assessing leakage at geologic CO_2 storage sites: Evaluating a CO_2 and CH_4 soil gas anomaly at the Cranfield CO_2-EOR site. *Chemical Geology*, *454*, 93-104. The first author contributed an original fluid source interpretation, geochemical analysis, and numerical modeling.

fluids collected from wells within the field. Two hydrocarbon gas sources, one within the reservoir (Tuscaloosa) and one in the above-zone (Wilcox) were geochemically distinct.

Stable carbon isotopes ($\delta^{13}C$) of CH_4 in the anomaly were similar to those of the reservoir, but stable hydrogen isotopes (δD) indicated that anomalous gases originate from an undetermined microbial source rather than either of the subsurface gas reservoirs. Hydrocarbon geochemical parameters were therefore not only useful for attribution, but were also found to have a high potential for leading to inaccurate conclusions because of alteration via CH_4 oxidation. Noble gases and introduced tracers proved least effective for attribution in this case. The most useful indicator was radioactive isotopes of CO_2 and CH_4, which contained >100% modern carbon indicating a negligible input, if any, from the reservoir.

2.1 INTRODUCTION

The possibility of fluid leakage from GCS operations is minimized by regulations and permitting processes that ensure that proper practices are followed for site selection, risk management, and environmental protection. However, any indication of potential leakage at GCS sites will need careful assessment. Indications of potential leakage may range from soil gas anomalies located by reconnaissance monitoring to public complaints about visual land changes, to environmental damage. Once an anomaly has been identified, source attribution will be critical to determining the need for next steps such as establishing liability, quantifying emissions for credit accounting, or instigating remediation activities (e.g., Dixon and Romanak, 2015). Accurate gas source attribution techniques will clearly be required independent of the potential for GCS sites to leak.

Whereas source attribution is critical to identifying whether an anomaly represents leakage, a lack of anomalies at GCS sites means that few empirical opportunities for developing attribution techniques exist. Most investigations into near-surface leakage have used controlled releases of a known origin to focus on developing tools and methods for locating anomalies or observing associated environmental impacts (e.g., Spangler et al., 2010; Smith et al., 2013; Feitz et al., 2014; Moreira et al., 2014). Few investigations have therefore benefitted from the opportunity to attribute real gas anomalies of unknown origin at active CO_2 injection sites. At a CO_2-EOR site in the Illinois Basin, Illinois, USA, a leak from an underground CO_2 pipeline became obvious from frozen ground and dust movement (Wimmer et al., 2011). In addition, a soil gas anomaly at a pilot project at Pump Canyon, New Mexico, USA, was found to originate from infrastructure failure (Wells et al., 2013). Perfluorocarbon tracers mixed into the injection gas were detected in the soil gas, thereby indicating well or pipeline leakage as the fluid source. In both of these cases, attribution was straightforward, perhaps because signals resulted from surface infrastructure leakage.

To date, perhaps one of the best pragmatic opportunities for developing and testing CO_2 source attribution techniques occurred in 2011, when landowners near the Weyburn CO_2 enhanced oil recovery (CO_2-EOR) site claimed that soil CO_2 on their property originated from injection operations. A study commissioned by the Kerr Farm landowners using CO_2 and hydrocarbon concentration and stable isotopic data concluded leakage (Lafleur, 2010; 2011). However, multiple independently-collected datasets including radioactive carbon isotopes (Trium, 2011), process-based soil gas ratios (Romanak et al., 2013; 2014), and noble gas isotopes (Sherk et al., 2011; Gilfillan et al.,

2014) were used to refute the leakage claim, indicating that CO_2 had formed in the near-surface by biological processes. At the Kerr Farm, attribution was relatively simple because of agreement of process-based ratios, noble gases and radioactive isotopes. However, the complexity of near-surface environments in CO_2-EOR settings such as described by Wolaver et al. (2013), will most likely create scenarios in which attribution is more problematic and requires a more diverse and highly tested toolset.

The latter scenario was the case when a localized (~300 m^2) soil gas anomaly of high CO_2 (up to 44%) and CH_4 (up to 47%) detected during reconnaissance monitoring near a plugged and abandoned well at the Cranfield CO_2-EOR site. The localized site became known as the "P-site." The attribution assessment by Romanak et al. (2012) was the first application of a process-based approach to assessing the origin of a surface anomaly. The method showed a systematic change in process-based soil gas ratios from simple respiration at the background site, to methane oxidation, and finally to exogenous gas input at the anomaly center near the well. We report herein the results of our attempt to further attribute the source of exogenous gas to explain to what degree the gas originated from reservoir leakage.

2.2 OBJECTIVES AND APPROACH

Our objective was to use a number of geochemical techniques to reduce the uncertainty in the origin of the surface gas anomaly at Cranfield. A secondary objective was to assess the usefulness of each technique for attribution and to begin to develop a framework for assessing exogenous gas at complex GCS sites. Our approach was to conduct a multi-parameter assessment of the anomaly over 6 years using stable and radioactive isotopes of CO_2 and CH_4, light hydrocarbon concentrations, noble gases, and

introduced tracers of SF_6 and PFT over time. A full characterization of gases within the sedimentary column was undertaken using mud gas samples during a new well drill and downhole fluid samples from wells throughout the field to provide information about potential gas sources of the anomaly.

2.3 PROJECT SETTING AND PREVIOUS WORK

As part of the U.S. Department of Energy's Regional Carbon Sequestration Partnerships (RCSP) Program, a depleted oil field in Cranfield, MS, USA (~25 km east of Natchez, MS, USA) was studied to evaluate and develop GS monitoring technologies. Approximately 25 organizations collaborated in the Cranfield project to store >5 million metric tons of CO_2 from 2012 through 2015 and publish at least 20 peer-reviewed publications addressing GS development, many in a special issue of the International Journal of Greenhouse Gas Control volume 18 (e.g., Nicot et al., 2013).

Cranfield surface geology is generally characterized by loess deposits with a vertical relief of tens of meters in which two streams have incised into alluvium (Hovorka et al., 2011). Hardwoods and pine dominate the flora. The shallow subsurface (0-500m) contains a shallow freshwater aquifer (Catahoula) (TDS < 1,000 mg/L) overlying several more saline confined aquifers (Jackson-Vicksburg Group) (Yang et al., 2013). Below the aquifers, the Eocene Wilcox Group (1,200 – 2,100 m) consists of thick interbedded sandstones formed by transgression and advancement of strand plain and deltaic deposition (Echols and Malkin, 1948; Nicot et al., 2013).

The primary hydrocarbon reservoir at Cranfield is the Cretaceous Lower Tuscaloosa Formation (~3000m) (Hovorka et al., 2011). These upward-fining sandstones and conglomerates are point-bar and channel features deposited during a transgressive

cycle during fluvial to shelf sedimentation (Spooner, 1964; Berg and Cook, 1968). The entire Tuscaloosa Formation is overlain by thick calcareous mudstones that serve as the confining system for hydrocarbon and CO_2 storage.

Above the Tuscaloosa, hydrocarbon production began in the Wilcox Formation in the early 1940s and ultimately produced ~12 MMbbl oil and 3 Bcf of gas over the following 40 years (Nicot et al., 2013). However, these volumes are relatively small when compared with the ~37 MMbbl oil and >672 Bcf of gas produced from the Lower Tuscaloosa Formation from 1944 through 1965 (Weaver, L.K., 1966). Gas production from both the Wilcox and Tuscaloosa was reinjected in the Lower Tuscaloosa for pressure management until field abandonment in 1966 (Hovorka et al., 2011).

In 2008, the oil field operator began EOR in the lower Tuscaloosa sands by injecting CO_2 sourced from a natural accumulation in Jackson Dome, MS, USA (Hovorka et al., 2013). Anthropogenic CO_2 was not used because regional power plants and other emission sources had not been considering CO_2 capture at that time (Hovorka et al., 2013). After staged increases in the number of injection wells and injection rates, 5.3 million metric tons of CO_2 had been stored (injected minus recycled) as of January 2015.

A rigorous leakage risk assessment of Cranfield field by Nicot et al. (2013) concluded that poor cementing in plugged and abandoned wells has made the historic wells the most likely fluid migration pathways. More than 287 wells penetrate the sealing formation (Anahuac shale) and 11% of wells with cement bond logs (n=9) contained poor or questionable cement quality. In contrast to wells, two faults exist at the depth of the Tuscaloosa. Neither fault is a likely CO_2 leakage pathway to surface: one fault penetrates

the Lower Tuscaloosa below the original oil-water contact, whereas the second fault appears to terminate in overlying mudstone, according to seismic imaging. Conclusions of the risk assessment suggest that any evaluation of groundwater (Yang et al., 2013; 2015) and/or soil gas (Romanak et al., 2012; this publication) should be focused near well sites.

Shallow groundwater compositions sampled from 14 wells from 2008 through 2012 reported by Yang et al. (2013) did not indicate widespread upward gas migration. Dissolved light hydrocarbons were <0.04 ppm and the concentrations of carbonate species were undersaturated with respect to calcite (Yang et al., 2013). Stable carbon isotopes of dissolved inorganic carbon (-25 to -14‰) were consistent with typical groundwater values (-25 to -5‰) rather than injectate CO_2 (-2.63‰) (Lu et al., 2012).

Initial near-surface surveillance was focused on measuring soil gas near and below the well pads of plugged and abandoned (P&A) wells (Romanak et al., 2009). Although 11 P&A well pads were surveyed, only one well pad (47-1) was found to exhibit anomalous CH_4 and CO_2 concentrations (CH_4=13.79%, CO_2=7.35% at the time of detection) (Fig. 2.1). This well pad and an associated abandoned open pit were located on a hillslope (Fig. 2.1c: Romanak et al, 2012). The 47-1 had been drilled in 1948 to produce oil from the Tuscaloosa Formation, but it was plugged and abandoned in 1967 (Figs. 2.2 and 2.3). Vadose zone measurements began in 2009 before CO_2 injection started at the field later the same year. During the data collection period, well 47-1 was recompleted from a P&A well to a producing well in June 2010. Continued sampling of the anomaly over 6 years yielded concentrations of CO_2 (up to 44%) and CH_4 (up to 47%) in soil gas up to a ~5 m depth.

Initial attribution of the anomaly by Romanak et al. (2012) was accomplished using a process-based assessment of fixed soil gases. This method was developed as a simplified screening option for attribution not requiring extensive baseline measurements or expensive sample analysis. The initial conclusion was that the anomaly represented an exogenous gas that required further attribution assessment (Hingst, 2013) (Fig. 2.4). We therefore conducted additional testing with geochemical parameters to further determine whether the origin was from the CO_2 storage reservoir, intermediate gas-rich intervals, or a different origin altogether (Fig. 2.4).

2.4 METHODS

Semi-permanent completions of nested stainless steel gas sampling ports were used to collect gas from depths ranging between 1 and 4 m at nine stations comprising several transects across the P-site well pad (for details see Romanak et al., 2012). One transect extended from a 1950s open pit across the well pad to a grassy area defined as a background area (Fig. 2.2). Soil gas was sampled several times per year from August, 2009 through February, 2014 and analyzed onsite and/or collected in Calibond gas bags for laboratory analysis. The following Methods subsections present the laboratories where each type of samples were analyzed.

2.4.1 LIGHT HYDROCARBONS

Hydrocarbons and isotopes were analyzed at Isotech Laboratories (Champaign, Illinois) for fixed gas and hydrocarbon concentrations, stable carbon isotopes of methane and CO_2, stable hydrogen isotopes of methane, and/or radioactive carbon isotopes of methane and CO_2. Gas concentrations and stable isotopes were measured via GC-IRMS (HP 6890/7890 interfaced to Thermo Scientific Delta V Plus). Radioactive carbon

isotopes were measured via Accelerator Mass Spectrometry. Carbon isotopic ratios were recorded relative to Vienna Pee Dee Belemnite standards and are presented in conventional delta notation.

2.4.2 WELL RECOMPLETION AND TRACER TEST

In June 2010, the field operator recompleted the P&A well near the soil gas anomaly (47-1) into a producing well (Fig. 2.3). Before the workover rig entered the well, a sampling port was drilled into the top of the well. A gas sample was collected with a peristaltic pump because the upper part of the well had not been pressurized.

After the upper cement plug had been drilled out, a second cement plug connected the bottom of the surface casing (555.3m) and the top of the production casing (584.9m) (Fig. 2.3). The original intent of the tracer test was to evaluate the integrity of this cement plug. Unfortunately, the production casing was patched to form a continuous string to the surface before it was possible for the tracers to be pressurized at this depth interval (Fig. 2.3). As an alternative, tracers were injected through the Tuscaloosa Formation perforations at 3090 to 3132 m. About 950 g of perfluorocarbon (PFT) and 8.6 kg of sulfur hexafluoride (SF_6) were injected into the well manifold followed by ~2,000 liters of brine to push the tracers into the formation. About one-third of the volume of the tracer was spilled at the surface near well 47-1 while it was being connected to the manifold. In January 2011, 10 samples were collected at soil gas stations for tracer analysis. These samples of soil gas collected before well recompletion (October, 2009, February, 2010 and June, 2010) were analyzed for PFT and SF_6 concentrations via GC-ECD at Oak Ridge National Laboratory.

2.4.3 NOBLES GASES

The soil gas anomaly and groundwater wells were sampled for noble gas concentrations and isotopes. In February 2010, soil gas from six stations was collected in pre-evacuated 1,000-cc stainless-steel cylinders. This sampling procedure was repeated at five soil gas stations in June 2010 during recompletion of well 47-1. The upper part of well 47-1 above the first cement plug was also sampled at that time (Fig. 2.3).

In November 2010, eight groundwater wells were sampled for noble gas analysis using internally polished copper tubes connected to high-pressure tubing to avoid atmospheric contamination. Groundwater wells were purged with a submersible pump for several hours until field parameters converged (temperature, dissolved oxygen, oxidation-reduction potential, and specific conductance). The downstream end of the copper tube was cold welded with a crimping tool before the upstream side was sealed.

Noble gas concentrations and isotopes were measured at Rouins Automated Rare Gas Analysis lab at the University of California Berkley and Lawerence Berkley National Lab (Berkeley, California). Sampled gas was purified in an all-metal gas purification line that was connected to an all-metal noble gas mass spectrometer. Analytical procedures used for noble gases are described in detail in Kennedy et al. (1985).

2.4.4 NOBLE GAS SOLUBILITY SIMULATIONS

The contribution of noble gases in the vadose zone that may have exsolved from groundwater was simulated using geochemical software PHREEQC (v3.0) (Parkhurst and Appelo, 2013). The initial aqueous solution was assumed to contain Cranfield average measured noble gas concentrations and total dissolved solids (TDS) (~135 mg/L) (Yang et al., 2013). Gas ebullition from organic matter was simulated by equilibrating equal

mole amounts of CO_2 and CH_4 at 0.5 mmol/L steps at constant atmospheric pressure. Altitude and water-vapor content were neglected in this modeling application. Separate model simulations were run using Henry coefficients calculated at 10° and 25° C (Ozima and Podesek, 2002) so that Cranfield ambient temperature could be modeled during sampling in February and June 2010, respectively. Dissolved CO_2 was equilibrated with other carbonate species (bicarbonate (HCO_3^-), carbonate (CO_3^{-2}), carbonic acid (H_2CO_3)) following equilibrium equations (Parkhurst and Appelo, 2013).

2.4.5 OVERBURDEN CHARACTERIZATION

In order that gases within the overburden could be characterized, mud gas was sampled during a new drill, and deep gases were also sampled at wellheads. While a new Cranfield well (CFU 70-2#1) was being drilled in October 2011, gas dissolved in drilling mud was sampled throughout the overburden every ~15 m from ~510 m to the Tuscaloosa reservoir at a depth of ~3,200 m. A gas-trap agitator was installed on the mud return line upstream of the shale shaker. Liberated gas was collected into Iso-tubes (Isotech Laboratories, Champaign, Illinois) at ~50 m intervals. Geomark Research, LTD (Lafayette, Louisiana) analyzed mud-gas samples for molecular composition and stable carbon isotopes of methane, ethane, and propane via gas chromatograph mass spectrometry (Agilent 6890).

Detailed geochemical analysis was undertaken on gas samples from wells completed in the Lower Tuscaloosa and Wilcox Formations. Lower Tuscaloosa Formation gas was sampled using wellhead, kluster, and U-tube techniques at eight wells across the field in December, 2009. Lu et al. (2012) provided well locations, methodology, and molecular composition results. Methane stable isotope data (δD and

$\delta^{13}C$) from the same samples were analyzed via mass spectrometry at UT-Austin labs (Thermo Scientific MAT 253).

In April 2012, two wells completed in the Wilcox Formation (Ella G Lees #28 and Lees-Ratcliffe unit) were sampled for gas at the wellhead into Calibond gas bags. Isotech Laboratories (Champaign, Illinois) measured molecular composition and methane stable isotopes via GC-IRMS (HP 6890/7890 interfaced to Thermo Scientific Delta V Plus).

2.5 RESULTS

2.5.1 HYDROCARBON AND CO_2 GAS GEOCHEMISTRY

The complete dataset of laboratory analysis of vadose zone gases, including light hydrocarbon and CO_2 concentrations, stable isotopes, and radioactive isotopes, are presented in online supplementary material Table S1 of the publication version of this chapter. Soil gas methane stable isotopes ranged from -31.6 to -65.8‰ for carbon and -197 to -281‰ for hydrogen. The vadose zone CO_2 stable carbon isotopes ($\delta^{13}C$-CO_2) ranged from -25.5 to -11.0‰.

Radioactive carbon isotopes were measured in CO_2 and/or CH_4 from the center of the anomaly (soil gas station 103), the background (BG) soil gas station, and a downhole fluid sample from a well penetrating the Wilcox Formation (Ella G. Lees #28). Results for all soil gas samples were >100% modern carbon (pMC) for both CO_2 and CH_4 (Table 2.1). In contrast to that of near-surface soil gas samples, methane carbon-14 from Wilcox gas contained 0.2 pMC. Carbon-14 was not measured on injectate or Tuscaloosa samples.

2.5.2 NOBLE GASES

The complete dataset of noble gas results is presented in Supplementary Information Table S2. Helium isotopic ratios ($^{3}He/^{4}He$) were normalized to the ratio in air (Ra, 1.4e-6). Helium isotopic ratios ranged from 0.857 to 1.236 for soil gas and well 47-1 and 0.26 to 0.51 for groundwater samples. The concentrations of ^{4}He, ^{22}Ne, ^{84}Kr, and ^{132}Xe ranged from 0.0007 to 0.0186, 0.0003 to 0.0063, 0.0005 to 0.0028, and 0.0000 to 0.0001 ppm respectively for groundwater samples and 0.0776 to 0.974, 0.0229 to 0.9096, 0.0093 to 0.7974, 0.0003 to 0.8572 ppm respectively for soil gas samples.

2.5.3 PFT AND SF_6

The complete dataset of tracer concentrations in soil gas are presented in Table S3 in online supplementary data. Concentrations of perfluorocarbon (PFT) were below detection limits for all samples. Sulfur hexafluoride (SF_6) was detected in 4 of the 10 soil gas samples collected after the tracer injection test with concentrations ranging from 104 to 815 pg/mL. Samples collected before the injection test were also analyzed and were found not to contain detectable SF_6 or PFT.

2.5.4 OVERBURDEN CHARACTERIZATION

Mud gas methane carbon isotopes ranged from -64.9 to -68.0‰ in the overburden interval from 648 to 2,373 m. These values increased from -58.6 to -42.2‰ in samples collected during drilling from 3,045 to 3,462 m (Fig. 2.5). Isotopic measurements from downhole fluid samples collected at 1,402 and 1,760 m were -65.8 & -67.4‰ for methane carbon isotopes and -184 to -188‰ for methane hydrogen isotopes, respectively. The molecular compositions of these two samples were dominated by methane (94.84 and 91.94%), yet ethane and heavier gaseous hydrocarbons (C2+) were also present (0.62 and 1.21%). Carbon and hydrogen stable isotopes ranged from -41.83 to -40.74‰ and -

165 to -173‰, respectively, in methane samples collected from the Tuscaloosa Formation.

2.6 DISCUSSION

2.6.1 HYDROCARBON AND CO_2 GAS GEOCHEMISTRY

Characterization of the $\delta^{13}C$ of CH_4 throughout the overburden (Fig. 2.5) indicates two isotopically distinct gases in the subsurface: one in the intermediate Wilcox Formation and one in the Tuscaloosa CO_2-EOR reservoir. The isotopic similarity between the Tuscaloosa and the surface anomaly, in addition to the proximity of the surface anomaly to the historic well, could easily lead to the conclusion of leakage; however, further analysis using methane-formation pathways suggests a different conclusion (Fig. 2.6).

Methane stable isotopes from the anomaly were compared with those of empirical models of formation processes and values from the Tuscaloosa and Wilcox Formations. Whereas our focus is not an understanding of methane formation pathways per se, they can serve as diagnostic tools for different potential source pools for the surface anomaly. In the deeper Tuscaloosa Formation, methane stable isotopes that include both $\delta^{13}C$ and δD clearly relate to a thermogenic genetic pathway following classifications by Schoell, 1983 (Fig. 2.6). The deepest mud gas sample (-42.2 ‰) agrees well with Tuscaloosa downhole samples (average = -41.3‰) (Lu et al., 2012) (Fig. 2.5). In contrast, methane stable carbon isotopes from the overburden Wilcox Formation are consistent with biogenic formation via CO_2 reduction (Fig. 2.6). Mud gas carbon isotopic values collected within the overburden (-64.9 to -68.0‰) are similar to values from Wilcox Formation downhole samples (-65.8 and -67.4‰) (Fig. 2.5). Our interpretation is

consistent with reports by other investigations on Wilcox reservoirs across Mississippi and Louisiana that were concluded to originate from CO_2 reduction ($\delta^{13}C$ range: -65.57 to -60.73‰; δD range: -196 to -188‰) (e.g., Warwick et al., 2008).

The near-surface anomaly appears to have a biogenic acetate fermentation pathway modified by oxidation (Fig. 2.6). Note that the hydrogen isotopic values on the y-axis of the Schoell plot distinguish acetate fermentation from thermogenic fluids because the carbon isotopic values from these two sources generally overlap. An assessment of fluid source based on a face-to-face comparison of carbon isotopes between the soil gas anomaly and Tuscaloosa fluid could result in an erroneous interpretation of leakage if hydrogen isotopes are not measured. Even so, a consideration of the effects of hydrocarbon oxidation is critical when formation pathways are used to attribute source.

Oxidation of methane created by acetate fermentation can cause data to shift into the thermogenic field (Templeton et al., 2006). Such effects of oxidation appear to have modified the geochemistry of many of the surface anomaly samples that exhibit enrichment in $\delta^{13}C\text{-}CH_4$ and $\delta D\text{-}CH_4$ relative to the acetate fermentation field. Modification by extreme oxidation seems particularly evident with the sample from station 103, which plots directly within the thermogenic field. Thus, a Schoell plot can potentially provide useful information for attribution, even though the effects of methane oxidation must be carefully considered.

Additional evidence for methane oxidation is shown in Figure 2.7 (modified from Whiticar, 1999). This plot shows the diagnostic relationships between $\delta^{13}C$ of CH_4 and

co-existing CO_2, supporting an acetate fermentation pathway modified by methane oxidation.

The presence of high concentrations of CO_2 coexisting with CH_4 is also consistent with acetate fermentation, which results in co-production of CO_2 and CH_4 (Lui and Whitman, 2008). A CO_2 component can therefore additionally arise from methane oxidation. The anomaly $\delta^{13}C$-CO_2 values (-25.5 to -11.0‰) generally align with typical biologic respiration values (-30 to -8‰) (Bowling et al., 2008) rather than injectate CO_2, which is not anthropogenic at Cranfield but sourced from a natural dome (-2.63‰) (Lu et al., 2012). Note that most anthropogenic CO_2 sources will be indistinguishable from natural respiration (Dixon and Romanak, 2015; Flude et al., 2016) and $\delta^{13}C$-CO_2 will not be adequate for attribution in these cases.

Continuing our analysis, we assessed the distribution of light hydrocarbons within the Cranfield soil gas anomaly and other potential gas sources using a Bernard Plot (Fig. 2.8). The soil gas anomaly contains high concentrations of methane, although relatively low concentrations of ethane and heavier hydrocarbons (avg. 0.011%), resulting in an average Bernard Ratio (C1/(C2+C3)) of 9,500. Bernard Ratios are generally >1,000 for microbial gas and <100 for thermogenic sources (Bernard et al., 1978). In comparison, average Tuscaloosa and Wilcox values (14.11 and 94.9, respectively) indicate contributions from thermogenic fluids, although the methane stable isotopes of Wilcox samples are significantly depleted (by at least 15‰) relative to the thermogenic field.

The high values of Bernard ratios observed in soil gas may still signify a potential thermogenic source even though high values typically indicate biogenic methane formation. Ethane and heavier hydrocarbons can be preferentially removed by sorption

and/or differential solubility during migration (Etiope et al., 2009). Additionally, microbes preferentially degrade C2+ alkanes in the near-surface, thereby increasing the Bernard ratio and $\delta^{13}C\text{-}CH_4$ (Kinnaman et al., 2007). Therefore, high Bernard ratios are non-unique because they can indicate biogenic formation, microbial oxidation, or seepage from deep intervals.

On the x-axis of the Bernard plot, the stable carbon isotopes of methane define biogenic and thermogenic formation pathways (Fig. 2.8). This classification is effective in offshore environments in which "biogenic" methane is typically formed by CO_2 reduction ($\delta^{13}C\text{-}CH_4$ <-55‰), which results in carbon isotopes lighter than thermogenic values (Bernard et al., 1978). The problem with using this technique in onshore environments is that carbon isotopic values of acetate fermentation generally overlap with thermogenic signatures as was discussed previously (Fig. 2.6). For example, the soil gas anomaly samples fall in an ambiguous area or the kerogen type 2 field on the Bernard plot, possibly leading to an incorrect interpretation of a source from a deep reservoir (Fig. 2.8).

Alternatively, oxidation of Wilcox samples is also a plausible interpretation for explaining the hydrocarbon geochemistry of the soil gas anomaly on this plot. Therefore, with the high potential for oxidation to modify both concentrations and isotopic ratios of hydrocarbons, traditional plots that classify origin on the basis of hydrocarbon parameters such as Bernard plots may have limited use for attributing surface anomalies and could easily risk false positive conclusions for leakage.

With the complexity that hydrocarbon oxidation adds to attribution, perhaps the parameter of most utility is carbon-14. Carbon-14 concentrations of >100 pMC for both

CO_2 and CH_4 precluded any significant contribution from older fluid sources. As a consequence of open-air nuclear weapons testing in the mid-twentieth century, atmospheric carbon-14 concentrations increased above the value in 1950 defined as 100% modern carbon (pMC). After radiocarbon produced in the atmosphere is fixed into organic matter, carbon-14 concentrations decrease at established decay rates. No biologic or geologic carbon-14 formation processes have been discovered (Klusman, 2011), although, contamination of drilling fluid has been known to add exogenous radiocarbon into near-surface environments (Richards et al., 2015).

Whereas each potential gas source in this study was not directly tested for carbon-14, considering that the half-life of radiocarbon is ~5,568 years, carbon from Jackson Dome and the Tuscalosa Formation are expected to be radiocarbon free. The carbon-14 measurement from Wilcox methane (0.2 pMC) is a clear and unambiguous indicator of older carbon.

Given that carbon-14 data indicate modern carbon, our current conclusion on attribution of the anomaly is microbial acetate fermentation of an undetermined source. There is neither indication of substantial amounts of modern organic matter buried within the vadose zone (Hingst, 2013) nor a clear indication of any influence from the nearby open pit. Because historic well pads are flat and cleared of trees, families living within the boundaries of the field commonly locate mobile homes in these areas, and waste from these homes is another potential but undocumented source. Yet, another explanation could be that drilling operations have contributed modern dissolved organic carbon (DOC) to groundwater systems which had subsequently metabolized to CO_2 and methane (Richards et al., 2015). Ultimately, the carbon source could be investigated no further,

once the fluid anomaly had been determined to be non-leakage, and the actual source of methyl fermentation remains unverified.

2.6.2 NOBLE GASES

Noble gases can be potentially valuable fluid source tools because their compositions are defined by physical processes and contributions from the atmosphere, crustal rocks, and mantle rather than biological reactions (Ozima and Podosek, 2002). We therefore evaluated these parameters in both groundwater and soil gas to assess their utility for source attribution in the near-surface. We will first discuss results from groundwater wells sampled field-wide to form the basis for overall trends in groundwater, and then we will focus on soil gas data collected locally at the P-site. No groundwater was available for sampling at the P-site.

Field-wide, groundwater noble gases have generally aligned with air-saturated water in one sample (44-2) lying along a mixing curve between air and air-saturated water (Figs. 2.9-2.11). With the exception of sample 44-2, which appears contaminated by atmosphere, groundwater noble gas concentrations are consistent with air-saturated water for xenon, krypton, and neon. The exception to air and air-saturated water trends was enriched helium concentrations, especially from well 31-F1.

Because helium is not retained by the Earth's gravitational field, the concentration in the atmosphere is low at 5.2 ppm. Hence, the ^{4}He concentrations could indicate input from crustal fluids containing radiogenic ^{4}He because concentrations are slightly higher than predictions from mixing calculations. The interpretation of excess ^{4}He at 31-F1 is corroborated by a low $^{3}He/^{4}He$ ratio (R/Ra = 0.257) in comparison with that of atmospheric values (R/Ra = 1.0). A contribution of Jackson Dome fluid is unlikely

because helium-3 is more abundant than helium-4 in injectate CO_2 (R/Ra = 3.99 and 4.73, Gyore et al., 2015). Yet, with the exception of enriched helium-4 concentrations, groundwater noble gas data did not indicate upward migration of injectate or reservoir fluids. Additionally, the low dissolved light hydrocarbon concentrations (max 0.37 ppm) measured over 14 groundwater sampling trips precluded extensive recent leakage (Yang et al., 2013).

Noble gas compositions from the soil gas anomaly generally plotted along a dilution line between atmospheric concentrations and zero, although some samples exhibited significant variation (Figs. 2.12-2.14). For example, many samples showed small enrichments in helium-4. Some of this variation may be explained by alteration occurring within the vadose zone from diffusion and solubility processes rather than signifying a contribution from an additional fluid source (Etiope et al., 2009). A meta-analysis of seeps from around the globe indicated that mass-dependent separation between light hydrocarbons occurs during transport, which may result from solubility and sorption processes. We plan to evaluate this argument in a separate paper.

We simulated the effects of noble gas concentration changes caused by transport of CO_2 flux from any exogenous source into in the vadose zone using a dusty gas model. The dusty gas model is a mathematical description of viscous and diffusive fluxes, coupled with the Knudsen diffusivity of the porous media (Ding et al., 2016). The addition of CO_2 into previously stagnant gases results in differential diffusion caused by mass differences between components (Evans et al., 2001; Ding et al., 2016). This fractionation effect has modeled experimental data using a dusty gas model that calculates changes in noble gas components on the basis of two end members: exogenous

CO_2 and atmospheric noble gas compositions. Model calculations following Evans et al., 2001 are presented as a percentage of exogenous CO_2 on noble gas graphs (Figs. 2.12-2.14). Several samples from the soil gas anomaly with relatively high xenon and helium concentrations relative to the atmospheric dilution line may have been caused by diffusion. However, four samples from February 2010 showed helium enrichments that were not consistent with diffusion model results.

An alternative explanation for deviation from the atmospheric dilution line is that exogenous CO_2 and/or CH_4 striped noble gases from water that co-existed in the vadose zone or from groundwater if gas bubbled up from below (Aeschbach-Hertig et al., 2008). We tested this hypothesis using numerical simulation software PHREEQC to calculate noble gas concentrations in the gas phase after CO_2 and CH_4 had been equilibrated with groundwater containing dissolved noble gases. This model assumed that the original aqueous solution was 1 Liter of water containing solutes that were based on measured Cranfield shallow groundwater samples. The average TDS (~135 mg/L) of all Cranfield groundwater analyses was simulated using pure sodium chloride as TDS. Dissolved noble gas concentrations in the model were defined as the average concentrations from Cranfield groundwater samples, excluding well 44-2, leading to model initial conditions similar to those of air-saturated water values. Simulation runs were conducted by incrementally combining equimolar gaseous CO_2 and CH_4, with the aqueous solution at constant atmospheric pressure until the gas volume had reached 1.9 L. The simulated noble gas concentrations in the gaseous phase at equilibrium are included in the graphs for simulated temperatures at 10° and 25° C.

When compared with the simulated fluid anomaly, the soil gas data with ^{4}He, ^{22}Ne, and ^{84}Kr enrichments may be explained by noble gas contributions from water (Figs. 2.12-2.14). Note that observed xenon enrichments are not consistent with either stripping or diffusion models. The gas-stripping and diffusion model results demonstrate the challenges associated with interpreting fluid sources using noble gases because processes occurring within the vadose zone can significantly influence compositions. Furthermore, open communication between soil gas and the atmosphere results in noble gas measurements of soil gas contaminated by air (Mackintosh and Ballentine, 2012). Consequently, noble gas measurements could be dominated by atmospheric signatures even if an anomaly had originated from depth, and thereby limit their effectiveness as an attribution tool.

2.6.3 INTRODUCED TRACERS – PFT AND SF_6

Injected tracers were ineffective in assessing fluid sources in this study. The spill of tracer at the surface near the recompleted well may have limited the value of the test. PFTs are historically difficult to work with owing to their low detection limits and "sticky" behavior, which creates a high potential for inadvertent contamination in unknown areas. Locations that showed PFT concentrations below detection limits were consistent with the interpretation of fluid isolation between zones (Table S3, online supplementary data associated with the publication version). However, the absence of PFT does not necessarily signify that fluid migration has not occurred. Detection of SF_6 was not correlated with high CO_2 or CH_4 concentrations (Fig. S1, online supplementary data associated with the publication version) and because of the contamination that

occurred at the surface during the test, fluid migration cannot be assumed to be the only possible source of tracer at the surface.

2.7 CONCLUSIONS AND IMPLICATIONS FOR GCS

On the basis of 6 years monitoring of a soil gas anomaly at the Cranfield CO_2-EOR site, this investigation evaluated approaches for attributing the source of a soil gas anomaly deemed "exogenous" by process-based or other monitoring approaches. We applied techniques using stable and radioactive isotopes, light hydrocarbons, noble gases and introduced tracers to identify parameters most suitable for providing the most cost-effective and accurate results for attributing the source. We have thus expanded the recommendations for attribution first proposed by Romanak et al. (2012) and refined in Dixon and Romanak (2015) for identifying the source of "exogenous" gases which may need further assessment.

We present our experiences of geochemical analyses (Table 2.2) for an anomaly in which in-situ aerobic respiration and surface infrastructure leakage has been ruled out. We found radiocarbon analysis (on CO_2 and/or CH_4) to be one of the most useful tools. Whereas carbon-14 is a relatively expensive and complex analysis (e.g., Klusman, 2011), and is probably not appropriate as a screening technique, radiocarbon can broadly distinguish modern carbon from older sources (Turnbull et al., 2017). At Cranfield, carbon-14 values of > 100 pMC on a soil gas anomaly having CH_4 and CO_2 concentrations as high as 109.9 and 106.7 pMC respectively, seem diagnostic without extensive characterization of the carbon-14 of other potential sources (e.g., the reservoir or injected CO_2); however in general care must be taken to distinguish and rule out other potential contributions. Anomalies with radiocarbon values of <100 pMC may still

originate from microbial processes or natural seepage. Examples of this scenario are CO_2 and CH_4 produced from the decomposition of coal (Scott et al., 1994), crude oil (Revesz et al., 1995), and dissolved organic carbon in old aquifers (Aravena et al., 1995).

Comparing soil gas concentrations and stable isotopes with other buoyant fluids and signatures of known formation processes can be effective *but should be performed with great care*. Schoell (1983) demonstrated that various formation pathways can be used to distinguish gas sources; however, we have found that in the near-surface, oxidation of methane or other hydrocarbons can add significant ambiguity into the interpretation. Furthermore, evaluation of fluids throughout the sedimentary column is important for a comparison with the near-surface anomaly.

An additional method is to compare the CO_2 composition of injectate with the soil gas anomaly. In the case of the P-site anomaly, the soil gas $\delta^{13}C\text{-}CO_2$ differed significantly from the injectate CO_2 sourced from Jackson Dome. Yet, the application of $\delta^{13}C\text{-}CO_2$ as a fluid source tool may be less effective at other sites because captured CO_2 $\delta^{13}C\text{-}CO_2$ is expected to fall within the range of natural variability (-30 to -8‰) (Dixon and Romanak, 2015; Flude et al., 2016).

The Bernard plot was difficult to apply as a fluid source tool at the P-site fluid anomaly. This plot was developed for offshore environments in which biogenic methane typically originates from CO_2 reduction rather acetate fermentation commonly found in onshore settings (Bernard, 1978). The problem with using the Bernard plot at the P-site was that the range of methane carbon isotopes for acetate fermentation overlaps significantly with the range of thermogenic signatures, and fluid anomaly samples

therefore plotted in an ambiguous or thermogenic region. For this reason, the Bernard plot should be used with caution when acetate fermentation is a potential fluid source.

Noble gas analysis was not useful at Cranfield, however, the sampling design and results made it difficult to evaluate noble gas as a leakage detection tool. One of the parameters (Neon-20) for assessing the degree of air contamination was not evaluated. However, measurements of Neon-22 are consistent with an air-derived source with minimal crustal or mantle contribution (Table S2; Fig. 2.11). Other datasets in this study (carbon-14, stable isotopes) suggested acetate fermentation of carbon with an unknown origin. Noble gas data, with the exception of helium-4 values, are consistent with this interpretation.

However, noble gas analysis could have value in evaluating groundwater anomalies in the future. Noble gases from groundwater have supported upward fluid migration interpretations in a wide swath of applications (Ballentine et al., 1991; Castro et al., 1998; Gilfillan, 2011; Darrah et al., 2014). Yet, one of the limitations of groundwater noble gas analysis is that upward fluid migration does not necessarily indicate leakage. For example, several groundwater samples in this study had helium-4 concentrations that were interpreted to originate from depth, but without coexisting CO_2 or CH_4 evidence indicative of leakage. Using noble gases in groundwater is therefore possible but may be difficult because it requires diligent characterization of multiple fluids within the overburden and careful consideration of potential alteration processes.

2.8 FIGURES AND TABLES

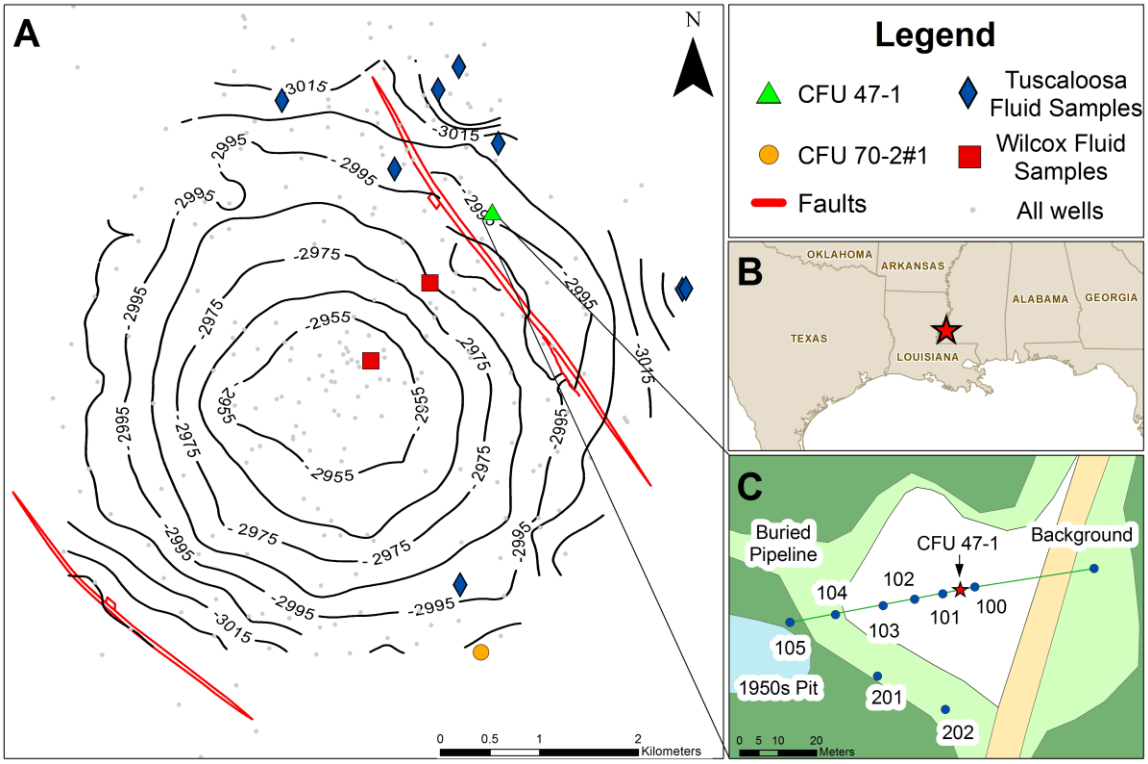

Figure 2.1. (A) Type log showing Tuscaloosa reservoir unit and Wilcox overburden package. (B) Field site schematic including well locations, Lower Tuscaloosa Formation contours, and faults. (C) Cranfield location (~20km east of Natchez, MS, USA.) C) Well 47-1, vadose zone sampling stations, 1950s pit, and buried pipeline locations.

Figure 2.2. Timeline of major well operations and fluid anomaly data collection period.

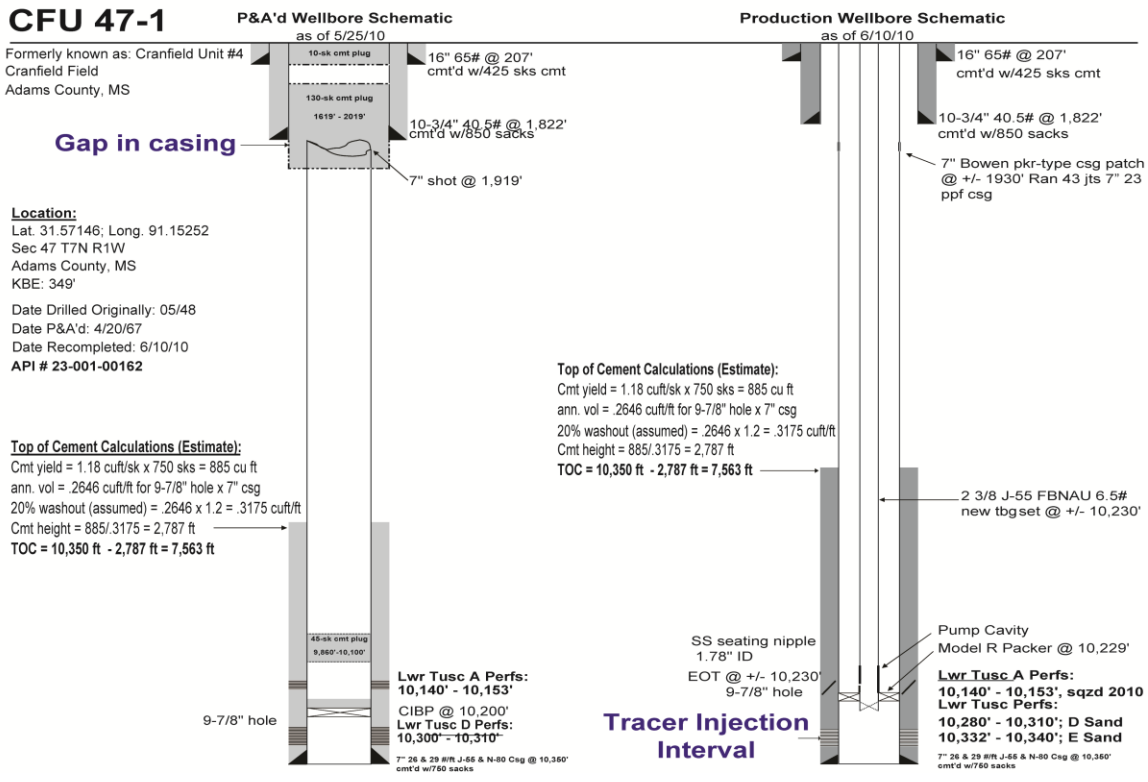

Figure 2.3. Schematics for the well nearby the soil gas anomaly (47-1) after plugged and abandonment (left) and recompletion (right).

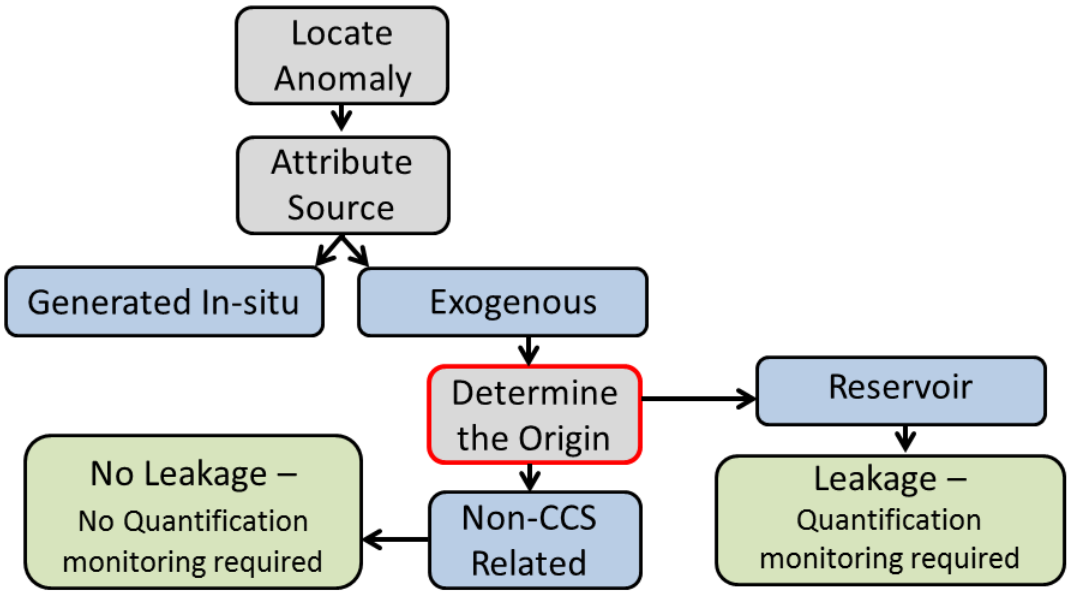

Figure 2.4. Flowchart describing the steps for anomaly source attribution in soil gas. This study addressed "determining the origin" of exogenous soil gas anomalies outlined in red. (Modified from Dixon and Romanak, 2015).

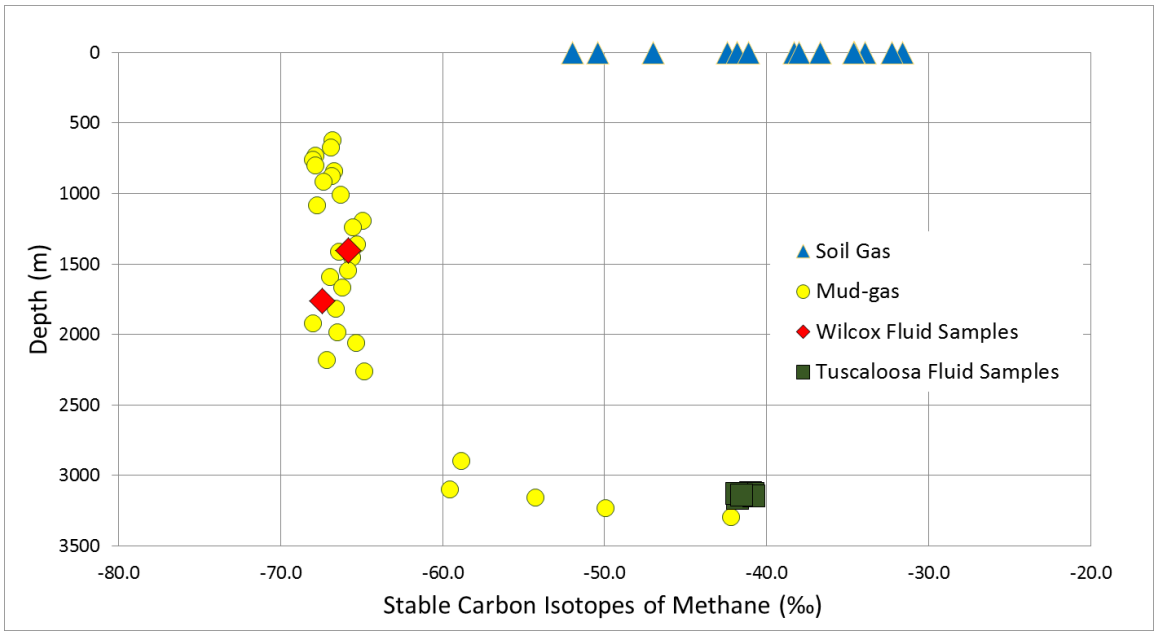

Figure 2.5. Stable carbon isotopes of methane ($\delta^{13}C\text{-}CH_4$) versus depth from liberated mud gas at well 70-2#1 (green circles). Also plotted are methane stable carbon isotopes from fluid samples collected from the Wilcox and Tuscaloosa Formations (red squares and yellow diamonds respectively). Values from the soil gas anomaly are shown as blue triangles.

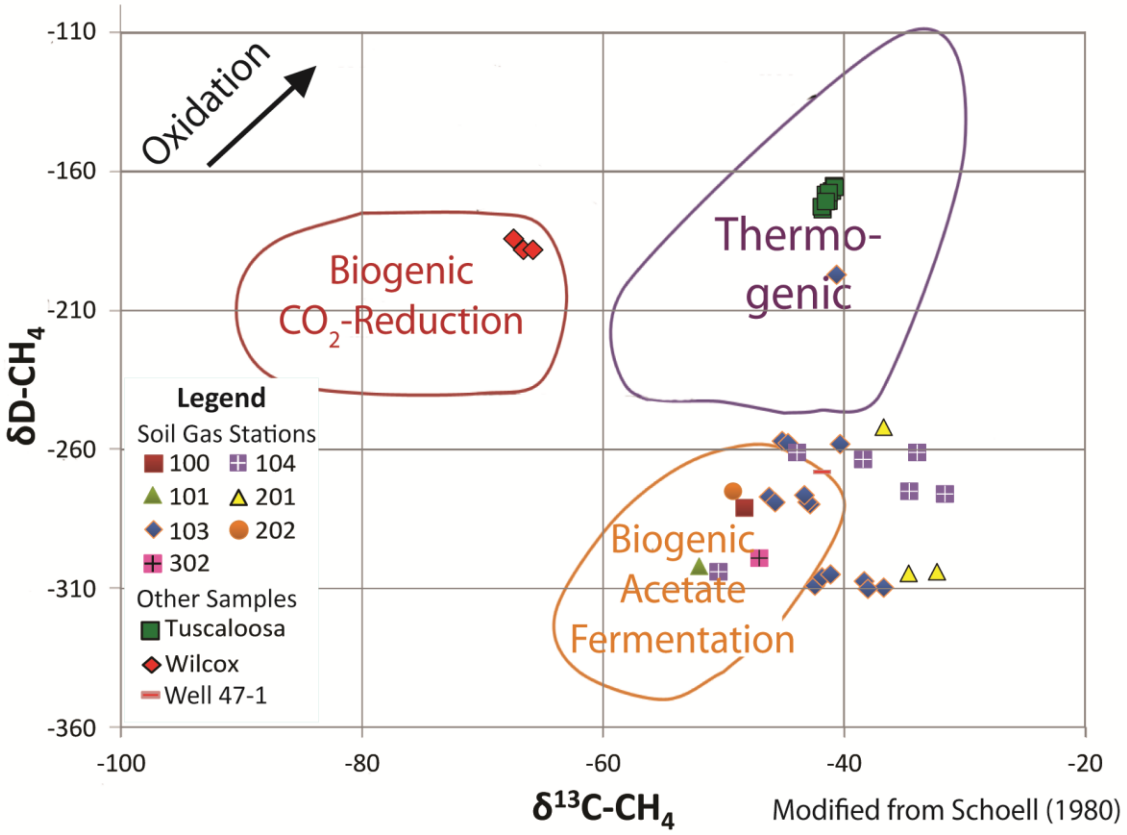

Figure 2.6. Schoell Plot modified from Schoell (1983). Stable carbon isotopes of methane ($\delta^{13}C\text{-}CH_4$) versus stable hydrogen isotopes of methane ($\delta D\text{-}CH_4$) for all samples.

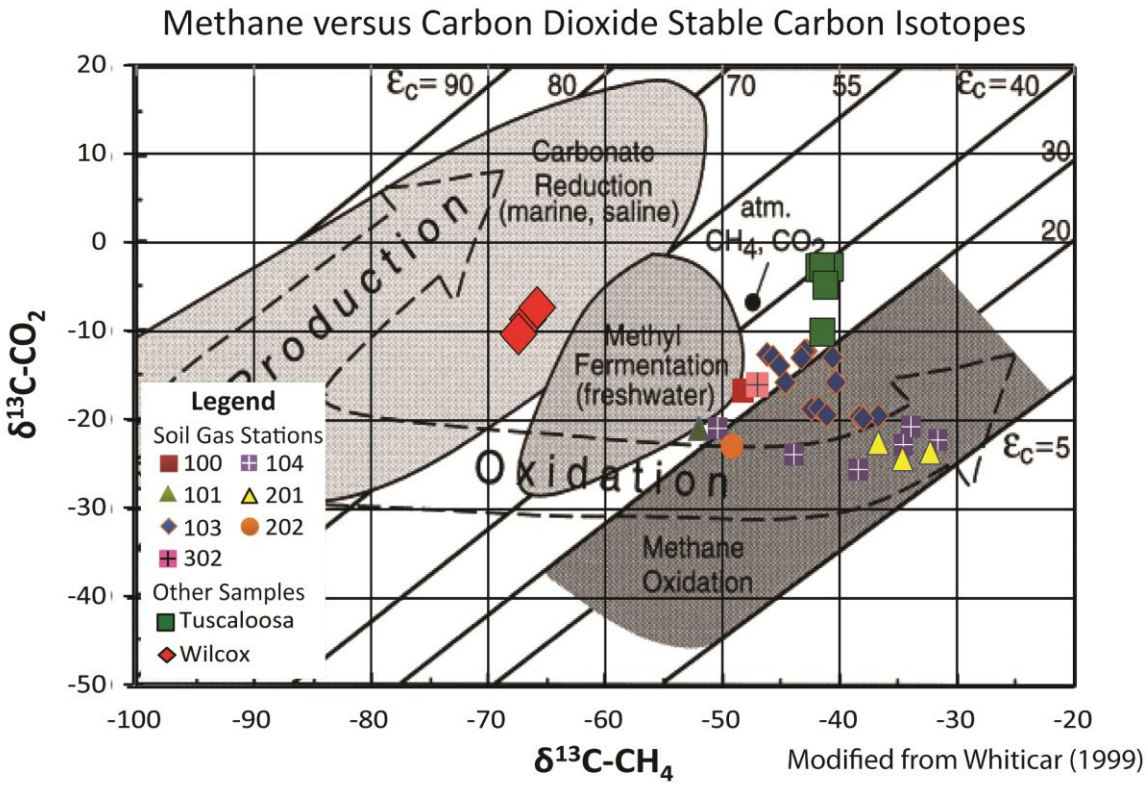

Figure 2.7. Methane stable carbon isotopes versus CO_2 stable carbon isotopes for soil gas, Tuscaloosa, and Wilcox samples. Modified from Whiticar (1999).

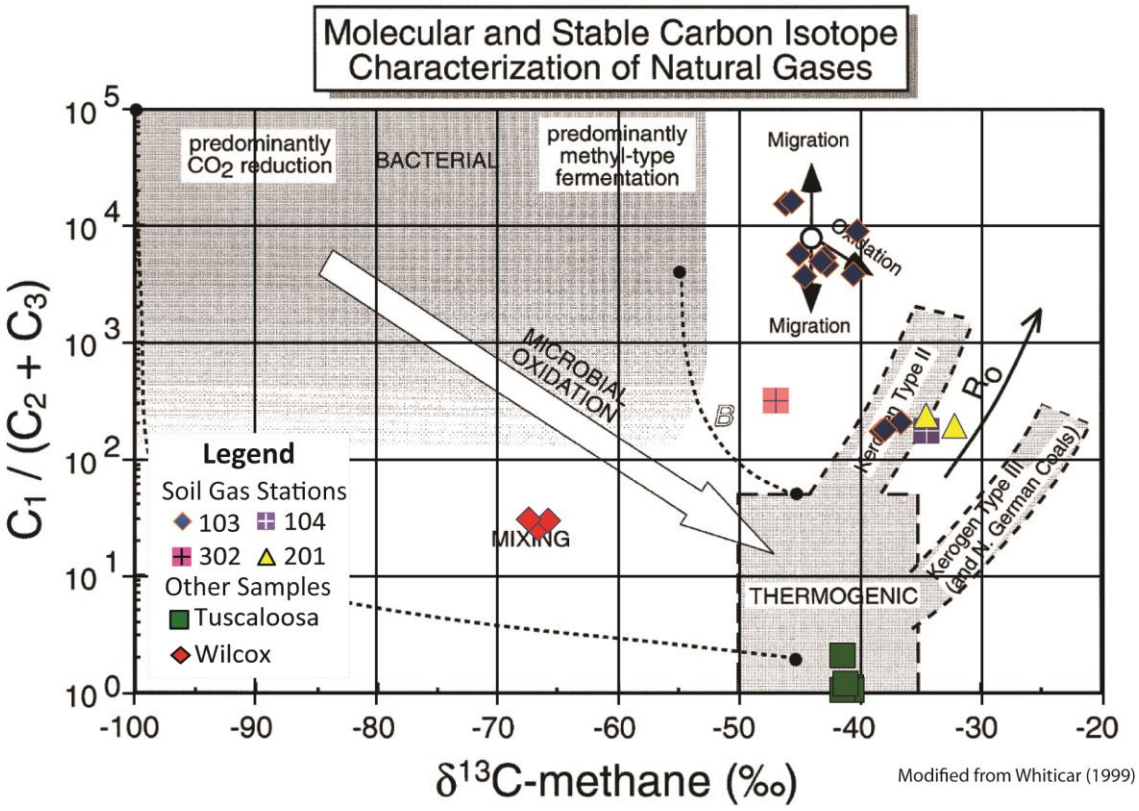

Figure 2.8. Methane stable carbon isotopes versus Bernard ratio for soil gas, Tuscaloosa, and Wilcox samples.

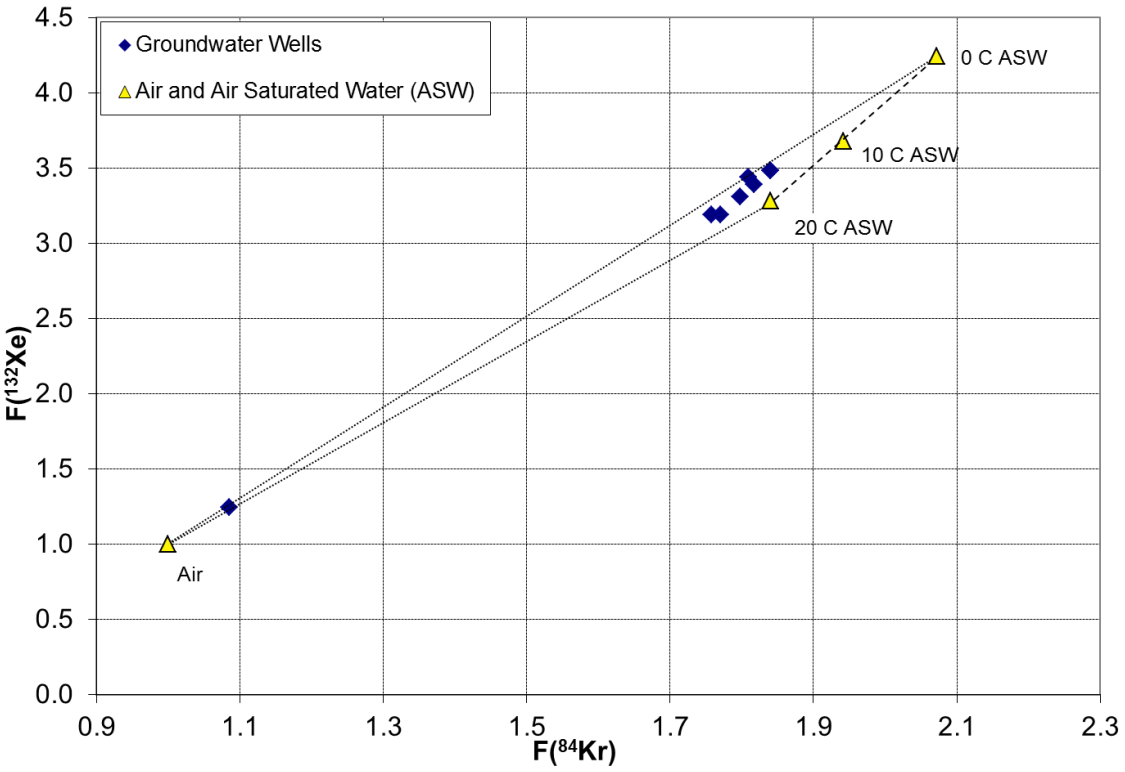

Figure 2.9. Groundwater concentrations (ppmV) of ^{84}Kr versus ^{132}Xe.

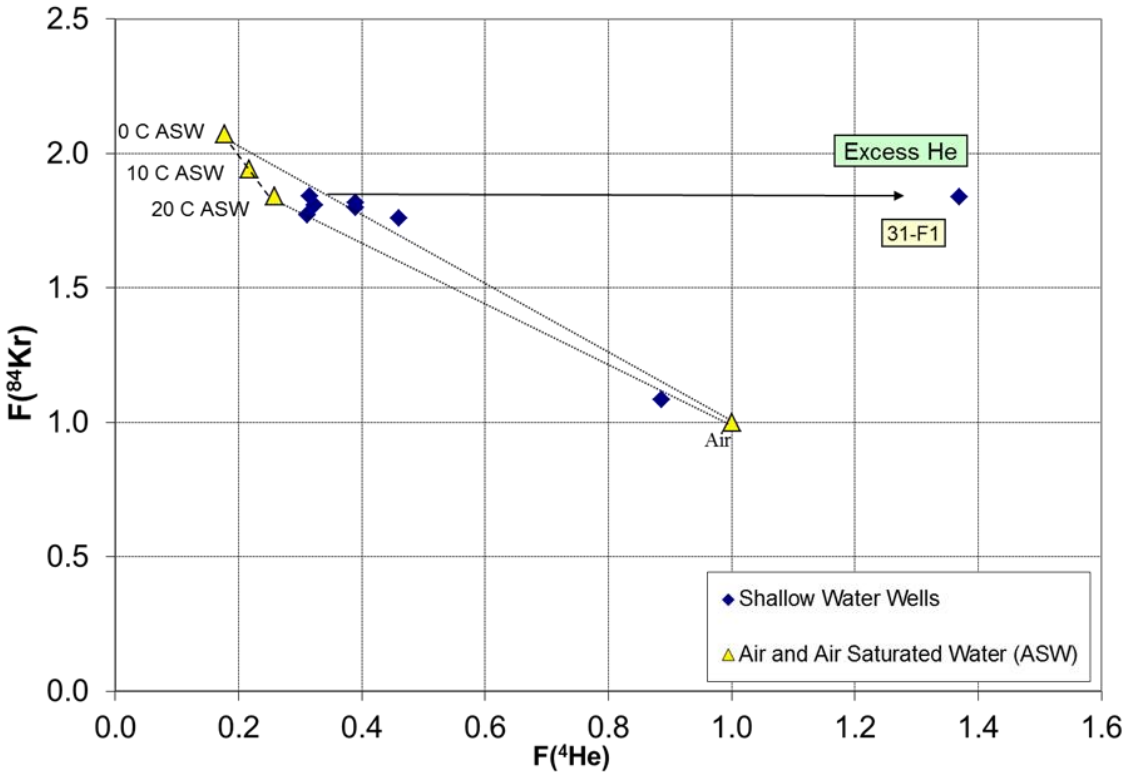

Figure 2.10. Groundwater concentrations (ppmV) of ^{22}Ne versus ^{84}Kr.

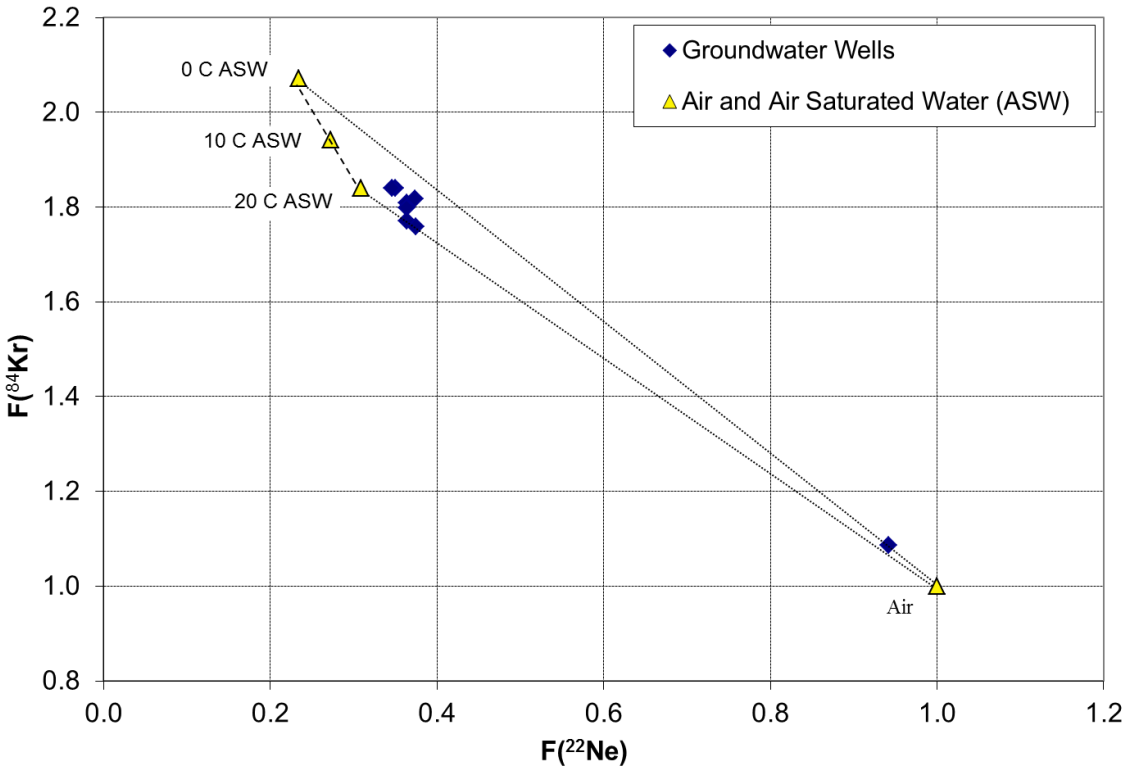

Figure 2.11. Groundwater concentrations (ppmV) of ^{4}He versus ^{84}Kr.

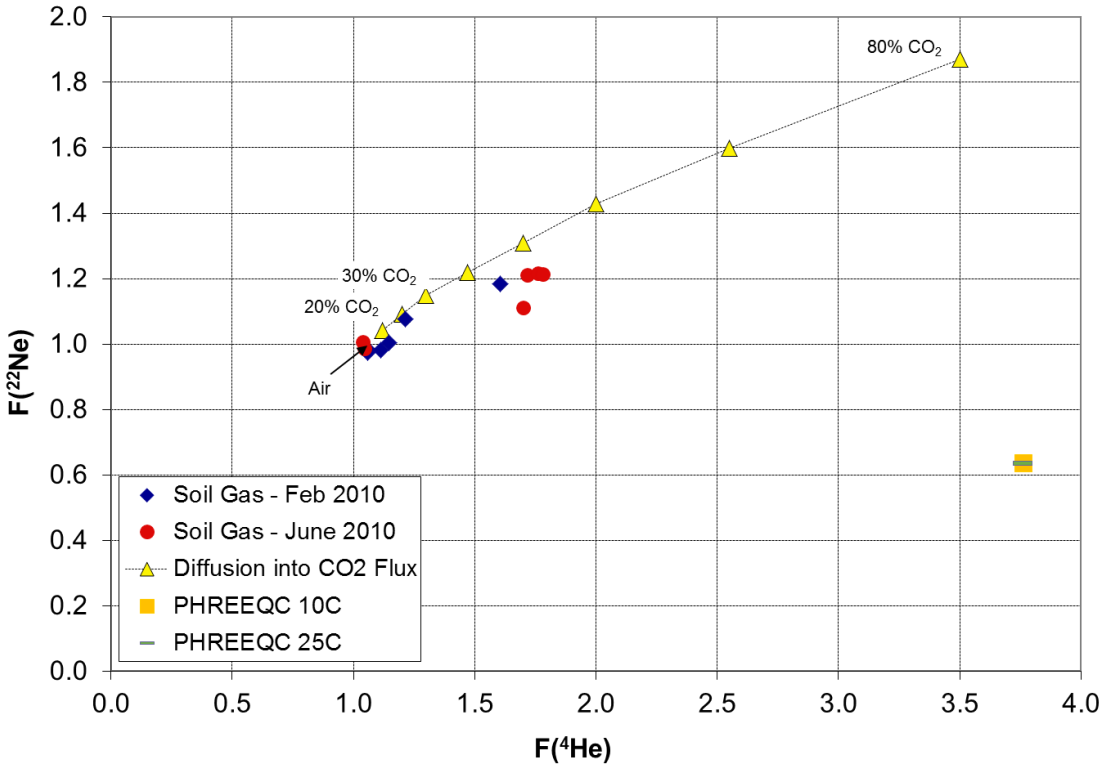

Figure 2.12. Soil gas concentrations (ppmV) of ^{4}He versus ^{22}Ne from Feb 2010 and June 2010. PHREEQC results are presented as a yellow square and blue dash for Henry coefficients at 10° and 25° C respectively.

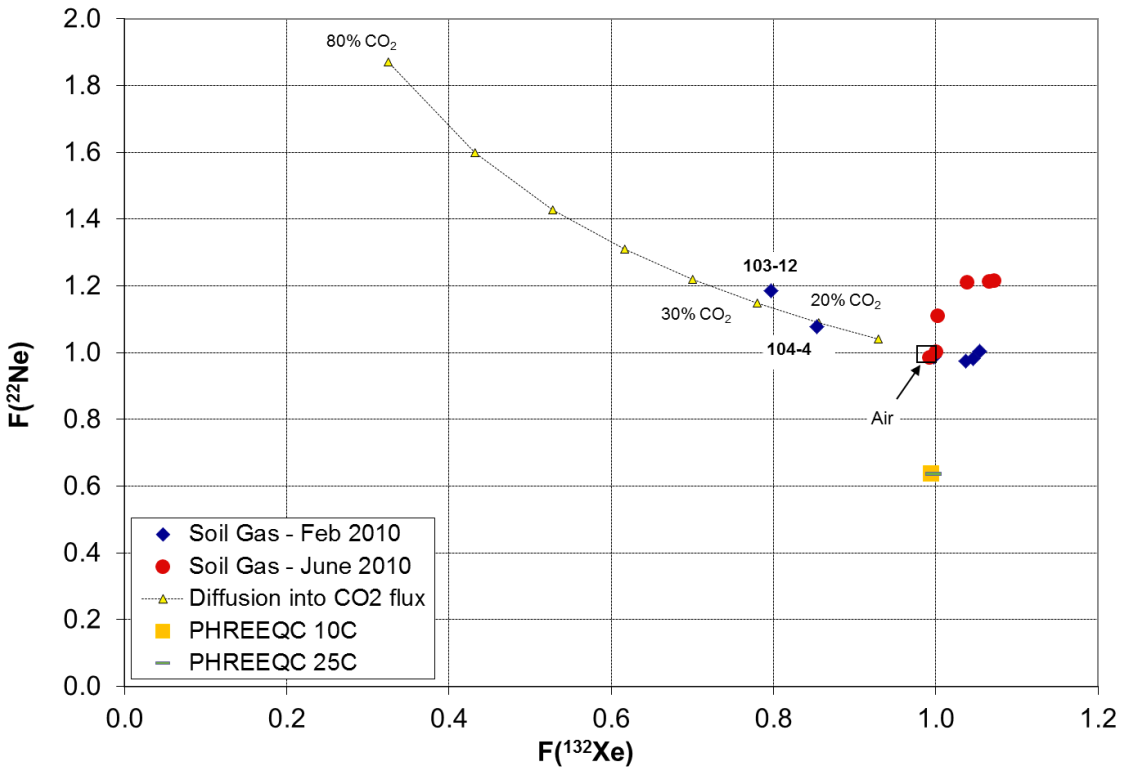

Figure 2.13. Soil gas concentrations (ppmV) of ^{132}Xe versus ^{22}Ne from Feb 2010 and June 2010. PHREEQC results are presented as a yellow square and blue dash for Henry coefficients at 10° and 25° C, respectively.

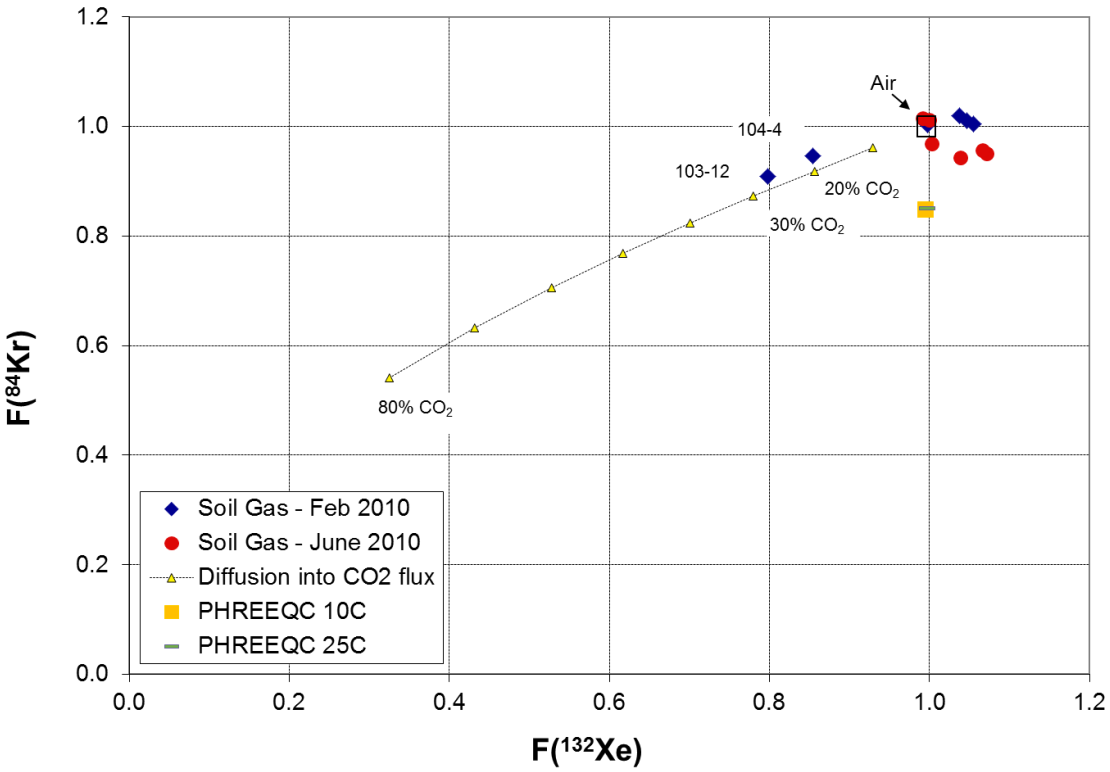

Figure 2.14. Soil gas concentrations (ppmV) of ^{4}He versus ^{22}Ne from Feb 2010 and June 2010. PHREEQC results are presented as a yellow square and blue dash for Henry coefficients at 10° and 25° C, respectively.

Table 2.1. Radiogenic carbon isotopes of CO_2 and CH_4.

Sampling Station (Date / Depth m)	**$^{14}CO_2$ (pMC)**	**$^{14}C_1$ (pMC)**
Station 103 – (Mar 2011 / 2.4m)	105.7	109.9
Station 103 – (Oct 2014 / 2.4m)	106.7	109.7
Background – (Mar 2011 / 3.6m)	102.8	
Background – (Aug 2014 / 3.6m)	104.8	
Ella G Lees #28 (Apr 2012 / 1780m)		0.2

Table 2.2. Fluid source attribution techniques, attribution outcome at Cranfield, and measurement effort required.

Fluid Source Attribution Techniques	Attribution Outcome at Cranfield	Measurement Effort Required
Radiocarbon of CO_2 and CH_4	Non-leakage	Minimal characterization, expensive analyses
Stable isotopes of CH_4	Somewhat Ambiguous	Characterization of reservoir/overburden CH_4, assessment of CH_4 oxidation
Stable carbon isotopes of CO_2	Non-leakage	Characterization of injectate CO_2, assessment of co-existing CH_4 oxidation
Bernard Plot	Ambiguous	Characterization of reservoir/overburden hydrocarbons, assessment of hydrocarbon oxidation
Noble gases	Ambiguous	Characterization of reservoir/overburden fluids, assessment of contamination by air, diffusion and interaction with groundwater

2.8 REFERENCES

Aeschbach-Hertig, W., El-Gamal, H., Wieser, M., & Palcsu, L. 2008. Modeling excess air and degassing in groundwater by equilibrium partitioning with a gas phase. *Water Resources Research*, 44(8). W08449, doi:10.1029/2007WR006454.

Aravena, R., Wassenaar, L.I., & Plummer, L.N., 1995. Estimating ^{14}C groundwater ages in a methanogenic aquifer. *Water Resources Research*, 31, 2307–2317.

Ballentine, C.J., O'nions, R.K., Oxburgh, E.R., Horvath, F., & Deak, J. 1991. Rare gas constraints on hydrocarbon accumulation, crustal degassing and groundwater flow in the Pannonian Basin. *Earth and Planetary Science Letters*, 105(1-3), 229–246.

Berg, R.L., & Cook, B.C., 1968. Petrography and origin of lower Tuscaloosa sandstones, Mallalieu field, Lincoln County, Mississippi. *Gulf Coast Association of Geological Societies Transactions* 18, 242–255.

Bernard, B. B. 1978. Light hydrocarbons in Marine Sediments. *Texas Agriculture and Mechanical University PhD Dissertation.*

Bowling, D.R., Pataki, D.E., & Randerson, J.T. 2008. Carbon isotopes in terrestrial ecosystem pools and CO_2 fluxes. *New Phytologist*, 178(1), 24–40.

Castro, M.C., Jambon, A., Marsily, G., & Schlosser, P. 1998. Noble gases as natural tracers of water circulation in the Paris Basin: 1. Measurements and discussion of their origin and mechanisms of vertical transport in the basin. *Water Resources Research*, 34(10), 2443–2466.

Darrah, T.H., Vengosh, A., Jackson, R.B., Warner, N.R., & Poreda, R.J. 2014. Noble gases identify the mechanisms of fugitive gas contamination in drinking-water wells overlying the Marcellus and Barnett Shales. *Proceedings of the National Academy of Sciences*, 111(39), 14076–14081.

Ding, X., Kennedy, B.M., Evans, W.C., & Stonestrom, D.A. 2016. Experimental studies and model analysis of noble gas fractionation in porous media. *Vadose Zone Journal*, 15(2). doi:10.2136/vzj2015.06.0095

Dixon, T., & Romanak, K.D., 2015. Improving monitoring protocols for CO_2 geological storage with technical advances in CO_2 attribution monitoring. *International Journal of Greenhouse Gas Control* 41, 29–40. https://doi.org/10.1016/j.ijggc.2015.05.029

Echols, D.J., & Malkin, D. 1948. Wilcox (Eocene) Stratigraphy, a key to production. *AAPG Bulletin* 32, 11.

Etiope, G., Feyzullayev, A., & Baciu, C.L., 2009. Terrestrial methane seeps and mud volcanoes: a global perspective of gas origin. *Marine Petroleum Geology* 26, 333–344.

Evans, W.C., Sorey, M.L., Kennedy, B.M., Stonestrom, D.A., Rogie, J.D., & Shuster, D.L. 2001. High CO_2 emissions through porous media: transport mechanisms and implications for flux measurement and fractionation. *Chemical Geology*, 177(1), 15–29.

Feitz, A., Jenkins, C., Schacht, U., McGrath, A., Berko, H., Schroder, I., Noble, R., Kuske, T., George, S., Heath, C. and Zegelin, S. 2014. An assessment of near surface CO_2 leakage detection techniques under Australian conditions. *Energy Procedia*, 63, 3891–3906.

Flude, S., Johnson, G., Gilfillan, S.M., & Haszeldine, R.S. 2016. Inherent tracers for carbon capture and storage in sedimentary formations: composition and applications. *Environmental Science & Technology*, 50(15), 7939–7955.

Gilfillan, S., Haszeldine, S., Stuart, F., Gyore, D., Kilgallon, R., & Wilkinson, M. 2014. The application of noble gases and carbon stable isotopes in tracing the fate, migration and storage of CO_2. *Energy Procedia*, 63, 4123–4133.

Györe, D., Stuart, F.M., Gilfillan, S.M., & Waldron, S., 2015. Tracing injected CO_2 in the Cranfield enhanced oil recovery field (MS, USA) using He, Ne and Ar isotopes. *International Journal of Greenhouse Gas Control*, 42, 554–561.

Hingst, M.C., 2013. Geochemical Effects of Elevated Methane and Carbon Dioxide in Near-Surface Sediments above an EOR/CCUS Site. The University of Texas at Austin, M.S. Thesis.

Hovorka, S.D., Meckel, T.A., Trevino, R.H., Lu, J., Nicot, J.P., Choi, J.W., & Freifeild, B.M. 2011. Monitoring a large volume CO_2 injection: year two results from SECARB project at Denbury's Cranfield, Mississippi, USA. *Energy Procedia*, 4, 3478–3485.

Hovorka, S.D., Meckel, & T.A., Treviño, R.H., 2013. Monitoring a large-volume injection at Cranfield, Mississippi—project design and recommendations, *International Journal of Greenhouse Gas Control* 18, 345–360.

Kennedy, B.M., Lynch, M.A., Reynolds, J.H., & Smith, S P. 1985. Intensive sampling of noble gases in fluids at Yellowstone: I. Early overview of the data; regional patterns. *Geochimica et Cosmochimica Acta*, 49(5), 1251–1261.

Kinnaman, F.S., Valentine, D.L. & Tyler, S.C., 2007. Carbon and hydrogen isotope fractionation associated with the aerobic microbial oxidation of methane, ethane, propane and butane. *Geochimica et Cosmochimica acta*, *71*(2), pp.271–283.

Klusman, R.W., 2011. Comparison of surface and near-surface geochemical methods for detection of gas microseepage from carbon dioxide sequestration. *International Journal of Greenhouse Gas Control*, 5, 1369–1392.

Lafleur, P. 2010. Geochemical Soil Gas Survey: A Site Investigation of SW30-5-13-W2M, Weyburn Field, Saskatchewan. *Petro-Find Geochem Ltd*., Saskatoon, SK.

Lafleur, P. 2011. *Geochemical Soil Gas Survey: A Site Investigation of SW30-5-13-W2M, Weyburn Field, Saskatchewan, Monitoring Project Number 2*. Petro-Find Geochem Ltd., Saskatoon, SK.

Liu, Y., & Whitman, W.B. 2008. Metabolic, phylogenetic, and ecological diversity of the methanogenic archaea. *Annals of the New York Academy of Sciences*, 1125(1), 171-189.

Lu, J., Kharaka, Y.K., Thordsen, J.J., Horita, J., Karamalidis, A., Griffith, C., & Hovorka, S.D., 2012. CO_2–rock–brine interactions in Lower Tuscaloosa Formation at Cranfield CO_2 sequestration site, Mississippi, USA. *Chemical Geology* 291, 269–277.

Mackintosh, S.J., & Ballentine, C.J. 2012. Using $^3He/^4He$ isotope ratios to identify the source of deep reservoir contributions to shallow fluids and soil gas. *Chemical Geology*, 304, 142–150.

Moreira, A.C.D.C.A., Landulfo, E., Nakaema, W.M., Marques, M.T., Medeiros, J.A., Musse, A.P.S., & Dobeck, L.M. 2014. The first Brazilian Field Lab fully dedicated to CO_2 MMV experiments: a closer look at atmospheric leakage detection. *Energy Procedia*, 63, 6215–6226.

Nicot, J.P., Oldenburg, C.M., Houseworth, J.E., & Choi, J.W., 2013. Analysis of potential leakage pathways at the Cranfield, MS, USA, CO_2 sequestration site. *International Journal of Greenhouse Gas Control*, 18, 388–400.

Ozima, M., & Podosek, F.A. 2002. *Noble Gas Geochemistry*. Cambridge, UKL Cambridge University Press. 286.

Parkhurst D. L. & Appelo C. A. J. 2013. Description of input and examples for PHREEQC version 3—a computer program for speciation, batch-reaction, one-dimensional transport, and inverse geochemical calculations: *U.S. Geological Survey Techniques and Methods*, book 6, chap. A43, 497 p.

Revesz, K., Coplen, T.B., Baedecker, M.J., Glynn, P.D., & Hult, M. 1995. Methane production and consumption monitored by stable H and C isotope ratios at a crude oil spill site, Bemidji, Minnesota. *Applied Geochemistry*, 10(5), 505–516.

Richards, L. A., Magnone, D., van Dongen, B.E., Ballentine, C.J., & Polya, D.A. 2015. Use of lithium tracers to quantify drilling fluid contamination for groundwater monitoring in Southeast Asia. *Applied Geochemistry*, 63, 190–202.

Romanak, K.D., Smyth, R.C., Yang, C., & Hovorka, S.D. 2009. Modeling shallow groundwater geochemistry and carbon isotopes: test of methodology for CO_2 storage evaluation at an EOR site, West Texas, USA, in *AGU Spring Meeting Abstracts.*

Romanak, K.D., Bennett, P.C., Yang, C., & Hovorka, S.D., 2012. Process-based approach to CO_2 leakage detection by vadose zone gas monitoring at geologic CO_2 storage sites. *Geophysical Research Letters* 39(15). DOI: 10.1029/2012GL052426

Romanak, K., Sherk, G.W., Hovorka, S., & Yang, C., 2013. Assessment of alleged CO_2 leakage at the Kerr farm using a simple process-based soil gas technique: implications for carbon capture, utilization, and storage (CCUS) monitoring. *Energy Proceedings*, 37, 4242–4248.

Romanak, K.D., Wolaver, B., Yang, C., Sherk, G.W., Dale, J., Dobeck, L.M., & Spangler, L.H. 2014. Process-based soil gas leakage assessment at the Kerr Farm: comparison of results to leakage proxies at ZERT and Mt. Etna. *International Journal of Greenhouse Gas Control*, 30, 42–57.

Schoell, M., 1983. Genetic characterization of natural gases. *AAPG Bulletin*, 67(12), 2225–2238.

Scott, A.R., Kaiser, W.R., & Ayers, W.B., Jr. 1994. Thermogenic and secondary biogenic gases, San Juan Basin, Colorado and New Mexico—implications for coalbed gas producibility. *AAPG Bulletin*, 78, 1186–1209.

Sherk, G.W., Romanak, K.D., Dale, J., Gilfillan, S.M.V., Haszeldine, R.S., Ringler, E.S., & Yang, C. 2011. The Kerr investigation: findings of the investigation into the impact of CO_2 on the Kerr property, final report. *IPAC Res. Inc., Regina, Saskatchewan, Canada*.

Smith, K.L., Steven, M.D., Jones, D.G., West, J.M., Coombs, P., Green, K.A., & Beaubien, S.E. 2013. Environmental impacts of CO_2 leakage: recent results from the ASGARD facility, UK. *Energy Procedia*, 37, 791–799.

Spangler, L.H., Dobeck, L.M., Repasky, K.S., Nehrir, A.R., Humphries, S.D., Barr, J.L., & Benson, S.M. 2010. A shallow subsurface controlled release facility in Bozeman, Montana, USA, for testing near surface CO_2 detection techniques and transport models. *Environmental Earth Sciences*, 60(2), 227–239.

Spooner, H.V., Jr. 1964. Basal Tuscaloosa sediments, east-central Louisiana. *AAPG Bulletin* 48, 1–21.

Templeton, A.S., Chu, K.H., Alvarez-Cohen, L., & Conrad, M.E. 2006. Variable carbon isotope fractionation expressed by aerobic CH_4-oxidizing bacteria. *Geochimica et Cosmochimica Acta*, 70(7), 1739–1752.

Trium, 2011. Site Assessment (SW-30-05-13-W2 M), Near Weyburn, Saskatchewan. *Trium Environmental Inc. and Chemistry Matters*, p. 50.

Turnbull, J.C., Keller, E.D., Norris, M.W., & Wilshire, R.M. 2017. Atmospheric monitoring of carbon capture and storage leakage using radiocarbon. *International Journal of Greenhouse Gas Control* 56, 93–101.

Warwick, P.D., Breland, F.C., & Hackley, P.C. 2008. Biogenic origin of coalbed gas in the northern Gulf of Mexico Coastal Plain, USA. *International Journal of Coal Geology* 76.1, 119–137.

Weaver, L.K. 1966. Cranfield Field, Cranfield Unit, Basal Tuscaloosa Reservoir, Adams and Franklin Counties, Mississippi. *Bureau of Mines.*

Wells, A.W., Diehl, J.R., Strazisar, B.R., Wilson, T.H., & Stanko, D.C., 2013. Atmospheric and soil-gas monitoring for surface leakage at the San Juan Basin CO_2 pilot test site at Pump Canyon New Mexico, using perfluorocarbon tracers, CO_2 soil-gas flux and soil-gas hydrocarbons. *International Journal of Greenhouse Gas Control* 14, 227–238.

Whiticar, M. J. 1999. Carbon and hydrogen isotope systematics of bacterial formation and oxidation of methane. *Chemical Geology*, *161*(1), 291–314.

Wimmer, B.T., Krapac, I.G., Locke, R., & Iranmanesh, A., 2011. Applying monitoring, verification, and accounting techniques to a real-world, enhanced oil recovery operational CO_2 leak. *Energy Proceedings* 4, 3330–3337.

Wolaver, B.D., Hovorka, S.D., & Smyth, R.C. 2013. Greensites and brownsites: implications for CO_2 sequestration characterization, risk assessment, and monitoring. *International Journal of Greenhouse Gas Control*, 19, 49–62.

Yang, C., Romanak, K., Hovorka, S.D., Holt, R.M., Lindner, J., & Trevino, R. 2013. Near-surface monitoring of large-volume CO_2 injection at Cranfield: early field test of SECARB phase III. *SPE Journal*, 18(03), 486–494.

Yang, C., Hovorka, S.D., Treviño, R.H., & Delgado-Alonso, J. 2015. Integrated framework for assessing impacts of CO_2 leakage on groundwater quality and monitoring-network efficiency: case study at a CO_2 enhanced oil recovery site. *Environmental Science & Technology*, 49(14), 8887–8898.

Chapter 3: Assessment of Shallow Subsea Hydrocarbons as a Proxy for Leakage at Offshore Geologic CO_2 Storage Sites

Abstract

This study is part of a multi-year effort to characterize offshore GCS potential along the Texas Gulf Coast. Previous efforts estimated CO_2 storage capacity and identified prospective storage sites. To further characterize the suitability of specific sites, a novel high-resolution 3D seismic dataset (P-cable™) was acquired. A seismically discontinuous zone was interpreted as a vertical chimney structure with possible shallow (<100 m below seafloor) gas pockets presumably sourced from a deeper thermogenic source. In an attempt to link focused gas flow from the shallow gas pockets up to the seafloor, this study investigated geochemical compositions from gases extracted from 23 piston core samples recovered between 2.56 and 3.50 meters subseafloor. We report concentrations for light hydrocarbons and stable carbon isotopes of methane which did not indicate hydrocarbon migration upwards from the seismic anomalies. Geochemical signatures were consistent with typical background values observed within the first few meters of subsea sediment that is heavily influenced by microbial activity. These results, considered along with the seismic anomalies, are consistent with episodic migration events over >1,000 a timescales.

3.1 INTRODUCTION

GCS is an important technology in stabilizing global emissions while still acknowledging the role of fossil fuels in meeting global energy demand. To date, most GCS pilot projects and commercial applications have stored CO_2 in onshore geologic formations. Yet, offshore GCS is an attractive option because of proximity to coastal emission sources, existing pipeline infrastructure, large-scale CO_2 storage capacity, and reduced health and safety risks. Previous large-scale offshore GCS projects (Sleipner and Snohvit in Norway, and Santos Basin in Brazil) have demonstrated the technical feasibility of CO_2 injection. The viability of offshore CO_2 storage was supported at Sleipner and Snohvit by decadal-period monitoring, which did not observe CO_2 migration above the sealing formations (Eiken et al., 2011).

While upward fluid migration above the primary sealing intervals is an unlikely possibility, risk assessment protocols during GCS site selection will likely require evaluations of potential leakage scenarios. Gas pipes or chimneys, geological features whereby light hydrocarbons (methane, ethane, and propane) have naturally migrated through offshore sediments, have been targeted as an important area of research, because of their potential to act as conduits for CO_2 migration. These features are abundant across the Gulf of Mexico (Roberts and Carney, 1997) and the North Sea (Loseth et al., 2003), and were documented within 10 km of Sleipner (Nicoll, 2012) and Snohvit (Tasianas et al., 2016). Gas migration mechanisms have been classified as episodic or continuous mobilization through either fractures in consolidated sediments (Roberts and Nunn, 1995), or soft sediment (Cartwright, 2007). Numerical simulations indicated that up to $2.5e10^9$ m^3/km^2 of gas may migrate upward through these features during episodic events

(Roberts and Carney, 1997). In a GCS case, this could accelerate potential upward migration of CO_2 and release into ocean waters.

Geochemical characterization of gas migrating through chimneys or pipes is still poorly developed. Episodic seepage may not be identifiable with geochemical evidence during the dormant periods (up to 1000s of years) between events (Leifer and Boles, 2005). Gay et al. (2006a;b) documented continuous seepage of light hydrocarbons above a gas chimney in offshore Congo. They found that the geochemical compositions were a mixture of thermogenic and biogenic signatures. In the Gulf of Mexico, offshore seepages also have been studied (Bernard et al., 1976; Hood et al., 2009) but light hydrocarbon migration from a gas chimney, observed on high-resolution seismic imaging, has not been investigated to our knowledge.

To assess the potential for gas chimneys to transmit stored CO_2 from depth, we used geochemical assessment above several anomalies measured using high-resolution 3D seismic images acquired in the Gulf of Mexico (GoM) (Meckel and Mulcahy, 2016). The goals of this study were to learn if these seismic anomalies represented possible seepage pathways from depth to surface and to assess the potential for hydrocarbon geochemical analysis to be used for future marine environmental monitoring. The approach included (1) measuring gases in the near-surface sediments above and near the structures, and (2) attributing their origin to either gas migration or near-surface processes. In so doing, we also aim to provide insights into using these techniques for signal attribution (e.g., Romanak et al., 2012, 2014; Anderson et al., 2017) and to assess if gas migration rates and frequency of episodic events associated with gas chimneys are a significant risk for CO_2 storage. The value of this dataset would be that light

hydrocarbons could be compared with Gulf of Mexico reservoir compositions to interpret alteration during migration.

3.2 BACKGROUND

Light hydrocarbons originate from two types of processes: thermal degradation of organic matter (thermogenic) or microbially-mediated anaerobic reactions (biogenic). Thermogenic light hydrocarbons are formed by heating oil or kerogen to produce methane, ethane, propane, butane, and pentane (C1 – C5) (Allen and Allen, 2013). Within the category of biogenic hydrocarbons, the two primary methanogenic reactions are methyl group fermentation and CO_2 reduction.

These formation pathways (thermogenic, biogenic – methyl fermentation, and biogenic – CO_2 reduction) are commonly interpreted from two geochemical plots: the Schoell plot and the Bernard plot. The Schoell plot uses stable carbon and hydrogen isotopes of methane to distinguish between all three formation pathways (Schoell, 1983). However, microbes can consume light hydrocarbons after they are formed, which leaves the remaining stable isotopes heavier. Light hydrocarbons altered by microbes are shifted upward on both axes on the Schoell plot.

The Bernard plot compares stable carbon isotopes of methane to the "Bernard Ratio" (concentrations of CH_4 / (C_2H_6 + C_3H_8)) (Bernard, 1978). The Bernard plot assumes that biogenic methane originates from CO_2 reduction, which is typical in offshore environments. Thermogenic gas is classified as having low Bernard ratios (<100) and heavy stable carbon isotopes (>-55 ‰). Biogenic gas is defined by high Bernard ratios (>1,000) and light stable carbon isotopes (<-60 ‰). After hydrocarbon generation, microbial consumption can occur and increase the Bernard ratio by

preferentially oxidizing ethane and propane to methane (Kinnaman et al., 2007). Altered compositions are shifted toward higher values on both axes on the Bernard plot.

Because gas compositions plot as 'thermogenic' on the Bernard and Schoell plots and because high hydrocarbon concentrations (> 100,000 ppm) are often observed near structural features or disturbed sediment such as pockmarks, slumps, or scars (Abrams, 2005), active macroseeps are relatively easy to identify geochemically. Yet, identifying passive microseeps (defined as < 100ppm) from background remains challenging. Methane through pentane (C1-C5) in concentrations less than 100 ppm are ubiquitous within the first two meters of marine sediment, due to biological processes, as observed from regional surveys in the North Sea (Faber and Stahl, 1984), Alaska (Abrams, 1992), and Gulf of Mexico (Bernard, 1978). These studies show that shallow sediment hydrocarbons can exist in three separate phases: free gas in pore space, dissolved gas in formation water, or gas adsorbed to sediment interfaces.

Field sampling for sediment collection and seepage identification usually targets the first several meters of sediment on the assumption that biological transformation is minimal in this zone. Yet, previous coring surveys that measured vertical hydrocarbon profiles documented less alteration and higher hydrocarbon concentrations below the zone of biological activity (1.5 to 5m) (Abrams, 1993; Hood et al., 2002; Faber et al., 1990) (Fig. 3.1). While migrating hydrocarbons are not generally oxidized in this lower zone, bacterial methanogenesis is a favorable redox process and can add biogenic methane to the overall composition (Whiticar, 1999).

Identifying light hydrocarbon formation processes and alteration is apparent in vertical hydrocarbon and isotopic composition profiles. An example profile from Faber et

al. (1990) shows low free gas concentrations of methane and ethane from a Gulf of Mexico shelf core at subseafloor depths <2.5 meters, presumably from microbial consumption (Fig. 3.1). However, higher concentrations of sorbed gas with stable carbon isotopes (-35 to -40 ‰) and Bernard ratios (<25) are indicative of a thermogenic source. A Schoell plot identified the low concentrations of hydrocarbons in the first few meters as thermogenic rather than biogenic. These hydrocarbons may have migrated from depth to seabed from previously active seepage and remained sorbed to near-seafloor sediments.

However, sorbed gas compositions do not necessarily identify an anomaly. Bernard (1978) compiled a background dataset showing that Gulf of Mexico Bernard ratios overlapped with thermogenic values (Fig. 3.2). The implication of results from Faber et al. (1990) is that, in the upper zone, data aligning with thermogenic signatures can still be characterized as background rather than active seepage.

Yet below this zone, Faber et al.'s hydrocarbon compositions were shown to align with biogenic values. A separate indicator of background or seepage is the ratio of ethane to ethene, which is commonly ~0.5 in background samples but orders of magnitude higher in seepage because ethene is a by-product of microbial reactions but not of thermogenic cracking (Bernard, 1978).

The key conclusion of prior work is that thermogenic signatures within the first few meters below the seafloor do not necessarily signify active hydrocarbon migration from depth. Thus, the successful use of hydrocarbons as proxies will require the ability to discern if and to what degree, other processes have altered or formed the geochemical signal that is observed.

3.3 FIELD SITE AND GEOLOGY

The field site for this study is located approximately five kilometers offshore of San Luis Pass, TX, USA. (Fig. 3.3). The Miocene stratigraphy occurs at depths of approximately 1.5 to 2.5 km subseafloor, and is generally characterized by large-scale progradational clastic wedges separated by transgressive shales (Galloway et al., 2011). Sediment loading and salt evacuation caused strike-parallel growth faults, regionally known as the Clement-Tomas fault system. Pliocene- and Pleistocene-aged stratigraphic features are controlled by the paleo-Brazos River system, sea level, and climate factors (Abdullah et al., 2004). Within the late Quaternary and Holocene (the last 150,000 years), a series of five eustatically-driven cycles deposited coarse-grained deltaic lobes overlaid by transgressive muds (Abdullah et al., 2004). At the San Luis Pass field site, Meckel and Mulcahy (2016) interpreted two incised valleys that cut down during lowstands and subsequently filled during transgressions.

A 2005 conventional 3D seismic survey over the study area identified a deep (>1,500 m subseafloor) salt dome and associated faulted anticlinal structure through the Miocene reservoir and seal intervals. While one interpretation is that this specific structure was never charged with hydrocarbons, despite productive gas discoveries laterally in the region, an alternative interpretation is that poor fault seal and/or top seal quality may have allowed vertical gas migration to shallower intervals. The conventional seismic survey design and resolution (peak frequency = ~25 Hz) could not resolve shallower geologic and structural features in the uppermost 330 m that may aid in evaluating the two contrasting interpretations.

In October 2013, high-resolution 3D (HR3D) seismic data were acquired using a P-Cable™ system (*Geometrics, Inc*.) offshore San Luis Pass (Fig. 3.3) (Meckel and Mulcahy, 2016). In the southwest portion of the survey, sixteen negative amplitude anomalies (~40 - 150 milliseconds (msec) two-way travel time (TWTT), 30 – 1000 m max length, <3 m thick) were interpreted as shallow gas accumulations. The shallowest anomaly at 40 msec corresponds to a subseafloor depth of approximately 11.5 m (Mulcahy, 2015). Mulcahy (2015) and Meckel and Mulcahy (2016) provided a thorough description of the stratigraphic setting, seals, and structural features associated with these shallow seismic anomalies.

If these seismic anomalies are gas pockets that are migrating to the seafloor, seafloor features have not been observed at this site. Pockmarks, slumps, craters, or mud volcanos on the order of meters to 10s of meters are associated with seepage termination points (Gay et al., 2006; Eichhubl et al., 2000). Yet, Osmond (2016) conducted a CHIRP sub-bottom survey at this site (frequency 700 – 12,000 Hz, up to 73 ms TWTT) that documented nearly continuous seismic reflectors within the first 2 ms. Consequently, piston core locations were chosen above and adjacent to seismic anomaly locations.

3.4 METHODS

In February, 2015, sea-floor sediment samples were collected along transects above the shallow seismic anomalies. Dissolved gases in these sediment samples were analyzed to determine the degree to which these seismic anomalies represent fluids that migrated from depth. A 1,000-kilogram piston core system (TDI-Brooks Incorporated, College Station, TX) was used to retrieve 23 sediment and fluid samples, including a "background" sample located over 1 km away from the area of seismic anomalies (Fig.

3.3). For these samples, intended core locations and actual core locations varied by an average of 3.7 m due primarily to sea conditions. The maximum core length retrieved in this survey was 2.75 m; core system hit refusal at a hard, light brown clay layer. This is far shallower than the shallowest of the geophysical anomalies, at approximately 11.5 m subseafloor. The coring equipment by this vendor has penetrated up to 12 m at another site (Bernard et al., 2013).

Immediately after the cores were retrieved, sediment samples were prepared for hydrocarbon analysis. The bottommost 20 cm of core sediment were cut and placed into 0.5 L metal cans containing 160 mL of sterile, hydrocarbon-free seawater. The headspace was flushed with nitrogen, and then the cans were frozen onboard the ship. After sample transport to a laboratory at *TDI-Brooks Incorporated* (College Station, TX, USA), the deepest samples from each core were warmed to 40^0 C for four hours and vigorously agitated. Headspace gas was analyzed for light hydrocarbon concentrations and methane stable carbon isotopes via a gas chromatograph (Varian, model 3400) coupled to a mass spectrometer (Finnigan, model MAT 252, GC-C-IRMS). Stable carbon isotopes of methane ($\delta^{13}C\text{-}CH_4$) were only measured for samples with methane concentrations of at least 8 ppm. Carbon isotopic ratios are reported in the conventional delta notation and measured relative to Vienna Pee Dee Belemnite (Coplen, 1995).

$$\delta^{13}C_{PDB}\ (‰) = [(R_{sample}/R_{std}) - 1] \times 1000$$

The CO_2 concentrations are not reported herein due to analytical uncertainty. The sampling and analysis methods of *TDI-Brooks Inc.* are designed solely for hydrocarbon analysis and the addition of seawater to the sample introduced enough uncertainty to

disqualify CO_2 measurements. In retrospect we would have collected water samples directly from the core slurry for subsequent dissolved inorganic carbon (DIC) analysis.

3.5 RESULTS AND DISCUSSION

Measured gas concentrations and stable isotopes for 23 samples are shown in Table 3.1. Low but detectable amounts of light hydrocarbons were observed in concentrations up to 18.70 ppmV. Methane was the most abundant light hydrocarbon component, but heavier alkanes and alkenes were also observed. The concentrations of pentane and heavier components were below the detection limits of the GC-C-IRMS for all samples and are not reported herein. For samples with at least 8 ppm of methane (n=5), the stable carbon isotopes of methane ($\delta^{13}C\text{-}CH_4$) ranged from -57.84 to -40.11 (‰). Stable carbon isotope analysis was not possible on samples with methane less than 8 ppm. The relatively low methane concentrations precluded analysis of stable hydrogen isotopes. The ratios of methane to ethane and propane ("Bernard ratio": C1/(C2+C3)) ranged from 7.13 to 122.00. Methane stable isotopes plotted against the Bernard ratio (Bernard plot) generally aligned with empirical values of thermogenic sources (Fig. 3.2).

Figure 3.4 shows the geochemical analyses overlain on a map of the seismic anomalies. Some of these samples lie directly above seismic anomalies while others did not. Light hydrocarbon concentrations were slightly higher in the southeastern and eastern areas compared to other parts of the survey. The average methane concentrations (6.23 ppm) and Bernard ratio (32.60) were generally similar to the values taken 1.04 km from the nearest anomaly (4.63 ppm and 23.15, respectively), although this single sample is insufficient to establish baseline compositions. Methane stable isotope values did not form consistent spatial trends in relation to underlying seismic anomalies (Fig. 3.5). The

lack of a strong spatial correlation between hydrocarbon compositions and underlying seismic anomalies supports the view that hydrocarbons are not indicators of deep gas migration at this site, although lateral migration is possible (Figs. 3.4 and 3.5).

Figure 3.6 shows data from this study plotted on the vertical profile of Faber et al. (1990) measured from a separate site within the Gulf of Mexico. Whereas Faber's data represent one core, and our data represent several locations, the comparison is still useful for illustrating the potential effects of sampling depth on our results. The results from this study are similar to those reported by Faber et al. (1990). In doing so, we show the correlation of our geochemical data within the zones of biological activity. As with Faber et al. (1990), Bernard ratios and methane stable isotopes from this study were consistent with thermogenic signatures (Fig. 3.6 C and D).

It is unclear if the hydrocarbons in the first few meters relate to remnant hydrocarbon migration or altered microbial fluids. These sources could be resolved on the Schoell plot, but low methane concentrations precluded analyzing stable hydrogen isotopes. Similarly, the geochemical results from this study were not distinguishable from extensive background values measured along the Texas shelf reported by Bernard (1978) and shown in Table 3.2. Methane through propane concentrations measured in this study were within the range of Bernard's baseline values (Fig. 3.2), and the Bernard ratios measured in this study are also similar to typical background values. Additionally, the ratio of ethane to ethene (ranging from 0.23 to 0.73, average of 0.46) (Table 3.1) were similar to background signatures of 0.50 and therefore did not strongly indicate active ethane input from depth.

The conventional piston cores could not penetrate a hard clay layer at 2.75 m. Seepage of methane from depth to below the shallow clay layer cannot be ruled out. These data illustrate a potential challenge in interpreting light hydrocarbon sources. An erroneous conclusion in the absence of extensive background data would be that hydrocarbons from depth are actively migrating to the seafloor because, as previously shown, the Bernard ratios and stable isotopes align with thermogenic signatures associated with deep hydrocarbon generation (Fig. 3.2). The dilemma for the geochemical interpreter is to resolve compositions that simultaneously appear as thermogenic and as typical background when using hydrocarbons as proxies for leakage.

If methane concentrations at this site had been adequate for stable hydrogen isotope analysis, a Schoell plot would have yielded additional information on the origin of the light hydrocarbons. However, even at background concentrations, hydrogen isotopes may have indicated migration from depth, as interpreted by Faber et al. (1990) or microbial methane oxidation that would also shift Bernard ratios and stable carbon isotopes from thermogenic to biogenic signatures. Regardless, neither of these interpretations were strong indicators of continuous active seepage to the seafloor in our study.

3.6 CONCLUSIONS

In this study, we investigated light hydrocarbon compositions above a gas chimney to evaluate potential alteration during migration. The lack of hydrocarbons that originated from depth did not establish a relationship with underlying seismic anomalies, because of the presence of a dense, clay-rich unit that prevented or slowed the upward transport of light hydrocarbons being investigated. Yet, this negative finding has valuable

implications for conceptual models of gas flow in chimneys. The hard clay layer that limited coring penetration may serve as a gas seal. This interpretation is consistent with deeper stratigraphic features, including channel fill and erosional features observed on seismic imaging, preventing upward gas migration at this site (Meckel and Mulcahy, 2016).

The continuity of this clay-rich "reflector" from a CHIRP survey at this site, and a lack of pockmarks and slumps (Osmond, 2016) that would disrupt the unit, indicates that the first several meters of subseafloor sediments were not disturbed by any gas migration event. If gas migration to the seafloor has not occurred since charging the shallowest seismic anomaly (at 11.5 m subseafloor) in the Pleistocene-aged Beaumont formation, the frequency of episodic events would be >10,000 years. In the case that events are more frequent, the lack of observed seepage may be explained by gas dispersal and/or attenuation within pore space of permeable layers. As an example, during a controlled release experiment of CO_2 at 11 m subsea in the North Sea the gas formed a small chimney feature, yet 85% of CO_2 remained trapped in the subsurface (Blackford et al., 2014). Consequently, the lack of light hydrocarbons originating from depth in this study is consistent with infrequent migration events (>10,000 years) and/or multiple trapping mechanisms (stratigraphic and residual), thereby indicating higher potential of successful CO_2 storage at GCS sites with gas chimneys.

3.7 FIGURES AND TABLES

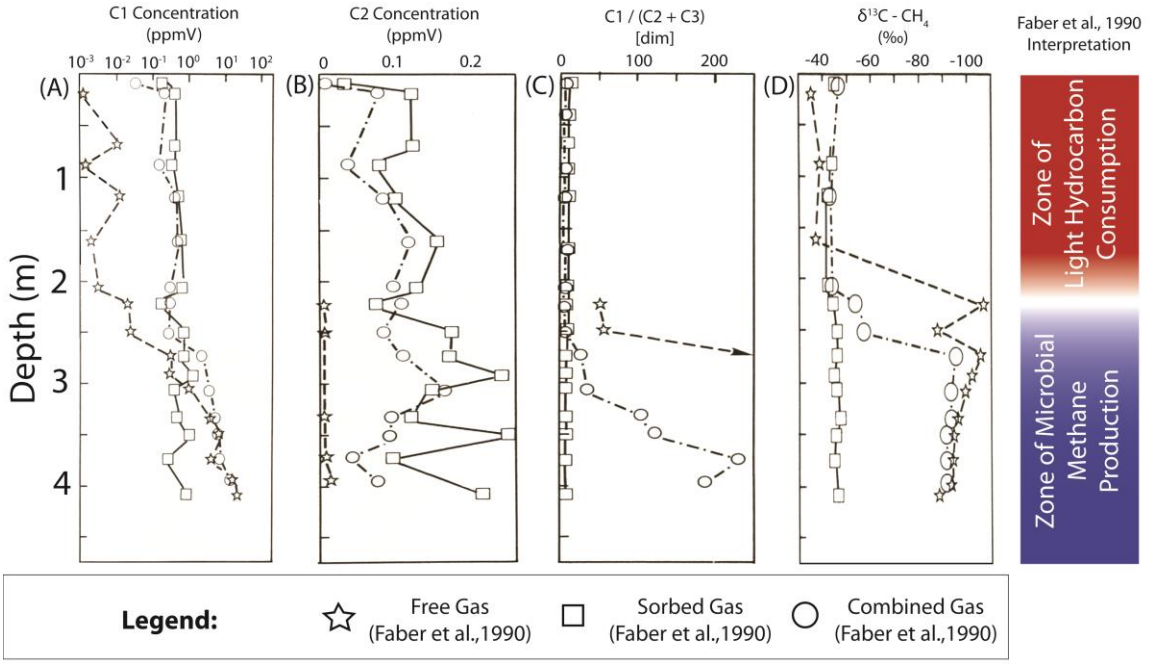

Figure 3.1. Vertical profiles of (A) methane, (B) ethane, (C) Bernard ratio, (D) stable carbon isotopes from Faber et al. (1990). In the top zone, microbes oxidize hydrocarbon to dissolved inorganic carbon (DIC). In the lower zone, microbes produce methane via CO_2 reduction (modified from Faber et al., 1990).

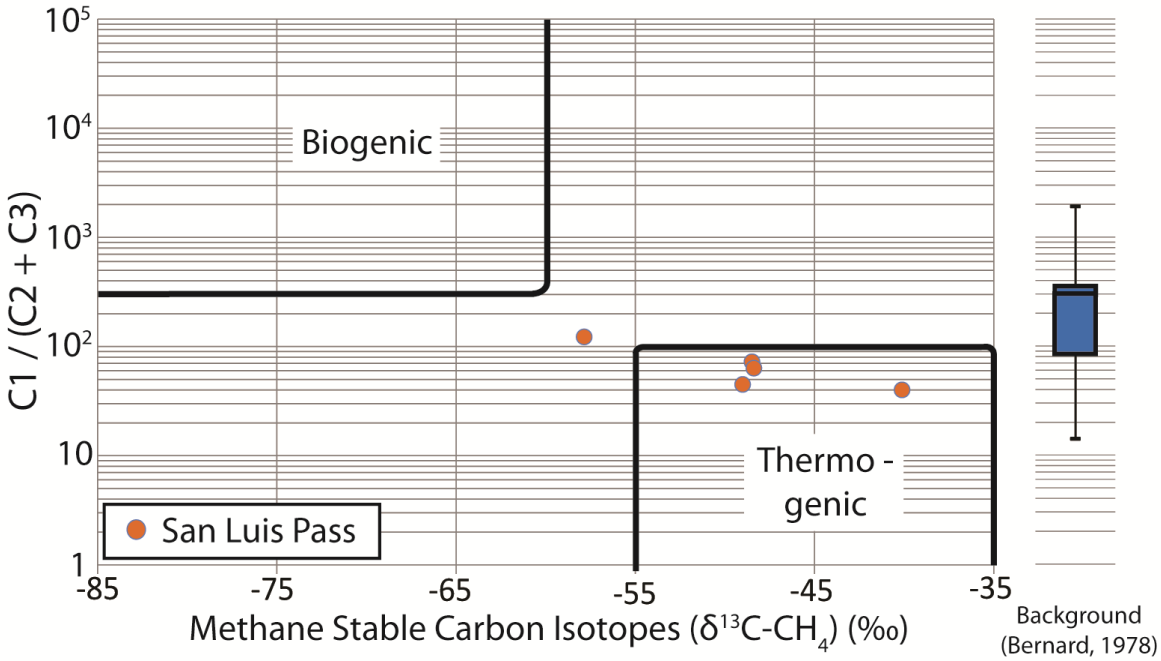

Figure 3.2. Bernard plot with methane stable carbon isotopes versus Bernard ratio (orange circles). The stable carbon isotopes of methane collected from sediment cores are shown as orange circles. A box and whiskers plot of background Bernard ratios is shown in blue. The overlapping Bernard ratios among background and thermogenic values indicate that active seepage is a unique interpretation from thermogenic methane.

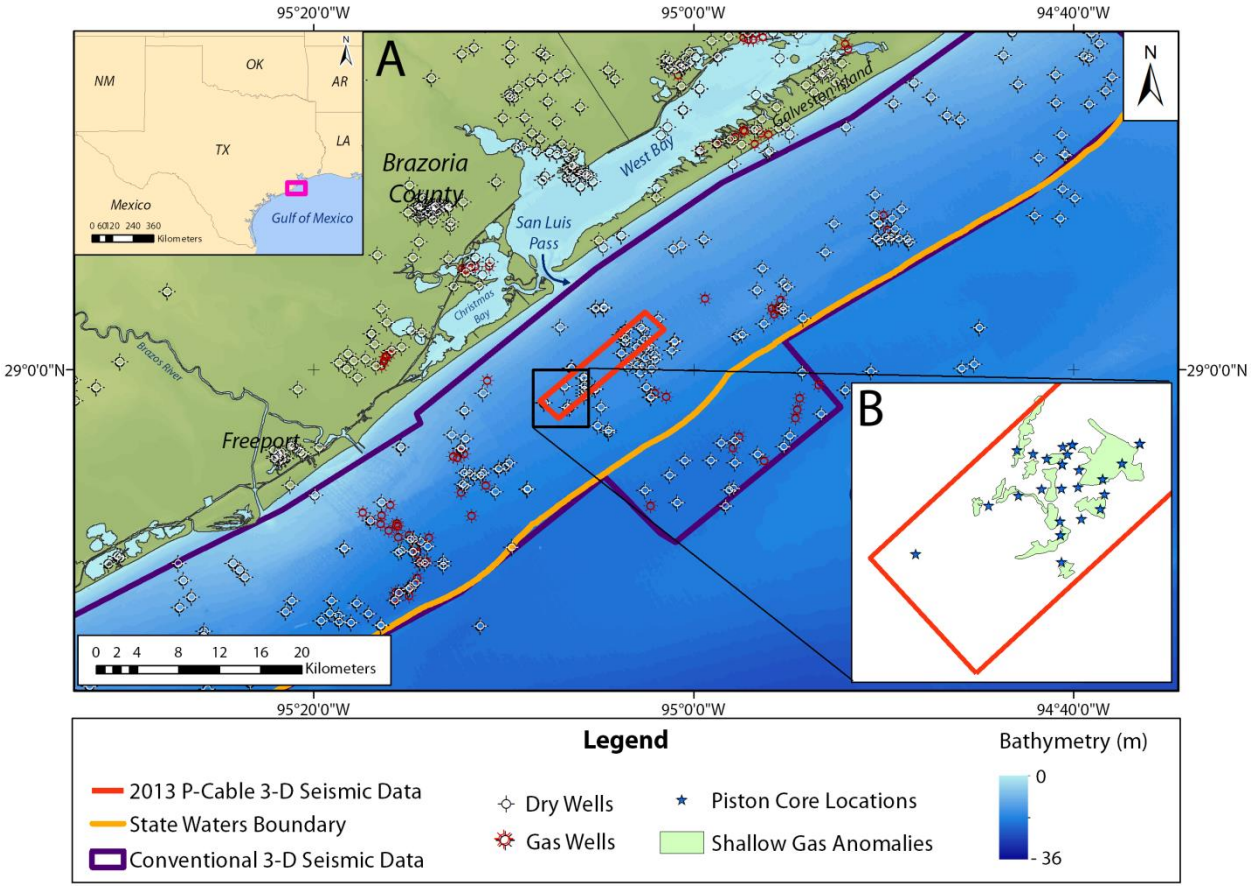

Figure 3.3. Field site offshore San Luis Pass. Inset in upper left shows location in Texas. (A) Locations of the high resolution seismic survey (red), conventional seismic survey extent (purple), Texas state water boundary (orange), gas wells (red asterisks) and dry wells (black crosses). (B) Piston core locations (blue stars) and locations of shallow gas anomalies projected to the surface (green polygons) (modified from Meckel and Mulcahy, 2016, and Osmond, 2016).

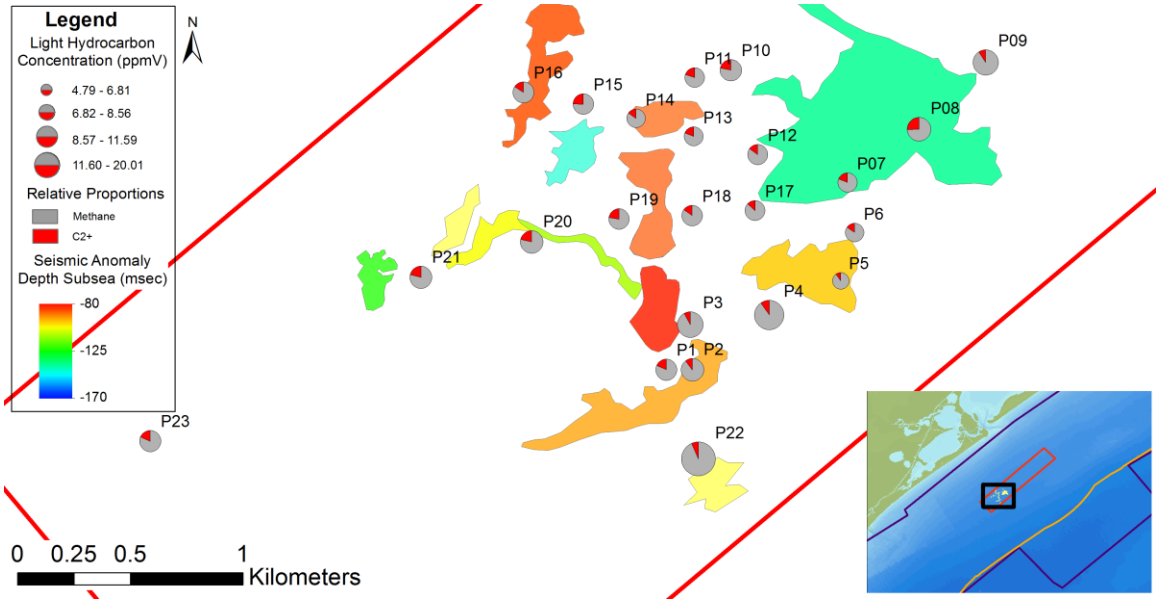

Figure 3.4. Pie plots indicate light hydrocarbon concentrations (size of pie), with the relative amount of methane represented in gray. The relative amounts of ethane and heavier components (C2+) are represented in red.

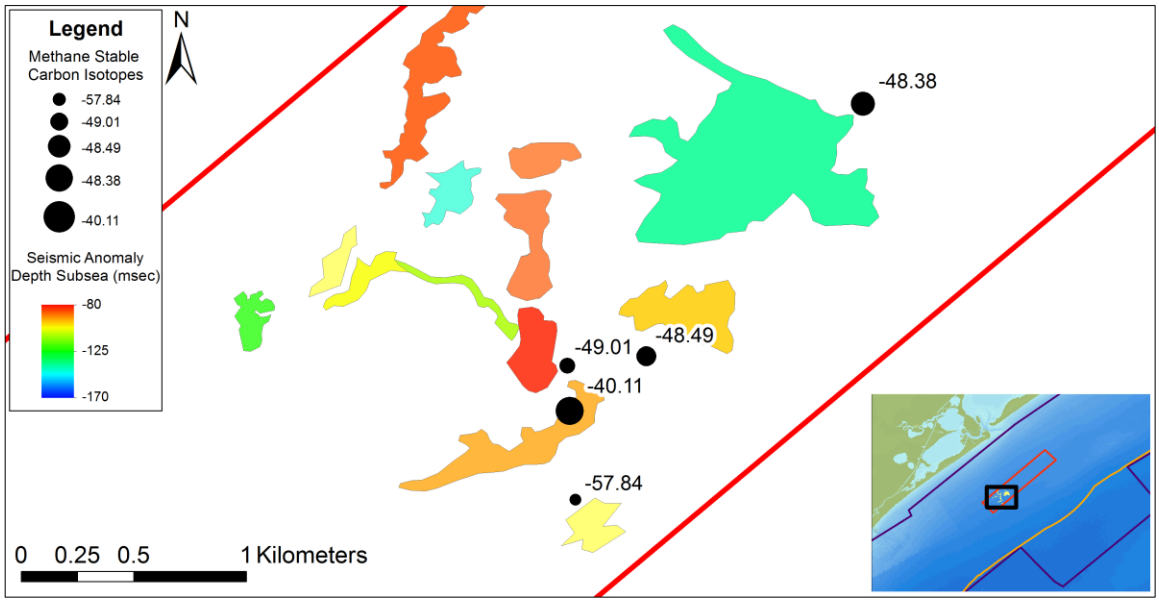

Figure 3.5. Ratio of methane stable carbon isotopes (per mil) (size of pie). Methane stable carbon isotopic values did not form consistent spatial trends in relation to underlying seismic anomalies.

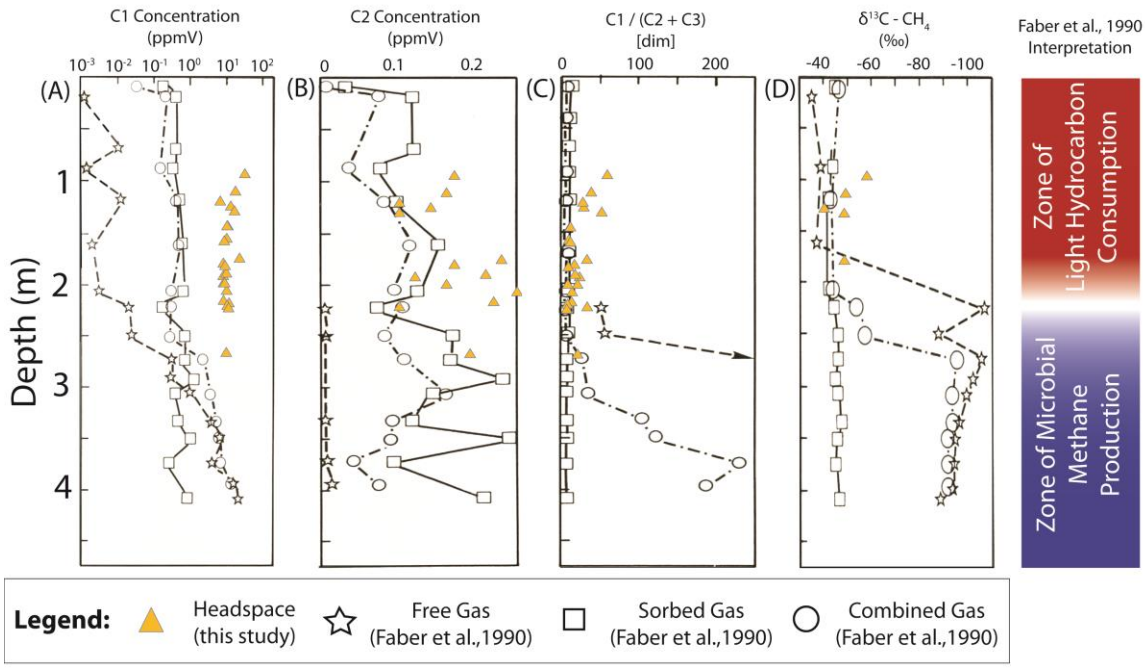

Figure 3.6. (A) Methane, (B) ethane, (C) Bernard ratio, and (D) stable carbon isotope data from this study (yellow triangles) plotted on the vertical profiles reported by Faber et al. (1990) from the Gulf of Mexico. The data from this study are consistent with typical values within the zone of light hydrocarbon consumption.

Table 3.1. Dissolved light hydrocarbon and CO_2 concentrations and stable carbon isotopes of methane. The symbol '-' signifies below detection limits.

CORE #	Methane	Ethene	Ethane	Propene	Propane	i-Butane	Butenes	n-Butane	CO_2	Bernard Ratio	Ethane / Ethene	$\delta^{13}C\text{-}CH_4$
Units	**ppmV**	**ppmV**	**ppmV**	**ppmV**	**ppmV**	**ppmV**	**ppmV**	**ppmV**	**ppmV**	**[dim]**	**[dim]**	**‰**
P1	6.31	0.66	0.25	0.25	0.17	0.01	0.05	0.04	10,489	23.17	0.52	
P2	8.07	0.46	0.14	0.13	0.13	0.01	0.02	0.04	3,399	39.90	0.54	-40.11
P3	10.70	0.47	0.16	0.12	0.11	0.01	0.01	0.02	992	44.74	0.54	-49.01
P4	13.60	0.81	0.23	0.21	0.17	0.02	0.02	0.03	2,514	72.18	0.31	-48.49
P5	4.32	0.26	0.10	0.06	0.05	-	-	-	94	22.00	0.73	
P6	5.15	0.51	0.12	0.18	0.09	0.01	0.02	0.02	2,869	33.36	0.23	
P7	5.23	0.56	0.22	0.23	0.15	0.01	0.02	0.04	1,577	24.73	0.36	
P8	7.24	1.09	0.48	0.42	0.34	0.01	0.07	0.09	8,596	12.83	0.63	
P9	10.14	0.69	0.10	0.12	0.09	0.01	0.01	0.02	369	63.07	0.23	-48.38
P10	6.34	0.78	0.35	0.30	0.24	0.02	0.05	0.05	1,320	63.07	0.67	
P11	5.48	0.64	0.26	0.19	0.17	0.02	0.02	0.03	12,595	17.22	0.64	
P12	6.08	0.49	0.14	0.29	0.11	0.01	0.01	0.01	1,025	16.58	0.36	
P13	5.17	0.58	0.17	0.25	0.12	0.02	0.03	0.03	3,053	32.63	0.41	
P14	5.24	0.53	0.16	0.13	0.08	0.01	0.02	0.02	2,462	16.48	0.33	
P15	5.62	0.79	0.35	0.30	0.26	0.02	0.03	0.07	8,797	26.56	0.65	
P16	6.51	0.72	0.10	0.24	0.09	0.02	0.03	0.03	867	14.76	0.24	
P17	6.15	0.49	0.19	0.14	0.09	0.01	0.01	0.02	1,045	25.43	0.27	
P18	6.23	0.54	0.21	0.17	0.12	0.02	0.03	0.01	907	37.23	0.44	
P19	5.76	0.78	0.34	0.27	0.23	0.02	0.03	0.02	11,210	27.18	0.63	
P20	7.08	0.67	0.29	0.25	0.60	0.03	0.01	0.09	2,233	16.55	0.55	
P21	6.74	0.83	0.34	0.34	0.22	0.02	0.03	0.05	1,577	7.13	0.52	
P22	18.70	0.72	0.17	0.22	0.14	0.01	0.03	0.02	720	21.39	0.23	-57.84
P23	6.49	0.67	0.31	0.22	0.20	0.01	0.02	0.03	9,780	122.00	0.61	
Average	6.16	0.31	0.14	0.07	0.09	0.02	0.01	0.02	2,912	33.92	0.46	

Average does not include P23, the control sample.

3.8 REFERENCES

Abdullah, K., Anderson, J., Snow, J., & Holdford-Jack, L. (2004). The Late Quaternary Brazos and Colorado Deltas. *Offshore Texas, USA—Their evolution and the factors that controlled their deposition: SEPM Special Publication*, *79*, 237–269.

Abrams, M. A. (1992). Geophysical and geochemical evidence for subsurface hydrocarbon leakage in the Bering Sea, Alaska. *Marine and Petroleum Geology*, 9(2), 208–221.

Abrams (1996). Distribution of Subsurface Hydrocarbon Seepage in Near-Surface Marine Sediments, in: D. Schumacher and M. A. Abrams, eds., Hydrocarbon migration and its near-surface expression: *AAPG Memoir* 66, p. 1–14.

Abrams, M. A. (2005). Significance of hydrocarbon seepage relative to petroleum generation and entrapment. *Marine and Petroleum Geology*, *22*(4), 457–477.

Allen, P. A., & Allen, J. R. (2013). *Basin analysis: principles and application to petroleum play assessment.* Oxford, UK: John Wiley & Sons. 632.

Anderson, R. K., Scalan, R. S., Parker, P. L., & Behrens, E. W. (1983). Seep oil and gas in Gulf of Mexico slope sediment. *Science*, *222*(4624), 619–621.

Azam, F. (1998). Microbial control of oceanic carbon flux: the plot thickens. *Science*, 280(5364), 694.

Bernard, B. B., Brooks, J. M., & Sackett, W. M. (1976). Natural gas seepage in the Gulf of Mexico. *Earth and Planetary Science Letters*, *31*(1), 48–54.

Bernard, B. B. (1978). Light hydrocarbons in marine sediments. PhD Dissertation. Texas A&M University.

Bernard, B. B., Orange, D. L., Brooks, J. M., & Decker, J. (2013, May). Interstitial Light Hydrocarbon Gases in Jumbo Piston Cores Offshore Indonesia: Thermogenic or Biogenic?. In *Offshore Technology Conference*. Offshore Technology Conference.

Blackford, J., Stahl, H., Bull, J. M., Berges, B. J., Cevatoglu, M., Lichtschlag, A., Connelly, D., James, R.H., Kita, J., Long, D. & Naylor, M. (2014). Detection and impacts of leakage from sub-seafloor deep geological carbon dioxide storage. *Nature Climate Change*, *4*(11), 1011–1016.

Blackford, J., Bull, J. M., Cevatoglu, M., Connelly, D., Hauton, C., James, R. H., Lichtschlag, A., Stahl, H., Widdicombe, S., & Wright, I. C. (2015). Marine baseline and monitoring strategies for carbon dioxide capture and storage (CCS). *International Journal of Greenhouse Gas Control*, *38*, 221–229.

Cartwright, J., Huuse, M., & Aplin, A. (2007). Seal bypass systems. *AAPG Bulletin*, *91*(8), 1141–1166.

Coplen, T. B. (1995). Reporting of stable hydrogen, carbon, and oxygen isotopic abundances. *Geothermics*, *24*(5-6), 707–712.

Dixon, T., & Romanak, K. D. (2015). Improving monitoring protocols for CO_2 geological storage with technical advances in CO 2 attribution monitoring. *International Journal of Greenhouse Gas Control*, *41*, 29–40.

Eichhubl, P., Greene, H. G., Naehr, T., & Maher, N. (2000). Structural control of fluid flow: offshore fluid seepage in the Santa Barbara Basin, California. *Journal of Geochemical Exploration*, *69*, 545–549.

Eiken, O., Ringrose, P., Hermanrud, C., Nazarian, B., Torp, T. A., & Høier, L. (2011). Lessons learned from 14 years of CCS operations: Sleipner, In Salah and Snøhvit. *Energy Procedia*, *4*, 5541–5548.

Faber, E. W., J. Stahl, M. J. Whiticar, J. Lietz, & J. M. Brooks, 1990, Thermal hydrocarbons in Gulf Coast sediments, *in*: Gulf Coast oils and gases: Proceedings of the Ninth Annual Research Conference, SEPM and Mineralogist Foundation, New Orleans, October 1, p. 297–307.

Faber, E., & Stahl, W. (1983). Analytic procedure and results of an isotope geochemical surface survey in an area of the British North Sea. *Geological Society, London, Special Publications*, *12*(1), 51–63.

Galloway, W. E., Whiteaker, T. L., & Ganey-Curry, P. (2011). History of Cenozoic North American drainage basin evolution, sediment yield, and accumulation in the Gulf of Mexico basin. *Geosphere*, 7(4), 938–973.

Gay, A., Lopez, M., Cochonat, P., Levaché, D., Sermondadaz, G., & Seranne, M. (2006a). Evidences of early to late fluid migration from an upper Miocene turbiditic channel revealed by 3D seismic coupled to geochemical sampling within seafloor pockmarks, Lower Congo Basin. *Marine and Petroleum Geology*, 23(3), 387–399.

Gay, A., Lopez, M., Cochonat, P., Levaché, D., Sermondadaz, G., & Seranne, M. (2006). Evidences of early to late fluid migration from an upper Miocene turbiditic channel revealed by 3D seismic coupled to geochemical sampling within seafloor pockmarks, Lower Congo Basin. *Marine and Petroleum Geology*, *23*(3), 387–399.

Hood, K. C., Wenger, L. M., Gross, O. P., & Harrison, S. C. (2002). Hydrocarbon systems analysis of the northern Gulf of Mexico: Delineation of hydrocarbon migration pathways using seeps and seismic imaging. *Surface exploration case histories: Applications of geochemistry, magnetics, and remote sensing: AAPG Studies in Geology*, *48*, 25–40.

Hunt, J. M. (1990). Generation and Migration of Petroleum from Abnormally Pressured Fluid Compartments (1). *AAPG Bulletin*, *74*(1), 1–12.

Laubmeyer, G., 1933, A new geophysical prospecting method: *Zeitschrift fiir Petroleum*, v. 29, no. 18, p. 1–4.

Leifer, I., & Boles, J. (2005). Measurement of marine hydrocarbon seep flow through fractured rock and unconsolidated sediment. *Marine and Petroleum Geology*, *22*(4), 551–568.

Løseth, H., Wensaas, L., Arntsen, B., & Hovland, M. (2003). Gas and fluid injection triggering shallow mud mobilization in the Hordaland Group, North Sea. *Geological Society, London, Special Publications*, *216*(1), 139–157.

Lower, S. K. (1999). Carbonate equilibria in natural waters. *Simon Fraser University*, *544*.

MacDonald, I. R., Sager, W. W., & Peccini, M. B. (2003). Gas hydrate and chemosynthetic biota in mounded bathymetry at mid-slope hydrocarbon seeps: Northern Gulf of Mexico. *Marine Geology*, *198*(1), 133–158.

Marzec, P., Sechman, H., Kasperska, M., Cichostępski, K., Guzy, P., Pietsch, K., & Porębski, S. J. (2016). Interpretation of a gas chimney in the Polish Carpathian Foredeep based on integrated seismic and geochemical data. *Basin Research*. http://dx.doi.org/10.1111/bre.12216

Meckel, T. A., & Mulcahy, F. J. (2016). Use of novel high-resolution 3D marine seismic technology to evaluate Quaternary fluvial valley development and geologic controls on shallow gas distribution, inner shelf, Gulf of Mexico. *Interpretation*, *4*(1), SC35–SC49.

Mulcahy, F.J. (2015). Use of high resolution 3D seismic data to evaluate Quaternary valley evolution history during transgression, offshore San Luis Pass, Gulf of Mexico. University of Texas at Austin. Master's of Science Thesis.

Nicoll, G. D. (2012). *Evaluation of the Nordland Group overburden as an effective seal for the Sleipner CO_2 storage site (offshore Norway) using analytical and stochastic modelling techniques* (Doctoral dissertation, University of Edinburgh).

Osmond, J.L. (2016). Fault seal and containment failure analysis of a Lower Miocene structure in the San Luis Pass area, offshore Galveston Island, Texas inner shelf. University of Texas at Austin. Master's of Science Thesis.

Roberts, H. H., & Carney, R. S. (1997). Evidence of episodic fluid, gas, and sediment venting on the northern Gulf of Mexico continental slope. *Economic Geology*, *92*(7–8), 863–879.

Roberts, S. J., & Nunn, J. A. (1995). Episodic fluid expulsion from geopressured sediments. *Marine and Petroleum Geology*, *12*(2), 195IN1203-202IN3204.

Romanak, K. D., Bennett, P. C., Yang, C., & Hovorka, S. D. (2012). Process-based approach to CO2 leakage detection by vadose zone gas monitoring at geologic CO_2 storage sites. *Geophysical Research Letters*, *39*(15). L15405, doi:10.1029/2012GL052426.

Romanak, K. D., Wolaver, B., Yang, C., Sherk, G. W., Dale, J., Dobeck, L. M., & Spangler, L. H. (2014). Process-based soil gas leakage assessment at the Kerr Farm: Comparison of results to leakage proxies at ZERT and Mt. Etna. *International Journal of Greenhouse Gas Control*, *30*, 42–57.

Schoell, M. (1983). Genetic characterization of natural gases. *AAPG bulletin*, *67*(12), 2225–2238.

Tasianas, A., Mahl, L., Darcis, M., Buenz, S., & Class, H. (2016). Simulating seismic chimney structures as potential vertical migration pathways for CO_2 in the Snøhvit area, SW Barents Sea: model challenges and outcomes. *Environmental Earth Sciences*, *75*(6), 504. https://doi.org/10.1007/s12665-016-5500-1

Wallace, K. J. (2013) Use of 3-dimensional dynamic modeling of CO_2 injection for comparison to regional static capacity assessments of Miocene sandstone reservoirs in the Texas State Waters, Gulf of Mexico. University of Texas at Austin. Master's of Science Thesis.

Yang, C., Dai, Z., Romanak, K. D., Hovorka, S. D., & Treviño, R. H. (2014). Inverse modeling of water-rock-CO2 batch experiments: Potential impacts on groundwater resources at carbon sequestration sites. *Environmental science & technology*, *48*(5), 2798–2806.

Chapter 4: Light Hydrocarbon and Noble Gas Migration as an Analog for Potential CO_2 leakage: Numerical Simulations and Field Data from Two Hydrocarbon Systems

Abstract

In assessing observed fluid anomalies or leakage allegations above geologic CO_2 storage sites, a direct comparison of injectate and anomaly compositions may be insufficient to determine if injection is the source of the fluid. Chemical matches may be non-unique and alteration can modify fluid chemistry during migration. This study evaluates natural light hydrocarbon migration and alteration, and noble gas stripping as analog for CO_2 migration. Three hydrocarbon systems were sampled in the groundwater and deeper gas bearing intervals above the reservoirs. Light hydrocarbons and noble gas upward migration were also modeled, including phase changes and sorption. Validated model results from the hydrocarbon analog system are applied to models of CO_2 migration and alteration to provide tools that can be used to better attribute leakage signal.

4.1 INTRODUCTION

Fluid leakage from geological CO_2 sites is not expected because regulation and permitting processes ensure that best practices are followed for site selection, risk management, and environmental protection. However, concerns about errors that lead to leakage require that operators develop plans to monitor and account for this possibility. Indications of potential leakage requiring assessment include anomalies in air, soil, and water, as well as public concerns about various types of changes. In the case that an anomaly is observed, attribution methods are needed to determine if the source of the anomaly is leakage of the injected CO_2 or other changes in the geosystem not related to injection (Dixon and Romanak, 2015). If leakage from the reservoir is identified, it may be necessary to establish liability, quantify emission for carbon accounting, and/or investigate remediation strategies. Improvements in attribution techniques that establish gas sources strengthen current GCS monitoring methods.

Leakage events or allegations are rare at GCS or CO_2-EOR sites; therefore, only a few field opportunities exist to evaluate techniques for identifying fluid sources. In 2011, landowners outside the Weyburn CO_2-EOR project claimed that land changes on their property were caused by CO_2 leakage. Multiple research teams interpreted near-surface CO_2 to have originated from natural biological processes. Geochemical tools used included stable and radioactive carbon isotopes, the process-based method, and noble gases (Sherk et al., 2011; Romanak et al., 2013). At the Cranfield CO_2-EOR site, high concentrations of CO_2 and CH_4 in soil gas near a well were evaluated to determine if they were caused by leakage. As with the Weyburn example, natural biological production

rather than leakage were interpreted as the fluid source using stable and radiogenic isotopes and noble gases (Anderson et al., 2017).

In both the Weyburn and Cranfield anomalies, fluid source attribution was relatively straight-forward because geochemical tools clearly identified biogenic fluids. However, the complexity of GCS sites allows for the possibility that current approaches could less effective for actual leakage cases. For example, in a case in which fluid migrates through the sedimentary column and interacts with rocks and fluids along the flow path, the geochemical composition of fluids in soil gas or groundwater may be quite different from the source fluids in the reservoir. For this reason, we investigate the processes that cause geochemical alteration during migration and how these effects can be incorporated into fluid source attribution techniques.

Our approach is to investigate the extent to which natural systems serve as an analog for potential CO_2 migration. There are no natural or man-made CO_2 seeps along the Gulf Coast, however, light hydrocarbon seepage (methane, ethane, propane, butane, and pentane) is common (Bernard et al., 1978; Hood et al., 2002).

We investigate hydrocarbon systems at three CO_2-EOR sites to determine the degree to which hydrocarbons reach the surface and to assess the limits of these interpretations. Light hydrocarbon seepage may provide a means to consider how CO_2 may migrate upward and interact with the natural system. In cases of non-isolation at other field sites (stacked reservoirs or seepage), there are clear patterns of enrichment of lighter geochemical components after migration (Ballentine et al., 1991; Etiope et al., 2009; Ma et al., 2009).

Samples from these three sites should be considered "baseline" and not misinterpreted as the results of monitoring a CO_2 injection site for leakage. We cannot directly study the CO_2 system at these sites to develop attribution techniques because no CO_2 leakage has been detected. However, this work is relevant to site monitoring because it is possible that in the future such techniques will be needed to deal with an incident or an allegation.

We focus on the hydrocarbon system, which is well represented at these locations because some hydrocarbons are detected all the way to the near-surface. In this investigation, we define overburden as gas-bearing intervals between groundwater and reservoir. We developed numerical simulations of gas migration and alteration to compare with field data.

The overall goal of this study is to use hydrocarbons systems to understand fluid alteration during upward migration. Then, forward models of CO_2 migration and alteration are investigated in order to attribute the source and migrated volumes of a potential future CO_2 anomaly. We consider preparation for such attribution, though novel at these sites, to be a skill that will be increasingly needed to meeting regulatory and public acceptance expectations.

4.2 FLUID MIGRATION AND GEOCHEMICAL ALTERATION

The concept of hydrocarbon seepage from source rock or reservoirs to the groundwater or the surface over geologic time is well known (Hunt, 1990). Gas migration occurs as continuous or episodic events when gas hydraulic head from buoyancy forces exceeds the capillary entry pressure of faults, natural fractures, or pores (Hunt, 1990). Hunt (1990) described typical events as gas periodically "burping" up to shallower

layers. Brown (2000) described the physical transport processes of continuous or episodic migration mechanisms. The source and alteration relationships between hydrocarbons reaching the near-surface and deeper accumulations is often complex because a wide array of water/rock interactions can occur (Abrams, 2005).

A compilation of light hydrocarbon data shows generally consistent patterns of alteration (Etiope et al., 2009). The proportion of methane generally increases relative to ethane and propane as a function of migration distance (Etiope et al., 2009). These field results and experiments indicate minimal changes in isotopic ratios from migration (Fuex et al., 1980).

The consistency in geochemical changes in both noble gas and hydrocarbons, whereby lighter components are enriched at shallower intervals, indicates that the same physical processes could influence these gases. This effect has been described as "chromotographic separation" (Etiope et al., 2009) or "elemental fractionation" (Hunt et al., 2012).

There is still uncertainty regarding the underlying processes that cause this alteration. Differential solubility and sorption, defined as physio-chemical partitioning between water and a solid substrate, are the most common interpretations (Deville et al., 2003; Etiope et al., 2009) and these explanations are consistent with core (Leythaeuser et al., 1985; Lu et al., 2015) and laboratory studies (Kettel et al., 1996). Yet, relatively few studies have modeled alteration processes at the field scale. Klusman (2003) modeled microseepage volumes and fluxes from a natural seep in Rangely Field, Colorado, but did not consider phase changes and sorption effects. Ma et al. (2012) modeled elemental fractionation of noble gases with static calculations of diffusion and differential solubility

to show that alteration effects aligned with field data. To our knowledge, light hydrocarbon alteration from solubility and sorption has not yet been investigated thoroughly. By quantifying these processes, interpretations of gas flowpaths and migrated volumes from changes in geochemical compositions and alteration models may be possible.

This study combines observations at hydrocarbon systems with geochemical alteration within natural CO_2 reservoirs. Previous work interpreted the path of CO_2 transport at Bravo Dome and St John's Dome by measuring phase changes of CO_2 and noble gases (He, Ne, Ar, Kr, and Xe) (Gilfillan et al., 2009, 2011). Supercritical CO_2 is a powerful solvent that can exsolve, or strip, noble gases dissolved in formation water and thereby provide a means to assess gas/water interactions (Warr et al., 2016). This investigation will couple CO_2 leakage simulations with noble gas phase behavior to understand how fluid compositions relate to migration scenarios.

4.3 APPROACH

Our approach was to assess and quantify alteration processes using a stepwise procedure. Light hydrocarbons and noble gases were collected and analyzed from available groundwater, overburden sands, and reservoirs at three hydrocarbon systems. These geochemical compositions from groundwater and overburden intervals were interpreted to determine if underlying intervals were potential fluid sources and the degree to which alteration occurred during migration. Field data were compared with models that quantified solubility and sorption to interpret the extent to which these processes could cause alteration. Then, forward models of CO_2 were run to theoretically evaluate how potential leakage may change during upward migration.

The models were designed to simulate episodic gas burping up to shallower permeable intervals and migrating laterally until the subsequent migration event. This migration scenario could transport gas volumes that classify as macro- rather than microseepage, but without an observable fault or wellbore as the pathway (Abrams, 2005). This scenario of gas transport was selected for detailed study because gas chimney structures, in which gas migrates as episodic events (Roberts and Carney, 1997), have been identified as leakage risks for offshore geologic storage (Jones et al., 2015).

We quantified gas burping with two types of models: (1) a static spreadsheet model in which gas is assumed to migrate to the next shallower layer and to be equilibrated with water and rock at hydrostatic conditions; and (2) compositional reservoir simulations using multiple stacked models that each have three layers: a gas-filled permeable layer, a faulted impermeable layer, and a water-filled permeable layer. After upward gas migration, the results of the top layer were used as initial conditions for the bottom layer of the next model at shallower depths. This geometry set-up is shown graphically in Fig. 4.7.

Gas migrates up through the faults from pressure differences and buoyancy while water from the top layer may migrate downward. We do not report rates and timing because each migration event is separated by unknown dormant periods (Roberts and Carney, 1997). These two model designs were constructed for three scenarios of gas migration: light hydrocarbons interacting with water, light hydrocarbons interacting with porous media, and CO_2 interacting with water saturated with noble gases.

4.4 FIELD SITE AND GEOLOGY

4.4.1 Site 1

The geology of Site 1 consists of the Pleistocene-aged freshwater Chicot aquifer (0– ~200 m below ground surface) and the Pliocene-aged freshwater confined Evangeline aquifer (~220– ~875 m) (Fig. 4.1).

A gas-productive Miocene-aged Jasper saline aquifer (~1000– ~1500 m) and a number of other hydrocarbon productive units overly a transgressive Anahuac confining unit that isolates the Oligocene–Miocene Frio strainplain-barrier island facies hydrocarbon reservoirs (Galloway et al., 1982). Frio reservoirs contained an estimated 690 MMbbl original oil in place and 115 bcf original gas in place. The structure of Site 1 reservoirs consists of rollover anticlines caused by a coastal growth fault. Ten well recompleted in above-zone intervals (~1655 and 1060 m) have been used for sampling and monitoring.

4.4.2 Site 2

Site 2 also produces hydrocarbons from Frio Formation reservoirs, but three geological features distinguish this site: deep salt intrusion resulting in extensive reservoir faulting at reservoir depth, fluvial–deltaic stratigraphic setting, and a thick overburden interval of locally hydrocarbon-bearing Miocene-aged sands. Below the Chicot, Evangeline, and Jasper aquifers, large-scale regression events deposited at least 14 progradational and aggradational Miocene-aged sands. Below the Miocene sands and Anahuac shale, Frio hydrocarbon reservoirs have produced over 575 MMbbl. Radiating from a principal fault, a network of smaller faults compartmentalizes reservoirs into at least 15 unique fault blocks (Halbouty, 1937). Fluids were not sampled in the Frio

reservoirs for gas components because of potential contamination by various fluids during past and current operations.

4.4.3 Site 3

The shallow subsurface (0–500 m) contains a shallow freshwater aquifer (Catahoula) overlying several more saline confined aquifers (Jackson-Vicksburg Group). Hydrocarbon production began in the Wilcox Group (1200-2200 m) but the primary reservoirs are fluvial to shelf sandstones and conglomerates in the Cretaceous Lower Tuscaloosa Formation (~3000 m) (Spooner, 1964; Hovorka et al., 2011). In terms of structural geology, deep salt intrusion caused a crestal graben feature with two faults at the Tuscaloosa depth interval (Nicot et al., 2013). From 1944 to 1965, approximately 37 million barrels of oil (MMbbl) and >672 billion cubic feet (bcf) of gas were produced from the Lower Tuscaloosa formation (Weaver and Anderson, 1966).

4.5 MATERIALS AND METHODS

4.5.1 Field Sampling and Laboratory Analysis

4.5.1.1 Sampling

At each site, multiple zones were sampled for light hydrocarbons (methane, ethane, propane, butane, and pentane) and noble gases (Fig. 4.1). At Site 1, eleven groundwater wells were sampled on eight sampling trips from 2012 to 2017. These PVC or steel cased wells were purged for at least three well storage volumes (~3 hours) or until field parameters stabilized (pH, oxidation-reduction potential, dissolved oxygen, and specific conductance). Groundwater was produced using a submersible pump (Grundfos 5E05) for seven wells, dedicated pumps for two wells, or from two artesian wells. Dissolved gas was pumped into 70 ml capped septa vials. Care was taken to remove any

gas bubbles while purging three volumes. Noble gases were sampled with a submersible pump from two Evangeline groundwater wells in February, 2017. Water was pumped through 3/8" refrigeration grade cooper tubes that were sealed by cold-welding with pinch off clamps. Atmospheric contamination was mitigated by allowing flow through the tubes for five minutes.

In February 2017, the field operator pumped brine from overburden sandstones (~1764 and 1740 m) for reinjection into deeper reservoirs. Brine samples were collected via ½" NPT fitting from two wellheads for dissolved hydrocarbon and noble gas analyses following the same procedure as groundwater sampling. As at site 1, reservoir fluids were not included in the sampling program.

At Site 2, groundwater sampling was conducted at one well in January 2017. Fresh groundwater was pumped with a Grundfos submersible pump from a PVC-cased well screened at an unknown depth. The sampling procedure at Site 2 was identical to Site 1 for both dissolved hydrocarbons and noble gases. Samples were transported on ice, maintained at 2^0 C and analyzed within one month.

In the overburden, two temporarily abandoned gas wells (perforation depths 1665 and 1858 m) were sampled for hydrocarbon composition and $\delta^{13}C\text{-}CH_4$. These relatively high pressure wells (~57.22 MPa / 8,300 psi) were purged for approximately ten minutes through a needle valve at the wellhead. Gas samples were collected in Isotubes steel cylinders (Isotech Laboratories, Champaign, IL) via Isotech's wellhead sampler. Noble gases were sampled in cooper tubes that were purged for five minutes to minimize atmospheric contamination.

At Site 3, fourteen groundwater wells were sampled between 2008 and 2012 (Yang et al., 2013). The concentrations of dissolved hydrocarbons were below 0.04 ppm in all groundwater samples. In April 2012, two wells completed in the overburden Wilcox Formation were sampled for gas at the wellhead and analyzed at Isotech Laboratories (Champaign, Illinois) (Anderson et al., 2017). In December 2009, nine wells from the Tuscaloosa reservoir were sampled for gas and analyzed at University of Texas at Austin laboratories (Lu et al., 2009).

4.5.1.2 Analysis

Groundwater hydrocarbon analysis was performed at the University of Texas laboratories following previously described methods (Nicot et al., 2017a; 2017b). Light hydrocarbons were analyzed for concentrations and $\delta^{13}C\text{-}CH_4$ via gas chromatography isotope ratio mass spectrometry (GC-IRMS). The concentrations of light hydrocarbons (methane, ethane, and propane) were calculated from measured headspace gas concentrations and Henry's Law relationships (Kampbell and Vandegrift, 1998). The detection limits for methane, ethane, and propane are 0.001, 0.002, and 0.003 mg/L respectively. Samples with dissolved methane concentrations greater than 0.3 mg/L were analyzed for stable carbon isotopes via GC-IRMS. Replicate analyses of $\delta^{13}C$ had standard deviations within +- 0.35 ‰.

Noble gas isotopes were measured at The Ohio State University Noble Gas Laboratory using either Thermo-Fisher Helix SFT or a Thermo-Fisher Argus VI+ mass spectrometers following previously reported methods (Darrah et al., 2012; 2015). Samples were purified in stainless steel and corning-1724 lines. Bulk gases were purified by consecutive exposure to a Zr-Al getter (SAES- ST-707) held at 450C and a SAES

SORB-AC cartridge held at 250 and then cooled to 25° C in an activated charcoal cold finger. The abundances of noble gases were calibrated with reference and cross-validated laboratory standards including an atmospheric standard, a series of synthetic natural gas standards obtained from Praxair, and a cross-validated natural MM-1 standard from Yellowstone National Park.

4.5.2 Fluid Sources

We present mixing analyses to estimate the percentage of thermogenic methane in groundwater. Groundwater methane was separated into biogenic and thermogenic end members using classifications of stable carbon and hydrogen isotopes. Ethane and propane in groundwater was assumed to originate from reservoirs, because only trace amounts are produced biogenically (Kim and Douglas, 1972).

With the dissolved concentrations of methane, ethane, and propane, we consider the composition of a gas in equilibrium with water that would reproduce the data. Hypothetical gas compositions were calculated with Henry's constants for methane, ethane, and propane at 21^0 C and the hydrostatic pressure associated with the depth of each groundwater well (Dhima et al., 1999). The Bernard ratios (Bernard et al., 1978) of this hypothetical equilibrium gas are compared with reservoir values as an indicator to assess alteration during upward migration. Noble gas sources are interpreted from signatures of the mantle, crust, and water in equilibrium with the atmosphere.

4.5.3 Numerical Simulations

4.5.3.1 Model Design

4.4.3.1.1 Static Model

The static model calculated how a hypothetical gas composition would change during transport from the reservoir to the surface by interacting with pure water and rock without initial sorbed components. The calculations were performed at eight arbitrary depth intervals following typical hydrostatic (0.997 Pa/m) and geothermal (0.032 C/m) gradients along the Texas Gulf Coast (Christie and Nagihara, 2016). After each calculation, half of the gas-phase moles were assumed to migrate to the next depth interval. Based on the gas volume from the ideal gas law, gas was assumed to contact the same volume of water and rock for solubility and sorption calculations, respectively. The bottommost layer was defined at 2,350 m and 18.2 MPa to represent overburden depths and pressures, respectively. The initial gas volume was calculated from a 1000 m by 1000 m by 150 m reservoir with 0.15 porosity and 0.2 residual water saturation. The relative amounts of methane, ethane, and propane in the initial compositions were identical to reservoir measurements at Site 2. The same geometry was used for the CO_2 model, but water contained air-saturated compositions following Benson and Krause (1976).

4.5.3.1.2 Dynamic Model

The static model was adapted into a fully compositional reservoir simulation to include effects occurring from transport. Our preliminary work using single dynamic model geometry from the reservoir to the surface resulted in vertical gas migration with minimal lateral migration. Therefore, we created eight separate models with no-flow

boundaries around all edges, but linked the results of the top layer to the initial conditions of the bottom layer of the following model (Fig. 4.7).

Each model consisted of 10 by 10 homogenous isotropic layers with 100 m length and width and 150 m height. Rather than using a "layered cake" geometry, layers were shaped like domes to simulate typical structural features associated with salt diapirism and roll-over anticlines (Hudec and Jackson, 2007) mapped at Sites 1, 2, and 3. The flow parameters through shale layers were designed to model transmissive natural fractures. Fracture rows were assigned through two center rows of the model geometry. In the simulation software CMG-GEM, fracture properties were chosen so that the fracture transmissivities were similar to ten fractures at 0.05 mm width and 1,000 md permeability.

Simulation times were intentionally long (40 years) with 1 month timesteps to allow for gas to equilibrate in the upper layer (i.e., no more flow). Relative permeability was calculated with quadratic relationships with 0.4 for immobile water saturation and 0.1 for immobile gas saturation.

4.5.3.2 Solubility Simulations

To simulate differential solubility, phase changes were modeled using the ideal Henry's Law (Eq. 1) in both the dynamic and static models. Our intention was not to avoid calibrating an equation of state to calculation phase changes. Equations of state account for the fact that mixtures of gases typically have difference solubilities than a pure gas and water. Experimental data from light hydrocarbon mixtures and water showed that the differences in fugacities between mixtures and pure light hydrocarbons were within the range of experimental error (Dhima et al., 1999). The reason that

pressure was used rather than chemical potential (i.e., fugacity) was because laboratory results were typically reported as pressure rather than fugacity.

A unique Henry's constant was used for each of the eight simulations. Henry's constants were compiled directly from experimental results for light hydrocarbons (methane, ethane, and propane) (Fig. 4.4).

Eq. 1 $$p = k_H * c$$

where p = partial pressure (kPa), k_H is Henry's constant (1/kPa), and c is mole fraction in the aqueous phase (dimensionless).

4.5.3.3 Sorption Simulations

The process of sorption, whereby light hydrocarbons form a film on the liquid or solid surfaces, is quantified in our models with the multi-component Langmuir model (Arri et al., 1992). The amount of gas-phase light hydrocarbons adsorbed depends on their partial pressure and isotherm constants (Langmuir constant and maximum moles adsorbed) (Eq. 2). The maximum amount of adsorbed gas depends on the presence of hydrophilic clay minerals and organic matter amount, type, and thermal maturity (Zhang et al., 2012). Zhang et al. (2012) measured methane adsorption onto dry shales at various temperatures. No data have been collected to quantify maximum moles of methane adsorbed; therefore, values for all simulation layers were chosen equal to the results from Woodford shales because this value (0.21 moles / kg-rock) was between Barnett and Green River results (0.16 and 0.24 moles / kg-rock, respectively). Langmuir constants for simulation layers 1–4, 5–7, and 8 were chosen as results at 35.4, 50.4, and 65.4 ^{0} C, respectively (Zhang et al., 2012) (Fig. 4.8). For the static model, the amount of gas

adsorbed per mass rock was interpolated for the pressure and temperature conditions of each of the eight layers.

Unlike methane, ethane and propane experiments have not been conducted on sedimentary rocks (Zhang, 2017, personal communication). The two processes that cause light hydrocarbon sorption are covalent bonding and Van der Waal forces (Loughlin et al., 1990). Ethane and propane sorption are modeled by scaling methane results by their molecular weight because Van der Waals forces are directly related to molecular mass (Dzychoshinskii et al., 2012). This approach is generally supported by light hydrocarbon sorption on zeolites that show ethane and propane sorption are similar to each other but higher than methane (Fig. 4.7) (Loughlin et al., 1990).

Eq. 2 $$\omega_i = \frac{\omega_{i,max} B_i y_{ig} p}{1 + p \sum_j B_j y_{jg}}$$

where B = Langmuir isotherm parameter, ω = moles of absorbed component per kg rock, p = pressure (kPa), y = mole fraction in the gas phase, i = individual gas component gas component, j = summation of total gas components.

4.5.3.4 CO_2 Stripping of Noble Gas Simulations

Noble gas stripping and CO_2 dissolution have been used to effectively document CO_2 migration direction at the field scale (Gilfillan et al., 2009). Pure CO_2 was initiated as the reservoir gas in the bottommost layer 2,250 m. As with light hydrocarbon simulations, experimental data did not require developing an equation of state. Warr et al. (2016) measured noble gas Henry's constants as a function of CO_2 density in a mixture of CO_2 water and noble gases. Trial simulations were run to determine the average CO_2 density in each layer. These densities were then applied to estimate noble gas Henry's constants in subsequent simulations using relationships in Warr et al. (2016).

The first group of simulations initiated overlying layers with dissolved noble gases at the same concentrations as air-saturated water (Benson and Krause, 1976). Then, CO_2 stripping simulations were tailored to field conditions at two sites to forward model a potential CO_2 leak. The initial dissolved noble gases in formation water are based on measured field data. Layers from surface to 1,200 m were defined with the average ^{3}He, ^{4}He, ^{36}Ar, and ^{40}Ar concentrations measured in groundwater samples. Below 1,200 m the initial dissolved noble gas concentrations were based on overburden gas analysis. The ^{3}He and ^{36}Ar were assumed to be air-saturated water concentrations. Then, ^{4}He and ^{40}Ar dissolved concentrations were chosen to maintain the same $^{3}He/^{4}He$ and $^{40}Ar/^{36}Ar$ ratios observed in gas samples at Sites 1 and 2.

4.6 RESULTS AND DISCUSSION

4.6.1 Fluid Source Interpretations

4.6.1.1 Light Hydrocarbons

The groundwater methane data from two sites are presented and compared to typical sources in Fig. 4.5. The percent of thermogenic methane in total methane at sites 1 and 2 is interpreted from a mixing trend assuming that reservoir methane at Site 2 is the thermogenic end member and the groundwater sample with the lightest carbon isotopes is the biogenic end member. At Site 1, the percentage of thermogenic methane ranges from 24.4 to 44.6% in the Evangeline aquifer and 0 to 41.59% in the Chicot aquifer.. The highest percentage of thermogenic methane was 85.4% from the groundwater sample at Site 2, which is strong evidence of seepage. This analysis was not possible for Site 3 because methane concentrations were too low.

Following the allocation of the percentage of methane allocated to a thermogenic source, Table 4.1 presents the Bernard ratios of hypothetical gases in equilibrium with groundwater that would result in the observed groundwater concentrations of thermogenic methane, ethane, and propane. These values are presented graphically in Fig. 4.6 along with the measured groundwater, overburden, and reservoir values. We consider the Bernard ratios of equilibrium gas to be altered thermogenic gas near the surface.

At Site 1, the higher Bernard ratios in the Evangeline and Chicot aquifers compared to overburden values could be explained by interaction with water and rock during migration (Etiope et al., 2009). An alternative explanation is that biogenic processes (variation in substrates, oxidation) control methane production and isotopic variation (Whiticar, 1999) and produce small amounts (<0.007 mg/L) of ethane and propane observed in wells 2 through 12 (Kim and Douglas, 1972)) (Table 4.2).

At Site 2, the equilibrium gas Bernard ratio is interpreted to have increased during migration from the reservoir because the methane stable isotopes of these two intervals agree (Fig. 4.9). The higher Bernard ratio of overburden gas indicates a biogenic contribution or separate migration pathway than to groundwater.

The end-member mixing model indicates that overburden gas at Site 3 includes a 30 to 40% thermogenic contribution (Fig. 4.5). However, upward fluid migration from the injection reservoir at 3 km depth is not interpreted as the source at Site 3 because overburden stable isotopes are within the range of regional signatures observed in the Wilcox formation ($\delta^{13}C$ -60.73 to -65.57 ‰, δD -188 to -196 ‰) (Warwick, 2004).

4.6.1.1 Noble Gases

In all of the samples from Fields 1 and 2, ratios of $^{4}He/^{20}Ne$ are significantly above the air ratio of 0.032 in all samples, thereby suggesting that contamination from air is negligible (Table 4.3). However, these samples can have noble gas components that originated from the atmosphere and dissolved into groundwater. The helium isotopic ratios relative to atmosphere (R/Ra values) vary from 0.017 to 0.059, which are generally consistent with crustal production (0.01 – 0.05, Oxburgh et al., 1986). The very low R values preclude a significant contribution of mantle helium (R/Ra ~ 8 to 35) (Graham et al., 2002).

The neon $^{20}Ne/^{22}Ne$ ratios show significant deviation from the atmospheric value of 9.78. Consequently, the neon measurements do not rule out a contribution of mantle ^{20}Ne ($^{20}Ne/^{22}Ne = 13.8$). However, neon $^{21}Ne/^{22}Ne$ ratios are similar to the atmospheric value and therefore do not indicate the addition of crustal ^{21}Ne.

The ratios of $^{40}Ar/^{36}Ar$ are all above the atmospheric value (295.5) and therefore reflect an addition of radiogenic ^{40}Ar. The overburden $^{40}Ar/^{36}Ar$ values are higher than groundwater samples which is consistent with production within the crust. The total amount of ^{40}Ar still contains significant atmospheric contributions and the $^{40}Ar_{rad}$ values reported here have been corrected for only radiogenic ^{40}Ar following Ballentine et al. (1991).

The $^{86}Kr/^{84}Kr$ ratios are very similar to the atmospheric value and therefore do not indicate an addition of crustal ^{86}Kr. With the exception of sample OB2 from Site 2, the ratios of $^{136}Xe/^{132}Xe$ are similar to the atmospheric value or slightly below. Therefore, only one sample may have additional ^{136}Xe from crustal production.

In summary, noble gas data do not indicate that groundwater components originated from depth at either site. Neon, krypton, and xenon were not valuable indicators because their ratios generally aligned with atmospheric values for both deep and shallow samples. The crustal components that are present (^{4}He, ^{40}Ar) are consistent with production in the crust rather than trends expected of upward migration. In contrast, Ballentine et al. (1991) documented $^{4}He/^{40}Ar$ ratios that increased by orders of magnitude at shallower depths in a stacked hydrocarbon system.

Groundwater noble gases at Sites 1 and 2 likely originated in-situ or dissolved from the atmosphere during recharge rather than from depth. Ratios of $^{4}He/^{40}Ar$ do not show discernable trends with depth and all values are within one order of magnitude of the crustal production value (4.92) (Ballentine et al., 1991). The noble gas compositions did not indicate upward fluid migration, yet this dataset is valuable as the initial conditions to forward model CO_2 migration and noble gas stripping.

4.6.2 Numerical Simulations

4.6.2.1 Light Hydrocarbon Solubility

Figure 4.7 presents static and dynamic model results of a gas with the same composition as the shallowest overburden sandstone at Site 2 migrating up and undergoing compositional changes as a result of hydrocarbon solubility. Saturation and Bernard ratios from the static model are presented as solid lines. For the dynamic model, these properties and the final pressures are shown as box and whiskers plots (minimum, maximum, Q1, Q3, mean, and median). The Bernard ratio mean (diamond symbols) was calculated from the total methane, ethane, and propane moles rather than from the mean value of the cells to weight the mean by the amount of gas in each cell.

The Bernard ratio from the static model increases 5.2%, from 59.2 to 62.3. The dynamic model mean agrees well with the static model results, although there is variation among cells, as shown in the box and whiskers plots. Simulated gas in cells at the edge of the plume were higher than the mean value, presumably from distillation as gas interacts with water during migration. The low Bernard ratios in models at 2050 m, 480 m, and 180 m occurred in cells with low gas saturation (< le-3). The differences between overburden and groundwater Bernard ratios at Site 2 may be interpreted as originating from solubility alteration.

There is a possibility that solubility simulations do not effectively model phase changes. The ideal Henry's Law does not account for interactions between components in a mixture of gases. However, experiments with multiple hydrocarbon components had solubility that could not be distinguished from two component results (Dhima et al., 1999). Therefore, the solubility model is not interpreted as causing the variation between simulations and field data. Actual light hydrocarbon solubility is expected to be lower than modeling results. The use of pure water in numerical simulations overestimates solubility, because the presence of dissolved solutes typical in Gulf Coast formation waters reduces solubility of light hydrocarbons (Dhima et al., 1999). Solubility is also overestimated by the reservoir simulator because phase equilibrium is calculated for the entire gridblock rather than only for water adjacent to a migration pathway. Other processes besides solubility are more likely responsible for causing chromatographic separation in light hydrocarbons.

4.6.2.2 Sorption

Figure 4.8 shows static and dynamic model results of gas composition changes from gas–rock interaction. Bernard ratios are not presented above 1250 m because gas saturation decreases below 1e-5 in the dynamic models. Changes in the Bernard ratios from both models are higher than differences between overburden and groundwater compositions at Site 1, indicating that sorption may cause alteration. In a separate static model, the volume of rock encountered by gas was decreased by one order of magnitude. The resulting Bernard ratios are similar to Site 1 field data and demonstrate how the degree of rock interaction strongly influences gas alteration.

Yet, the current experimental data poorly constrain sorption quantification. The experimental results used for the sorption calculation studied dry shale samples (Zhang et al., 2002). In actual sedimentary rocks, the presence of water coating grains reduces gas sorption (Zhang et al., 2002). Ethane and propane isotherms are estimated because experimental data do not exist for sorption on actual sedimentary rocks (Zhang, personal communication). The factors controlling sorption, including clay and organic matter composition, vary at the pore scale and, therefore, cause large uncertainty when upscaling to the sedimentary column.

Still, the interpretation of sorption as a key alteration process is consistent with core studies observing hydrocarbons sorbed to shales (Lu et al., 2015). Physical processes, such as diffusion, are less likely because significant isotopic fractionation would be expected to occur, but is not observed (Klusman, 2003). Microbial consumption of light hydrocarbons preferentially oxidizes C2+ alkanes (i.e., ethane and propane) (Kinnaman et al., 2007) and cannot be ruled out for Site 1. At Site 2, oxidation is unlikely because microbes concurrently oxidize methane with ethane and propane, but the

methane stable isotopes from this site do not show increases associated with oxidation (Fig. 4.8).

Future lab work is needed to evaluate methane, ethane, and propane sorption during transport. Sorption coupled with fluid transport has been quantified for methane flow through coals (Cui et al., 2009; Shabro et al., 2011) and its isotopic fractionation (Xia and Tang, 2012). An advantage of applying these models to laboratory experiments of natural gas flow through sedimentary rocks would be that seepage rates could be interpreted based on observed compositional changes.

4.6.2.3 CO_2 Stripping

Simulations of CO_2 migrating up through the sedimentary column show that concentrations of noble gases increase in the gas phase (Fig. 4.9). This alteration occurs from two processes. When CO_2 is in the supercritical phase (> ~1,000 m), CO_2 decreases the Henry's constant of argon, krypton, and xenon and, therefore, causes exsolution of gases originally dissolved in formation water. Gaseous CO_2 at depths shallower than ~1,000 m does not alter noble gas solubility. However, the solubility of CO_2 increases at lower temperatures (Fig. 4.9), thereby enriching the concentrations of noble gases at shallower depths.

Figure 4.9 shows simulation results of CO_2 reacting with formation water initiated with air-saturated water noble gas concentrations. The isotopic ratios of noble gases are not reported because they remain identical to air-saturated water values. The concentrations of krypton, argon, and xenon increase approximately one order of magnitude. Helium concentrations remain lower because supercritical CO_2 decreases the Henry's constant. The differences in noble gas concentrations among the static and

dynamic models are influenced by the volume of water contacted by CO_2. Warr et al. (2016) did not report results for neon.

The CO_2 is completely dissolved by 200 m, in contrast to other simulations in this study where light hydrocarbons reach the top layer. This observation supports previous work documenting solubility as a major trapping mechanism (Suekane et al., 2008).

These results are relevant to attributing the fluid source of a CO_2 anomaly at a GCS site. Migration of CO_2 to the near-surface is not expected, but some geochemical indicators, such as stable carbon isotopes, may coincidentally align with injectate values (Sherk et al., 2011). These simulations predict expected trends in noble gas changes in the unlikely case of leakage.

Several aspects of this modeling design may limit confidence in interpreting fluid sources. The assumptions of homogenous, isotropic, and zero-tilt porous media and relatively large gridblocks likely overestimate CO_2 and water interaction as actual CO_2 may finger along high-permeability pathways (Trevisan et al., 2017). As with uncertainties in rock properties, sampling from groundwater and overburden are insufficient to characterize dissolved fluids throughout the sedimentary column.

The presence of oil in overburden intervals would both increase the amount of CO_2 trapped in the dissolved phase and the noble gases stripped from oil (Kharaka and Specht, 1988). If methane or light hydrocarbons were dissolved in oil or formation water, they would exsolve in addition to noble gases. In that case, light hydrocarbons and noble gases may form a separate phase that precedes dense, supercritical CO_2 (Oldenburg et al., 2013). Yet, light hydrocarbons are not recommended as a fluid source indicator because

natural seepage, mixing with biogenic methane, and possible alteration make it difficult to diagnosis leakage.

4.7 IMPLICATIONS FOR GCS FLUID SOURCE ATTRIBUTION

This study investigated three hydrocarbon systems as a means to assess the potential for CO_2 migration from geologic storage. Two of the sites did show evidence of thermogenic hydrocarbons. The goal of this investigation was to understand the earth processes influencing light hydrocarbons during migration to then forward model potential CO_2 migration. Modeling results of phase changes could not account for compositional changes observed at these systems and seeps at other sites (Etiope et al., 2009).

We interpret sorption as the dominate alteration process, but a lack of experimental data limited the confidence in our predictive models. In the future, light hydrocarbon and CO_2 sorption data onto wet sedimentary rocks would allow for forward modeling of gas compositional changes for various migration pathways. Forward models using noble gases could be valuable for geologic storage risk assessments, anomaly attribution, and investigations of stacked reservoirs for oil and gas exploration (Ballentine et al., 1991). Developing these models has the potential to demonstrate that fugitive CO_2 is significantly attenuated by sorption in addition to solubility trapping (Gilfillan et al., 2009).

Quantifying the volumes and rates of fluid migrations is challenging because of the discontinuous nature of breakthrough and charging events (MacDonald et al., 2000). At Site 2, a soil gas survey at the beginning of field production documented significant thermogenic seepage (Horvitz, 1969). A repeat survey in 1968 showed less seepage

leading to the interpretation of seepage decline from field production and migration faster than 22 years. An analogous approach was taken at Coal Oil Point, CA indicating seepage attenuated also within 22 years (Quigley et al., 1999). While it is possible that continuous seepage terminated, another interpretation is that seepage occurred as episodic events and thereby migrates through the sedimentary column over 1,000 to 100,000 year timescales (Roberts and Carney, 1997). Consequently, the process of seepage at hydrocarbon systems does not indicate that significant CO_2 volumes will reach the near-surface during the GCS project lifespan. However, for the purposes of fluid anomaly attribution, migrated CO_2 is expected to be accompanied by elevated noble gas concentrations.

4.8 FIGURES AND TABLES

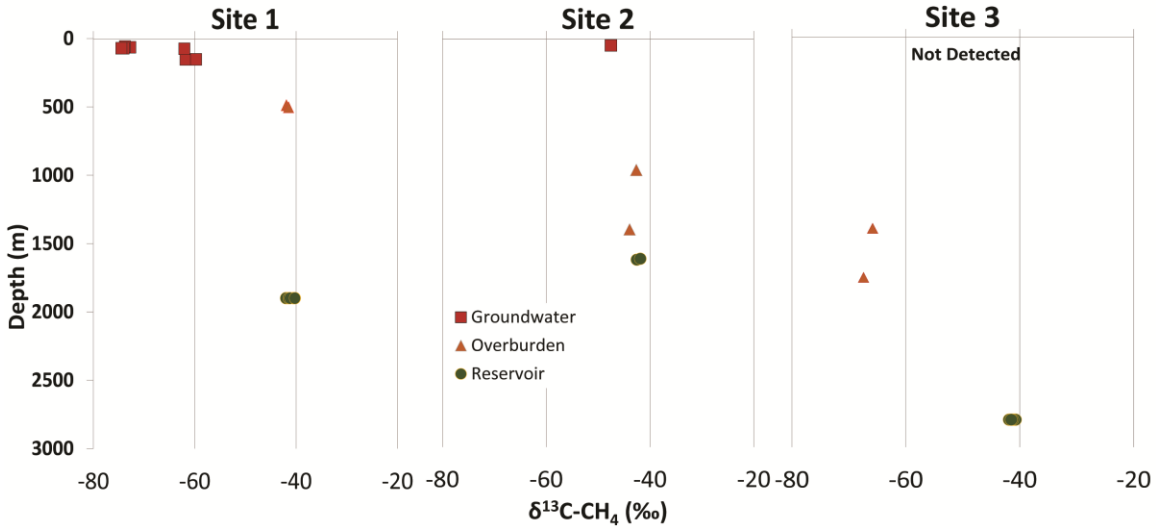

Figure 4.1. Methane carbon and hydrogen stable isotopes versus depth at each site showing the intervals sampled and analyzed.

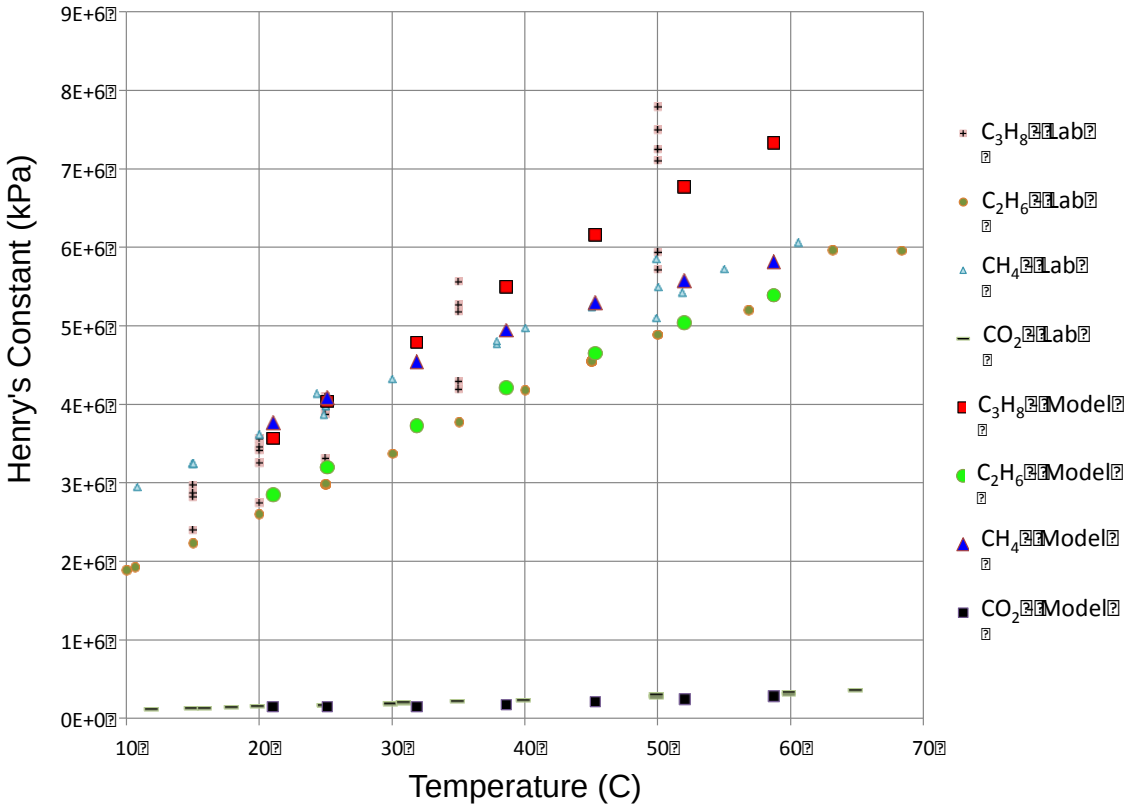

Figure 4.2. Henry's constants (kPa) of methane (CH_4), ethane (C_2H_6), propane (C_3H_8), and CO_2. CH_4: Krause and Benson, 1989; Crovetto et al., 1982. C_3H_8: Chapoy et al., 2004. CH_4, C_2H_6, and C_3H_8: Dhima et al., 1999. These data were interpolated to use at the temperatures associated with the geothermal gradient at selected depth intervals.

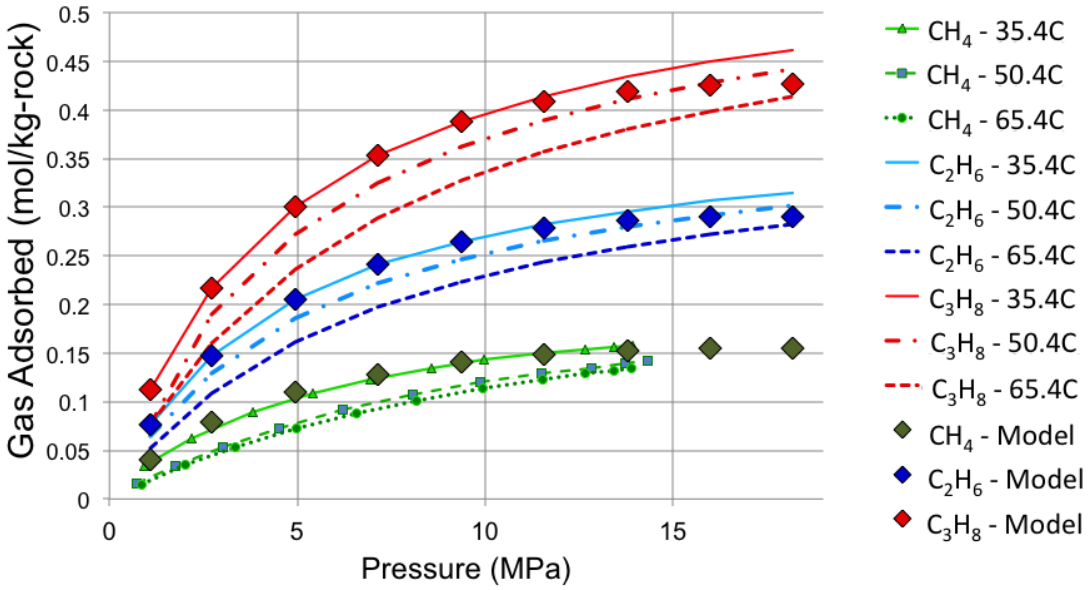

Figure 4.3. Langmuir isotherms for methane (CH_4), ethane (C_2H_6), and propane (C_3H_8). The green triangles, squares, and circles are methane laboratory results from Zhang et al. (2012). The blue and red lines are methane isotherms that have maximum adsorbed moles scaled to the molecular weights of ethane and propane, respectively. Green, blue, and red lines are isotherms used in the dynamic model. The diamonds are interpolated values for the static model.

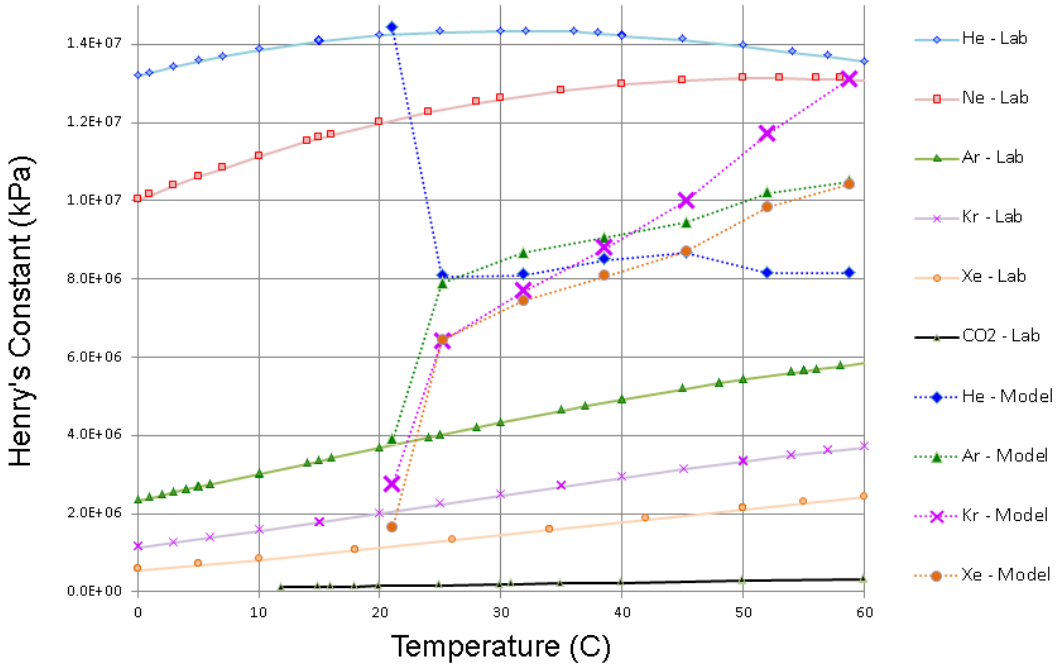

Figure 4.4. Henry's constants (kPa) for helium (He; blue diamonds), neon (Ne; red squares), argon (Ar; green triangles), krypton (Kr; pink x's), and xenon (Xe; orange circles) (Benson and Krause, 1989). These Henry's calculations were adjusted based on equations in Warr et al. (2016) as a function of CO_2 density. The CO_2 density was calculated at pressure and temperature of the model layers using CMG-GEM.

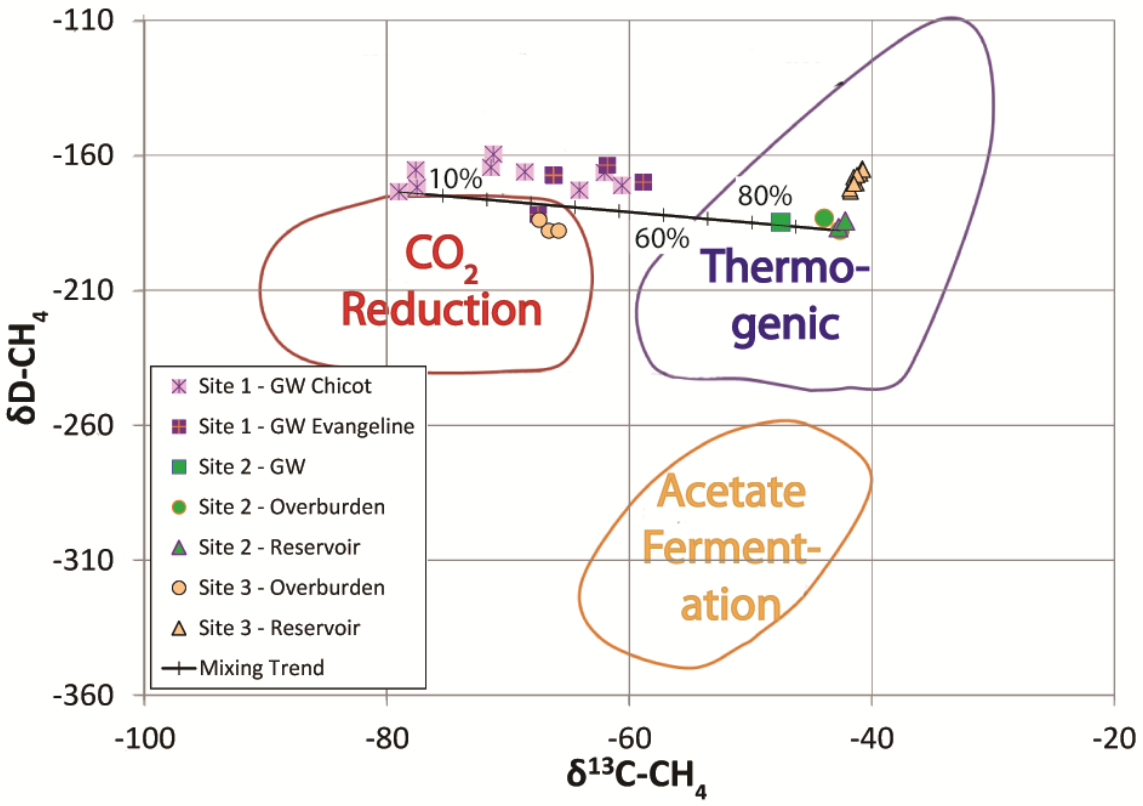

Figure 4.5. Stable carbon and hydrogen isotopes of methane along with classifications by Schoell (1980). The percent of thermogenic methane at sites 1 and 2 is interpreted from a mixing trend assuming that reservoir methane at Site 2 is the thermogenic end member and that the groundwater sample with the lightest carbon isotopes is the biogenic end member.

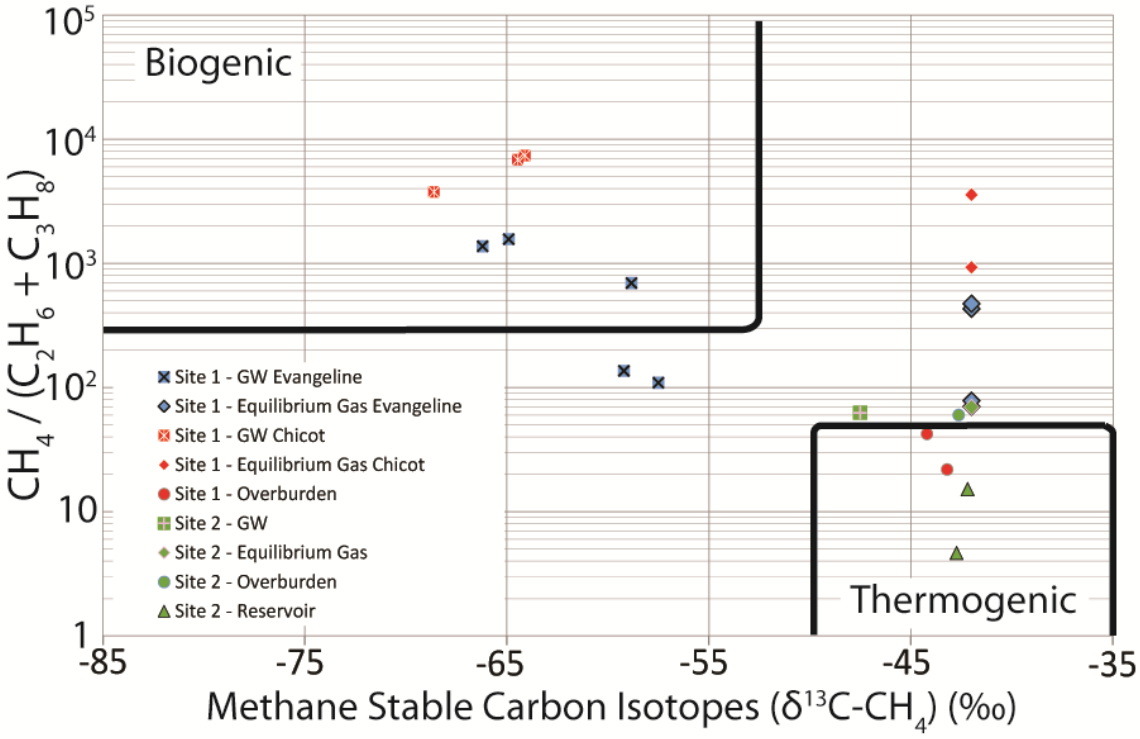

Figure 4.6. Methane stable carbon isotopes versus the Bernard ratio (methane / [ethane + propane]) for samples from sites 1 and 2 The Bernard ratios of groundwater samples have been adjusted based on the amount of thermogenic gas from the mixing trend in Fig. 4.5. Then, a hypothetical gas composition was calculated that would produce this thermogenic dissolved Bernard ratio.

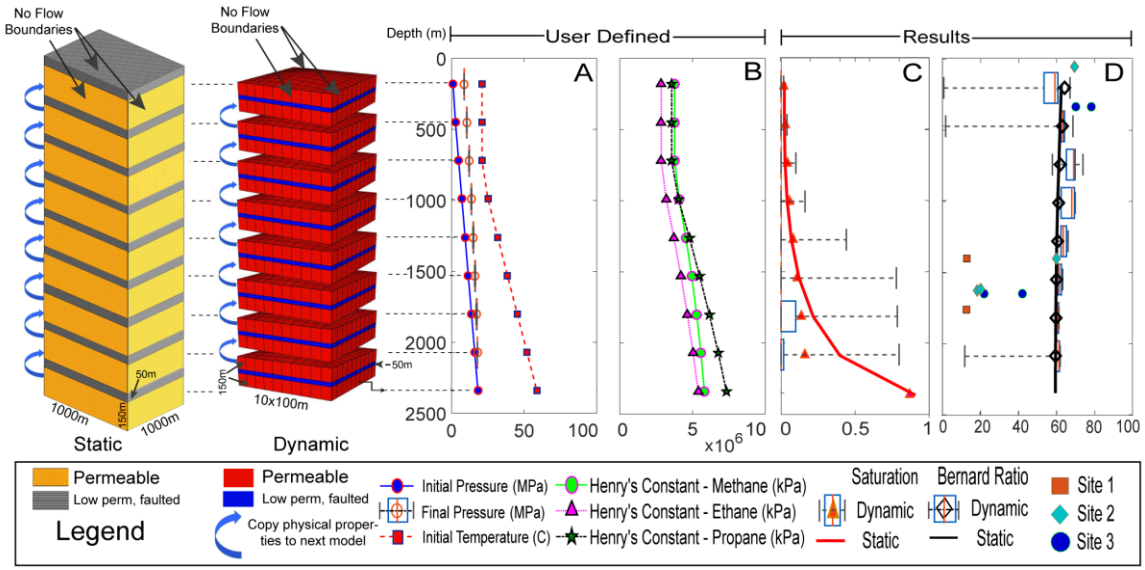

Figure 4.7. Static and dynamic results for solubility calculations. The two graphs on the left show the model geometries. For the static model, half of the gas moles are assumed to migrate to the next layer for the subsequent calculation. For the dynamic model, the gas mole fractions, pressures, and saturations of the top layer are set as initial conditions for the bottom layer. Panel A shows hydrostatic pressure and temperatures used for the static model and initial conditions of the dynamic model. Final pressures of the dynamic model are shown as box and whiskers plots. Panel B shows Henry's constants (kPa) versus depth (m). Panel C shows the saturation of the static model (red line) and dynamic model (box and whiskers plot; red triangle is mean weighted by moles in each cell). Panel D shows Bernard ratio increases from static (black line) and dynamic (box and whiskers plot) models. Field data from sites 1–3 are squares, diamonds, and circles, respectively.

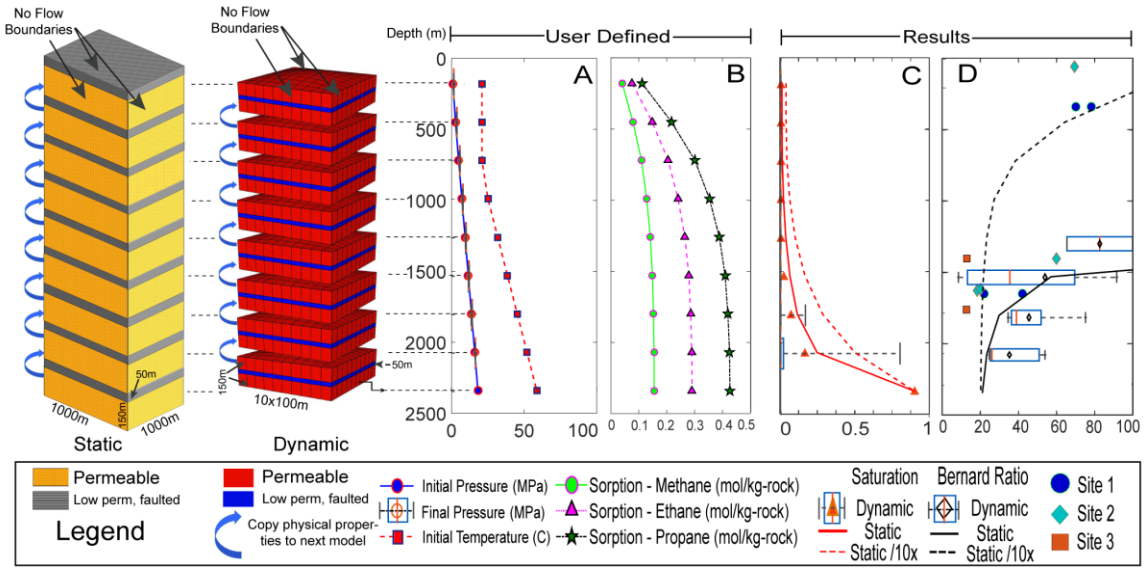

Figure 4.8. Static and dynamic results for sorption calculations. The two graphs on the left show the model geometries. Panel A shows hydrostatic pressure and temperatures used for the static model and initial conditions of the dynamic model. Final pressures of the dynamic model are shown as box and whiskers plots. Panel B shows sorption (moles/kg-rock) versus depth (m) used and input parameters. Panel C shows the saturation of the static model (red line) and dynamic model (box and whiskers plot; red triangle is mean weighted by moles in each cell). Panel D shows Bernard ratio increases from static (black line) and dynamic (box and whiskers plot) models. The dashed lines in panels C and D assume rock volume contacted by gas is an order or magnitude less. Field data from sites 1–3 are squares, diamonds, and circles, respectively.

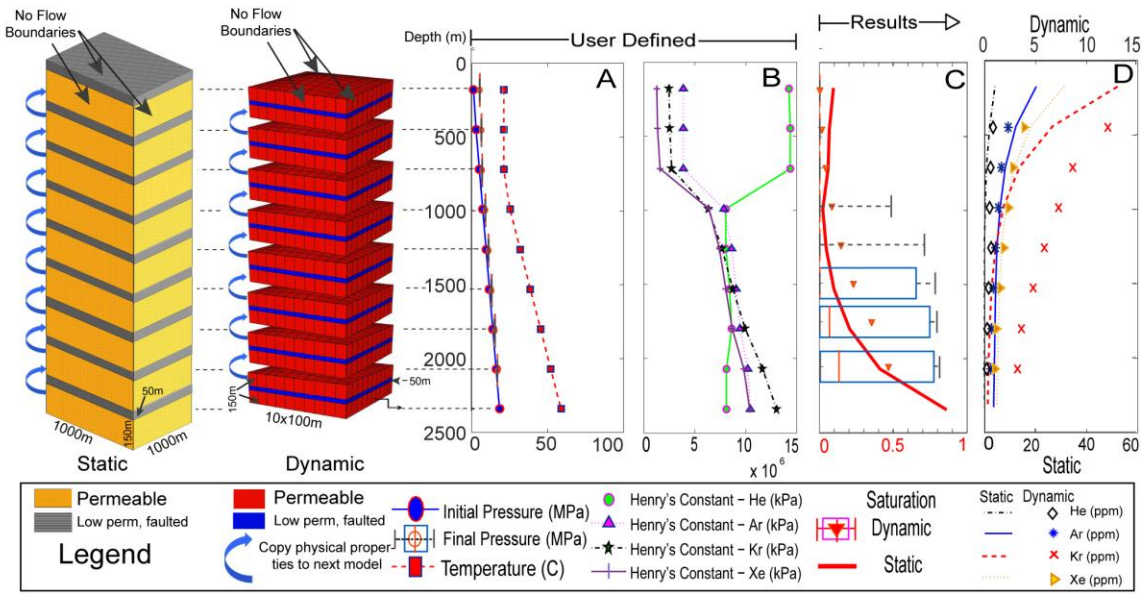

Figure 4.9. Static and dynamic results for CO_2 forward model. The two graphs on the left show the model geometries. For the static model, half of the gas moles are assumed to migrate to the next layer for the subsequent calculation. For the dynamic model, the gas mole fractions, pressures, and saturations of the top layer are set as initial conditions for the bottom layer. Panel A shows hydrostatic pressure and temperatures used for the static model and initial conditions of the dynamic model. Final pressures of the dynamic model are shown as box and whiskers plots. Panel B shows Henry's constants (kPa) versus depth (m). Panel C shows the saturation of the static model (red line) and dynamic model (box and whiskers plot; red triangle is mean weighted by moles in each cell). Saturation increases in the static model during the CO_2 phase change. Panel D shows the concentrations of helium, argon, krypton, and xenon.

Table 4.1. Hydrocarbon compositions and stable isotopes of groundwater samples. The Bernard ratios of a gas in equilibrium with groundwater were calculated with Henry's constants of 3,608,964, 2,595,146, and 3,411,162 kPa for methane, ethane, and propane, respectively.

Sample ID	Site Number	Date sampled	CH4 (mg/L)	C2H6 (mg/L)	C3H8 (mg/L)	δ13C-CH4	δD-CH4	Bernard Ratio	% Thermogenic	Bernard Ratio of Equilibrium Gas
GW1	1, E	11/8/2012	10.630	0.015	BDL	-58.83	-170.00	606.06	44.66	361.9
GW1	1, E	12/22/2015	20.716	0.169	0.021	-57.50		109.14	47.83*	70.15
GW1	1, E	3/23/2016	20.147	0.121	0.027	-59.20		136.18	43.76*	78.37
GW2	1, E	11/8/2012	11.370	BDL	BDL	-61.80	-163.70		31.68	
GW2	1, E	12/22/2015	9.903	0.007	BDL	-66.20	-167.56	969.45	24.83	306.4
GW2	1, E	3/21/2016	9.364	0.006	BDL	-64.90		1042.17		
GW3	1, C	10/30/2012	11.470	BDL	BDL	-62.02	-166.40		33.69	
GW3	1, C	12/22/2015	12.637	BDL	BDL	-71.40	-164.56		9.64	
GW3	1, C	3/22/2016	13.481	BDL	BDL	-71.44				
GW4	1, E	10/31/2012	17.980	BDL	BDL	-66.26	-167.30		24.44	
GW4	1, E	12/21/2015	23.537	BDL	BDL	-67.50	-181.99		35.26	
GW4	1, E	3/21/2016	16.299	BDL	BDL	-67.14				
GW5	1, C	12/21/2015	24.255	BDL	BDL	-60.60	-171.22		41.59	
GW5	1, C	3/21/2016	16.299	BDL	BDL	-60.9				
GW6	1, C	12/21/2015	11.042	0.003	BDL	-68.60	-166.22	1858.51	17.86	398.3
GW6	1, C	3/21/2016	12.224	BDL	BDL					
GW7	1, C	12/22/2015	11.946	BDL	BDL	-71.20	-159.67		5.53	
GW7	1, C	3/23/2016	12.635	BDL	BDL	-71.44				
GW8	1, C	12/22/2015	8.203	BDL	BDL	-77.60	-165.42		4.32	
GW8	1, C	3/21/2016	8.397	BDL	BDL	-76.65				
GW9	1, C	12/21/2015	15.578	0.002	BDL	-64.10	-172.98	3050.28	34.91	1249.9
GW9	1, C	3/22/2016	16.226	0.002	BDL	-64.45		3020.23		
GW10	1, C	12/21/2015	0.762	BDL	BDL	-75.00				
GW10	1, C	3/22/2016	4.664	BDL	BDL	-75.21				
GW11	1, C	12/21/2015	6.578	BDL	BDL	-77.50	-171.97		2.06	
GW11	1, C	3/23/2016	6.490	BDL	BDL	-75.65				
GW12	1, C	12/21/2015	7.901	BDL	BDL	-79.00	-173.58		0.01	
GW12	1, C	3/21/2016	7.833	BDL	BDL	-77.45				
GW1	2	1/21/2016	16.71	0.206	0.061	-47.51	-184.4	65.62	85.4	69.6

*Note: The percent thermogenic calculations in these samples from GW1, Site 1 assume that δD-CH4 is -170.0.

Table 4.2. Hydrocarbon compositions and stable isotopes of overburden gas samples.

Sample ID	Site Number	Type of Sample	Date Sampled	CH4 (ppm)	C2H6 (ppm)	C3H8 (ppm)	n-C4H10	i-C4H10	n-C5H12	i-C5H12	Bernard Ratio	δ13C CH4
Overburden 1	1	gas	1/30/17	83.11	2.79	1.01	0.75	0.48	0.42	0.32	21.86	-43.2
Overburden 2	1	gas	1/30/17	25.20	0.56	0.04	0.15	0.01	0.03	nd	42.29	-44.2
Overburden 1	2	gas	1/21/16	99.30	1.36	0.30	0.07	0.07	0.02	0.03	60.00	-41.8
Overburden 2	2	gas	1/21/16	101.97	nd	nd	Nd	nd	nd	0.00	NA	-42.5

Notes: ”nd” = not detected. ‘ ‘ = not analyzed. ”NA” is not applicable. The Bernard ratio is the concentrations of $CH_4/(C_2H_6+C_3H_8)$.

Table 4.3. Noble gas isotopic ratios for overburden and groundwater samples. Note: The ^{40}Ar concentration used in the $^{4}He/^{40}Ar$ ratio was corrected for atmospheric ^{40}Ar contributions samples following Ballentine et al. (1991).

Sample Name	Site Name	$\frac{R}{R_A}$	$\frac{^{21}Ne}{^{22}Ne}$	$\frac{^{40}Ar}{^{36}Ar}$	$\frac{^{82}Kr}{^{84}Kr}$	$\frac{^{136}Xe}{^{132}Xe}$	$\frac{^{4}He}{^{40}Ar_{rad}}$
Air Saturated Water		**1.0**	**0.0289**	**295.50**	**0.203**	**0.329**	
OB 1	Site 1	0.0378	0.0298	386.171	0.2048	0.3316	4.02
OB 2	Site 1	0.0502	0.0289	315.093	0.2035	0.3286	1.09
GW 1	Site 1	0.0324	0.0289	302.546	0.2034	0.3310	1.66
GW 2	Site 1	0.0380	0.0289	296.154	0.2036	0.3301	6.29
OB 1	Site 2	0.0166	0.0290	472.366	0.2107	0.3291	2.29
OB 2	Site 2	0.0208	0.0287	313.605	0.2030	0.3401	13.15
GW1	Site 2	0.0590	0.0296	306.699	0.2036	0.3145	0.23

4.9 REFERENCES

Abrams, M. A. (2005). Significance of hydrocarbon seepage relative to petroleum generation and entrapment. *Marine and Petroleum Geology*, *22*(4), 457–477.

Anderson, J. S., Romanak, K. D., Yang, C., Lu, J., Hovorka, S. D., & Young, M. H. (2017). Gas source attribution techniques for assessing leakage at geologic CO_2 storage sites: Evaluating a CO_2 and CH_4 soil gas anomaly at the Cranfield CO_2-EOR site. *Chemical Geology*, *454*, 93–104.

Arri, L. E., Yee, D., Morgan, W. D., & Jeansonne, M. W. (1992). Modeling coalbed methane production with binary gas sorption. In *SPE rocky mountain regional meeting*. Society of Petroleum Engineers.

Ballentine, C. J., O'nions, R. K., Oxburgh, E. R., Horvath, F., & Deak, J. (1991). Rare gas constraints on hydrocarbon accumulation, crustal degassing and groundwater flow in the Pannonian Basin. *Earth and Planetary Science Letters*, *105*(1–3), 229–246.

Benson, B. B., & Krause Jr, D. (1976). Empirical laws for dilute aqueous solutions of nonpolar gases. *The Journal of Chemical Physics*, *64*(2), 689–709.

Brown, A. (2000). Evaluation of possible gas microseepage mechanisms. *AAPG Bulletin*, *84*(11), 1775–1789.

Christie, C. H., & Nagihara, S. (2016). Geothermal gradients of the northern continental shelf of the Gulf of Mexico. *Geosphere*, *12*(1), 26–34.

Computer Modeling Group Ltd.: Calgary, Canada http://www.cmgroup.com/ (2015)

Crovetto, R., Fernández-Prini, R., & Japas, M. L. (1982). Solubilities of inert gases and methane in H_2O and in D_2O in the temperature range of 300 to 600 K. *Journal of Chemical Physics*, 76(2), 1077–1086.

Cui X., Bustin A. M. M. & Bustin R. M. (2009) Measurements of gas permeability and diffusivity of tight reservoir rocks: different approaches and their applications. *Geofluids* 9, 208–223.

Deville, E., Battani, A., Griboulard, R., Guerlais, S., Herbin, J. P., Houzay, J. P., Connelly, D., James, R.H., Kita, J., Long, D., & Prinzhofer, A. (2003). The origin and processes of mud volcanism: new insights from Trinidad. *Geological Society, London, Special Publications*, *216*(1), 475–490.

Dixon, T., & Romanak, K. D. (2015). Improving monitoring protocols for CO_2 geological storage with technical advances in CO_2 attribution monitoring. *International Journal of Greenhouse Gas Control*, *41*, 29–40.

Dhima, A., de Hemptinne, J. C., & Jose, J. (1999). Solubility of hydrocarbons and CO_2 mixtures in water under high pressure. *Industrial & engineering chemistry research*, *38*(8), 3144–3161.

Dzyaloshinskii, I. E., Lifshitz, E. M., & Pitaevskii, L. P. (2012). Van der Waals forces in liquid films. *Perspectives in Theoretical Physics: The Collected Papers of E\M\Lifshitz*, 425 p.

Etiope, G., Feyzullayev, A., & Baciu, C. L. (2009). Terrestrial methane seeps and mud volcanoes: a global perspective of gas origin. *Marine and Petroleum Geology*, *26*(3), 333–344.

Fuex, A. N. (1980). Experimental evidence against an appreciable isotopic fractionation of methane during migration. *Physics and Chemistry of the Earth*, *12*, 725–732.

Galloway, W. E., Hobday, D. K., & Magara, K. (1982). Frio formation of the Texas Gulf Coast Basin-Depositional systems, structural framework, and hydrocarbon origin, migration, distribution, and exploration potential. *Rep. Invest., Univ. Tex. Austin, Bur. Econ. Geol.;(United States)*, *122*.

Gilfillan, S. M., Lollar, B. S., Holland, G., Blagburn, D., Stevens, S., Schoell, M., Cassidy, M., Ding, Z., Zhou, Z., Lacrampe-Couloume, G., & Ballentine, C. J. (2009). Solubility trapping in formation water as dominant CO2 sink in natural gas fields. *Nature*, *458*(7238), 614–618.

Gilfillan, S. M., Wilkinson, M., Haszeldine, R. S., Shipton, Z. K., Nelson, S. T., & Poreda, R. J. (2011). He and Ne as tracers of natural CO 2 migration up a fault from a deep reservoir. *International Journal of Greenhouse Gas Control*, *5*(6), 1507–1516.

Graham, D. W. (2002). Noble gas isotope geochemistry of mid-ocean ridge and ocean island basalts: Characterization of mantle source reservoirs. *Reviews in mineralogy and geochemistry*, *47*(1), 247–317.

Halbouty, M. T. , (1937) "Geology and Economic Significance of Hastings Field", World Petroleum, September, pp. 26–51.

Hood, K. C., Wenger, L. M., Gross, O. P., & Harrison, S. C. (2002). Hydrocarbon systems analysis of the northern Gulf of Mexico: Delineation of hydrocarbon migration pathways using seeps and seismic imaging. *Surface exploration case histories:*

Applications of geochemistry, magnetics, and remote sensing: AAPG Studies in Geology, *48*, 25–40.

Horvitz, L. (1969). Hydrocarbon geochemical prospecting after thirty years (pp. 205–218). Southern Methodist University, Institute for the Study of Earth and Man, SMU Press.

Hovorka, S. D., Meckel, T. A., Trevino, R. H., Lu, J., Nicot, J. P., Choi, J. W., Freeman, D., Cook, P., Daley, T.M., Ajo-Franklin, J.B. & Butsch, R. J. (2011b). Monitoring a large volume CO_2 injection: Year two results from SECARB project at Denbury's Cranfield, Mississippi, USA. *Energy Procedia*, *4*, 3478–3485.

Hudec, M. R., & Jackson, M. P. (2007). Terra infirma: Understanding salt tectonics. *Earth-Science Reviews*, *82*(1), 1–28.

Hunt, J. M. (1990). Generation and migration of petroleum from abnormally pressured fluid compartments (1). *AAPG Bulletin*, *74*(1), 1–12.

Jones, D. G., Beaubien, S. E., Blackford, J. C., Foekema, E. M., Lions, J., De Vittor, C., West, J. M., Widdicombe, S., Hauton, C., and Queirós, A. M. (2015). Developments since 2005 in understanding potential environmental impacts of CO_2 leakage from geological storage. *International Journal of Greenhouse Gas Control.* DOI 10.1016/j.ijggc.2015.05.032.

Kampbell, D. H., & Vandegrift, S. A. (1998). Analysis of dissolved methane, ethane, and ethylene in ground water by a standard gas chromatographic technique. *Journal of chromatographic science*, *36*(5), 253–256.

Kettel, D. (1996). A method for processing adsorbed methane stable isotope data from the near surface based on fractionation. *AAPG Special Volumes.* In: Hydrocarbon Migration and Its Near-Surface Expression. 19-336.

Kinnaman, F.S., Valentine, D.L., & Tyler, S.C., 2007. Carbon and hydrogen isotope fractionation associated with the aerobic microbial oxidation of methane, ethane, propane and butane. Geochimica et Cosmochimica Acta *71* (2), 271–283.

Klusman, R. W. (2003). Evaluation of leakage potential from a carbon dioxide EOR/sequestration project. *Energy Conversion and Management*, *44*(12), 1921–1940.

Kharaka, Y. K., & Specht, D. J. (1988). The solubility of noble gases in crude oil at 25–100 C. *Applied Geochemistry*, *3*(2), 137–144.

Kim, A. G., & L. J. Douglas, 1972, Hydrocarbon gases produced in a simulated swamp environment: *United States Bureau of Mines Repository Inventory*. 7690, 15 p.

Leythaeuser, D., Mackenzie, A., Schaefer, R. G., & Bjoroy, M. (1984). A novel approach for recognition and quantification of hydrocarbon migration effects in shale-sandstone sequences. *AAPG Bulletin*, *68*(2), 196–219.

Loughlin, K. F., Hasanain, M. A., & Abdul-Rehman, H. B. (1990). Quaternary, ternary, binary, and pure component sorption on zeolites. 2. Light alkanes on Linde 5A and 13X zeolites at moderate to high pressures. *Industrial & Engineering Chemistry Research*, *29*(7), 1535–1546.

Lu, J., Larson, T. E., & Smyth, R. C. (2015). Carbon isotope effects of methane transport through Anahuac Shale—A core gas study. *Journal of Geochemical Exploration*, *148*, 138–149.

Ma, L., Castro, M. C., & Hall, C. M. (2009). Crustal noble gases in deep brines as natural tracers of vertical transport processes in the Michigan Basin. *Geochemistry, Geophysics, Geosystems*, *10*(6). Q06001, doi:10.1029/2009GC002475.

MacDonald, I. R., Buthman, D. B., Sager, W. W., Peccini, M. B., & Guinasso, N. L. (2000). Pulsed oil discharge from a mud volcano. *Geology*, *28*(10), 907–910.

Nicot, J. P., Oldenburg, C. M., Houseworth, J. E., & Choi, J. W. (2013). Analysis of potential leakage pathways at the Cranfield, MS, USA, CO_2 sequestration site. *International Journal of Greenhouse Gas Control*, *18*, 388–400.

Oldenburg, C. M., Doughty, C., & Spycher, N. (2013). The role of CO_2 in CH_4 exsolution from deep brine: Implications for geologic carbon sequestration. *Greenhouse Gases: Science and Technology*, *3*(5), 359–377.

Oxburgh, E. R., O'nions, R. K., & Hill, R. I. (1986). Helium isotopes in sedimentary basins. *Nature*, *324*, 632–635.

Quigley, D. C., Hornafius, J. S., Luyendyk, B. P., Francis, R. D., Clark, J., & Washburn, L. (1999). Decrease in natural marine hydrocarbon seepage near Coal Oil Point, California, associated with offshore oil production. *Geology*, *27*(11), 1047–1050.

Rice, D. D., & Claypool, G. E. (1981). Generation, accumulation, and resource potential of biogenic gas. *AAPG Bulletin*, *65*(1), 5–25.

Roberts, H. H., & Carney, R. S. (1997). Evidence of episodic fluid, gas, and sediment venting on the northern Gulf of Mexico continental slope. *Economic Geology*, *92*(7–8), 863–879.

Romanak, K., Sherk, G. W., Hovorka, S., & Yang, C. (2013). Assessment of alleged CO_2 leakage at the Kerr farm using a simple process-based soil gas technique: Implications for carbon capture, utilization, and storage (CCUS) monitoring. *Energy Procedia*, *37*, 4242–4248.

Shabro, V., Torres-Verdin, C., & Javadpour, F. (2011, January). Numerical simulation of shale-gas production: from pore-scale modeling of slip-flow, Knudsen diffusion, and Langmuir desorption to reservoir modeling of compressible fluid. In *North American Unconventional Gas Conference and Exhibition*. Society of Petroleum Engineers.

Sherk, G. W., K. D. Romanak, J. Dale, S. M. V. Gilfillan, R. S. Haszeldine, E. S. Ringler, B. D. Wolaver, & C. Yang. "The Kerr investigation: Findings of the investigation into the impact of CO_2 on the Kerr property, final report." *IPAC-CO_2 Inc., Regina, Saskatchewan, Canada* (2011).

Smith, S. P., & Kennedy, B. M. (1983). The solubility of noble gases in water and in NaCl brine. *Geochimica et Cosmochimica Acta*, *47*(3), 503–515.

Spooner Jr, H. V. (1964). Basal Tuscaloosa sediments, east-central Louisiana. *AAPG Bulletin*, *48*(1), 1–21.

Suekane, T., Nobuso, T., Hirai, S., & Kiyota, M. (2008). Geological storage of carbon dioxide by residual gas and solubility trapping. *International Journal of Greenhouse Gas Control*, *2*(1), 58–64.

Trevisan, L., R. Pini, A. Cihan, J. T. Birkholzer, Q. Zhou, A. GonzalezNicolas, & T. H. Illangasekare (2017), Imaging and quantification of spreading and trapping of carbon dioxide in saline aquifers using meterscale laboratory experiments, *Water Resources Research*, *53*, doi:10.1002/2016WR019749.

Weaver,L.K., Anderson,K.F., (1966). Cranfield Field, Cranfield Unit, Basal Tuscaloosa reservoir, Adams and Franklin Counties, Mississippi, in Oil Recovery from Gas-Cap Reservoirs: an Engineering Evaluation of Conservation Practices in Six Reservoirs. Interstate Oil Compact Commission, Oklahoma City, pp. 42–58.

Warr, O., Rochelle, C.A., Masters, A. and Ballentine, C.J. (2015) Determining noble gas partitioning within a CO_2 –H_2O system at elevated temperatures and pressures. *Geochimica et Cosmochimica Acta 159*, 112–125.

Warwick, P. D. (2004). Bacterial Reduction of CO_2: The Primary Origin of Low-Rank Coal Gas in the Northern Gulf of Mexico Coastal Plain, USA. *Abstracts of the 21th Annual Meeting of the Society for Organic Petrology*, Vol. 21.

Whiticar, M. J. (1999). Carbon and hydrogen isotope systematics of bacterial formation and oxidation of methane. *Chemical Geology*, *161*(1), 291–314.

Xia, X., & Tang, Y. (2012). Isotope fractionation of methane during natural gas flow with coupled diffusion and adsorption/desorption. *Geochimica et Cosmochimica Acta*, *77*, 489–503.

Yang, C., Romanak, K., Hovorka, S. D., Holt, R. M., Lindner, J., & Trevino, R. (2013). Near-surface monitoring of large-volume CO2 injection at Cranfield: Early field test of SECARB phase III. *SPE Journal*, *18*(03), 486–494.

Zhang, Tongwei, et al. "Effect of organic-matter type and thermal maturity on methane adsorption in shale-gas systems." *Organic Geochemistry* 47 (2012): 120–131.

Zhou, Zheng, Chris J. Ballentine, Martin Schoell, and Scott H. Stevens. "Identifying and quantifying natural CO 2 sequestration processes over geological timescales: the Jackson Dome CO 2 Deposit, USA." *Geochimica et Cosmochimica Acta* 86 (2012): 257–275.

Chapter 5: Conclusions

5.1 CONCLUSIONS

For millions of years, light hydrocarbons and CO_2 have been naturally generated in the earth and migrated up to shallower intervals. Upward fluid migration is classified as a ”problem” by some stakeholders when it is caused by industrial operations instead of natural processes (Jackson et al., 2013).

The emphasis on possible migration should not be a barrier for GCS or shale gas projects because of the lack of actual leakage cases. Field studies investigating high concentrations of CO_2 or light hydrocarbons above GCS or shale gas sites were shown to originate naturally (Jackson et al., 2013; Romanak et al., 2013; Gilfillan et al., 2017). This research intended to address leakage concerns by formalizing the process of attributing fluid anomalies with fundamental understanding of gas origin and alteration.

Investigation of an onshore anomaly in Chapter 2 was consistent with other field sites showing non-leakage. However, the value of this anomaly was as an opportunity to evaluate and compare geochemical tools in a CO_2 Enhanced Oil Recovery setting. These results demonstrated to stakeholders and the scientific community that non-leakage can be identified with the current geochemical tools available.

The geochemical approach to anomaly attribution is similar in an offshore environment, but fluid sampling is more challenging. Previous offshore carbon storage projects at Sleipner and Snohvit monitored for CO_2 but did not detect anomalies (Eiken et al., 2011). This research initiated offshore anomaly attribution with a coring survey

detailed in Chapter 3, but piston cores did not reach sufficient penetration depths for sampling. Future work is needed to evaluate alternative methodologies that ensure samples are taken at deeper zones. The value of Chapter 3 to the scientific community and GCS stakeholders is that gas chimneys structures observed on seismic do not necessarily signify that gas reaches the seafloor.

One of the challenges in interpreting fluid sources is predicting leakage compositions. A key missing dataset is CO_2 compositions that have migrated up through the sedimentary column at a continental margin. This research made progress on this issue by theoretically simulating gas migration undergoing two alteration processes in Chapter 4. These results are valuable because they show possible trends in alteration, but much work still remains.

The degree to which fluids are altered depends on their interaction with water and rock. There are a wide range of migration scenarios ("burping" (Hunt et al., 1999), migration up faults or fractures (Etiope et al., 2013), soft sediment mobilization (Loseth et al., 2009)) that each contact varying degrees of water and earth materials. This fact may be leveraged in the future so that gas pathways are interpreted from geochemical changes.

Interpretations of fluid pathway would require significant work investigating fluid flow and alteration. Ideally, alteration could be documented with meter-scale experiments of high-pressure, high temperature CO_2 migrating up through sedimentary rocks. Another valuable test would be to measure CO_2 compositions as it travels up through stacked, interconnected reservoirs. At the Sliepner GCS sites, CO_2 injection initiated in

the lower-most reservoir below the sealing formation and was observed to migrate up on 4D seismic (Eiken et al., 2011). If this geologic setting and field operations occur at other GCS sites, then sampling from wells penetrating these reservoirs could document CO_2 vertical migration and alteration.

5.2 REFERENCES

Eiken, O., Ringrose, P., Hermanrud, C., Nazarian, B., Torp, T. A., & Høier, L. (2011). Lessons learned from 14 years of CCS operations: Sleipner, In Salah and Snøhvit. *Energy Procedia*, *4*, 5541–5548.

Etiope, G., Drobniak, A., & Schimmelmann, A. (2013). Natural seepage of shale gas and the origin of "eternal flames" in the Northern Appalachian Basin, USA. *Marine and petroleum geology*, *43*, 178–186.

Gilfillan, S. M., Sherk, G. W., Poreda, R. J., & Haszeldine, R. S. (2017). Using noble gas fingerprints at the Kerr Farm to assess CO_2 leakage allegations linked to the Weyburn-Midale CO_2 monitoring and storage project. *International Journal of Greenhouse Gas Control*, *63*, 215–225.

Hunt, J. M. (1990). Generation and migration of petroleum from abnormally pressured fluid compartments (1). *AAPG bulletin*, *74*(1), 1–12.

Jackson, R. B., Vengosh, A., Darrah, T. H., Warner, N. R., Down, A., Poreda, R. J., Osborn, S.G., Zhao, K. & Karr, J. D. (2013). Increased stray gas abundance in a subset of drinking water wells near Marcellus shale gas extraction. *Proceedings of the National Academy of Sciences*, *110*(28), 11250–11255.

Løseth, H., Gading, M., & Wensaas, L. (2009). Hydrocarbon leakage interpreted on eismic data. *Marine and Petroleum Geology*, *26*(7), 1304–1319.

BIBLIOGRAPHY

Abdullah, K., Anderson, J., Snow, J., & Holdford-Jack, L. (2004). The Late Quaternary Brazos and Colorado Deltas. *Offshore Texas, USA—Their evolution and the factors that controlled their deposition: SEPM Special Publication*, *79*, 237–269.

Abrams, M. A. (1992). Geophysical and geochemical evidence for subsurface hydrocarbon leakage in the Bering Sea, Alaska. *Marine and Petroleum Geology*, *9*(2), 208–221.

Abrams (1996). Distribution of Subsurface Hydrocarbon Seepage in Near-Surface Marine Sediments, in: D. Schumacher and M. A. Abrams, eds., Hydrocarbon migration and its near-surface expression: *AAPG Memoir 66*, p. 1–14.

Abrams, M. A. (2005). Significance of hydrocarbon seepage relative to petroleum generation and entrapment. *Marine and Petroleum Geology*, *22*(4), 457–477.

Aeschbach-Hertig, W., El-Gamal, H., Wieser, M., & Palcsu, L. 2008. Modeling excess air and degassing in groundwater by equilibrium partitioning with a gas phase. *Water Resources Research*, 44(8). W08449, doi:10.1029/2007WR006454.

Allen, P. A., & Allen, J. R. (2013). Basin analysis: principles and application to petroleum play assessment. Oxford, UK: John Wiley & Sons. 632.

Anderson, R. K., Scalan, R. S., Parker, P. L., & Behrens, E. W. (1983). Seep oil and gas in Gulf of Mexico slope sediment. *Science*, *222*(4624), 619–621.

Anderson, J. S., Romanak, K. D., Yang, C., Lu, J., Hovorka, S. D., & Young, M. H. (2017). Gas source attribution techniques for assessing leakage at geologic CO_2 storage sites: Evaluating a CO_2 and CH_4 soil gas anomaly at the Cranfield CO_2-EOR site. *Chemical Geology*, *454*, 93–104.

Aravena, R., Wassenaar, L.I., & Plummer, L.N., 1995. Estimating ^{14}C groundwater ages in a methanogenic aquifer. *Water Resources Research, 31*, 2307–2317.

Arri, L. E., Yee, D., Morgan, W. D., & Jeansonne, M. W. (1992). Modeling coalbed methane production with binary gas sorption. In: *SPE Rocky Mountain Regional Meeting*. Society of Petroleum Engineers.

Azam, F. (1998). Microbial control of oceanic carbon flux: the plot thickens. *Science*, *280*(5364), 694.

Ballentine, C.J., O'nions, R.K., Oxburgh, E.R., Horvath, F., & Deak, J. 1991. Rare gas constraints on hydrocarbon accumulation, crustal degassing and groundwater flow in the Pannonian Basin. *Earth and Planetary Science Letters*, *105*(1-3), 229–246.

Berg, R.L., & Cook, B.C., 1968. Petrography and origin of lower Tuscaloosa sandstones, Mallalieu field, Lincoln County, Mississippi. *Gulf Coast Association of Geological Societies Transactions*, *18*, 242–255.

Benson, B. B., & Krause Jr, D. (1976). Empirical laws for dilute aqueous solutions of nonpolar gases. *The Journal of Chemical Physics*, *64*(2), 689–709.

Bernard, B. B., Brooks, J. M., & Sackett, W. M. (1976). Natural gas seepage in the Gulf of Mexico. *Earth and Planetary Science Letters*, *31*(1), 48–54.

Bernard, B. B. 1978. Light hydrocarbons in Marine Sediments. *Texas Agriculture and Mechanical University PhD Disseration.*

Bernard, B. B., Orange, D. L., Brooks, J. M., & Decker, J. (2013). Interstitial Light Hydrocarbon Gases in Jumbo Piston Cores Offshore Indonesia: Thermogenic or Biogenic?. In: *Offshore Technology Conference*. Offshore Technology Conference.

Blackford, J., Stahl, H., Bull, J. M., Berges, B. J., Cevatoglu, M., Lichtschlag, A., Connelly, D., James, R.H., Kita, J., Long, D. & Naylor, M. (2014). Detection and impacts of leakage from sub-seafloor deep geological carbon dioxide storage. *Nature Climate Change*, *4*(11), 1011–1016.

Bowling, D.R., Pataki, D.E., & Randerson, J.T. 2008. Carbon isotopes in terrestrial ecosystem pools and CO_2 fluxes. *New Phytologist*, 178(1), 24–40.

Brown, A. (2000). Evaluation of possible gas microseepage mechanisms. *AAPG Bulletin*, *84*(11), 1775–1789.

Cartwright, J., Huuse, M., & Aplin, A. (2007). Seal bypass systems. *AAPG Bulletin*, *91*(8), 1141–1166.

Castro, M.C., Jambon, A., Marsily, G., & Schlosser, P. 1998. Noble gases as natural tracers of water circulation in the Paris Basin: 1. Measurements and discussion of their origin and mechanisms of vertical transport in the basin. *Water Resources Research*, *34*(10), 2443–2466.

Christie, C. H., & Nagihara, S. (2016). Geothermal gradients of the northern continental shelf of the Gulf of Mexico. *Geosphere*, *12*(1), 26–34.

Computer Modeling Group Ltd.: Calgary, Canada http://www.cmgroup.com/ (2015)

Coplen, T. B. (1995). Reporting of stable hydrogen, carbon, and oxygen isotopic abundances. *Geothermics*, *24*(5–6), 707–712.

Crovetto, R., Fernández-Prini, R., & Japas, M. L. (1982). Solubilities of inert gases and methane in H_2O and in D_2O in the temperature range of 300 to 600 K. *The Journal of Chemical Physics*, *76*(2), 1077–1086.

Cui X., Bustin A. M. M. and Bustin R. M. (2009). Measurements of gas permeability and diffusivity of tight reservoir rocks: different approaches and their applications. *Geofluids 9*, 208– 223.

Darrah, T.H., Vengosh, A., Jackson, R.B., Warner, N.R., and Poreda, R.J. 2014. Noble gases identify the mechanisms of fugitive gas contamination in drinking-water wells overlying the Marcellus and Barnett Shales. *Proceedings of the National Academy of Sciences*, *111*(39), 14076–14081.

Deville, E., Battani, A., Griboulard, R., Guerlais, S., Herbin, J. P., Houzay, J. P., Connelly, D., James, R.H., Kita, J., Long, D. & Prinzhofer, A. (2003). The origin and processes of mud volcanism: new insights from Trinidad. *Geological Society, London, Special Publications*, *216*(1), 475–490.

Dhima, A., de Hemptinne, J. C., & Jose, J. (1999). Solubility of hydrocarbons and CO_2 mixtures in water under high pressure. *Industrial & engineering chemistry research*, *38*(8), 3144–3161.

Ding, X., Kennedy, B.M., Evans, W.C., and Stonestrom, D.A. 2016. Experimental studies and model analysis of noble gas fractionation in porous media. *Vadose Zone Journal*, *15*(2).

Dixon, T., and Romanak, K.D., 2015. Improving monitoring protocols for CO_2 geological storage with technical advances in CO_2 attribution monitoring. *International Journal of Greenhouse Gas Control 41*, 29–40.

Echols, D.J., and Malkin, D. 1948. Wilcox (Eocene) Stratigraphy, a key to production. *AAPG Bulletin* 32, 11.

Eichhubl, P., Greene, H. G., Naehr, T., & Maher, N. (2000). Structural control of fluid flow: offshore fluid seepage in the Santa Barbara Basin, California. *Journal of Geochemical Exploration*, *69*, 545–549.

Eiken, O., Ringrose, P., Hermanrud, C., Nazarian, B., Torp, T. A., & Høier, L. (2011). Lessons learned from 14 years of CCS operations: Sleipner, In Salah and Snøhvit. *Energy Procedia*, *4*, 5541-5548.

Etiope, G., Feyzullayev, A., and Baciu, C.L., 2009. Terrestrial methane seeps and mud volcanoes: a global perspective of gas origin. *Marine Petroleum Geology, 26*, 333–344.

Evans, W.C., Sorey, M.L., Kennedy, B.M., Stonestrom, D.A., Rogie, J.D., & Shuster, D.L. 2001. High CO_2 emissions through porous media: transport mechanisms and implications for flux measurement and fractionation. *Chemical Geology*, *177*(1), 15–29.

Faber, E. W., J. Stahl, M. J. Whiticar, J. Lietz, and J. M. Brooks, 1990, Thermal hydrocarbons in Gulf Coast sediments, *in*: Gulf Coast oils and gases: Proceedings of the Ninth Annual Research Conference, SEPM and Mineralogist Foundation, New Orleans, October 1, p. 297–307.

Feitz, A., Jenkins, C., Schacht, U., McGrath, A., Berko, H., Schroder, I., Noble, R., Kuske, T., George, S., Heath, C., and Zegelin, S. 2014. An assessment of near surface CO_2 leakage detection techniques under Australian conditions. *Energy Procedia*, *63*, 3891–3906.

Flude, S., Johnson, G., Gilfillan, S.M., and Haszeldine, R.S. 2016. Inherent tracers for carbon capture and storage in sedimentary formations: composition and applications. *Environmental Science & Technology*, *50*(15), 7939–7955.

Fuex, A. N. (1980). Experimental evidence against an appreciable isotopic fractionation of methane during migration. *Physics and Chemistry of the Earth*, *12*, 725–732.

Galloway, W. E., Hobday, D. K., & Magara, K. (1982). Frio formation of the Texas Gulf Coast Basin-Depositional systems, structural framework, and hydrocarbon origin, migration, distribution, and exploration potential. *Rep. Invest., Univ. Tex. Austin, Bur. Econ. Geol.;(United States)*, *122*.

Galloway, W. E., Whiteaker, T. L., & Ganey-Curry, P. (2011). History of Cenozoic North American drainage basin evolution, sediment yield, and accumulation in the Gulf of Mexico basin. *Geosphere*, *7*(4), 938–973.

Gay, A., Lopez, M., Cochonat, P., Levaché, D., Sermondadaz, G., & Seranne, M. (2006a). Evidences of early to late fluid migration from an upper Miocene turbiditic channel revealed by 3D seismic coupled to geochemical sampling within seafloor pockmarks, Lower Congo Basin. Marine and Petroleum *Geology*, *23*(3), 387–399.

Gay, A., Lopez, M., Cochonat, P., Levaché, D., Sermondadaz, G., & Seranne, M. (2006). Evidences of early to late fluid migration from an upper Miocene turbiditic channel revealed by 3D seismic coupled to geochemical sampling within seafloor pockmarks, Lower Congo Basin. *Marine and Petroleum Geology*, *23*(3), 387–399.

Gemery, P. A., Trolier, M., & White, J. W. (1996). Oxygen isotope exchange between carbon dioxide and water following atmospheric sampling using glass flasks. *Journal of Geophysical Research: Atmospheres*, *101*(D9), 14415–14420.

Gilfillan, S. M., Lollar, B. S., Holland, G., Blagburn, D., Stevens, S., Schoell, M., Cassidy, M., Ding, Z., Zhou, Z., Lacrampe-Couloume, G & Ballentine, C. J. (2009). Solubility trapping in formation water as dominant CO_2 sink in natural gas fields. *Nature*, *458*(7238), 614–618.

Gilfillan, S. M., Wilkinson, M., Haszeldine, R. S., Shipton, Z. K., Nelson, S. T., & Poreda, R. J. (2011). He and Ne as tracers of natural CO 2 migration up a fault from a deep reservoir. *International Journal of Greenhouse Gas Control*, *5*(6), 1507–1516.

Gilfillan, S., Haszeldine, S., Stuart, F., Gyore, D., Kilgallon, R., & Wilkinson, M. 2014. The application of noble gases and carbon stable isotopes in tracing the fate, migration and storage of CO_2. *Energy Procedia, 63*, 4123–4133.

Graham, D. W. (2002). Noble gas isotope geochemistry of mid-ocean ridge and ocean island basalts: Characterization of mantle source reservoirs. *Reviews in mineralogy and geochemistry*, *47*(1), 247–317.

Györe, D., Stuart, F.M., Gilfillan, S.M., & Waldron, S., 2015. Tracing injected CO_2 in the Cranfield enhanced oil recovery field (MS, USA) using He, Ne and Ar isotopes. *International Journal of Greenhouse Gas Control*, 42, 554–561.

Halbouty, M. T., (1937) "Geology and Economic Significance of Hastings Field", *World Petroleum*, September, pp. 26-–Hingst, M.C., 2013. Geochemical Effects of Elevated Methane and Carbon Dioxide in Near-Surface Sediments above an EOR/CCUS Site. The University of Texas at Austin, M.S. Thesis.

Hood, K. C., Wenger, L. M., Gross, O. P., & Harrison, S. C. (2002). Hydrocarbon systems analysis of the northern Gulf of Mexico: Delineation of hydrocarbon migration pathways using seeps and seismic imaging. *Surface exploration case histories: Applications of geochemistry, magnetics, and remote sensing: AAPG Studies in Geology*, *48*, 25–40.

Horvitz, L. (1969). Hydrocarbon geochemical prospecting after thirty years (pp. 205-218). Southern Methodist University, Institute for the Study of Earth and Man, SMU Press.

Hovorka, S.D., Meckel, T.A., Trevino, R.H., Lu, J., Nicot, J.P., Choi, J.W., & Freifeild, B.M. 2011. Monitoring a large volume CO_2 injection: year two results from SECARB project at Denbury's Cranfield, Mississippi, USA. *Energy Procedia*, 4, 3478–3485.

Hovorka, S.D., Meckel, T.A., & Treviño, R.H., 2013. Monitoring a large-volume injection at Cranfield, Mississippi—project design and recommendations, *International Journal of Greenhouse Gas Control* 18, 345–360.

Hudec, M. R., & Jackson, M. P. (2007). Terra infirma: Understanding salt tectonics. *Earth-Science Reviews*, *82*(1), 1–28.

Hunt, J. M. (1990). Generation and migration of petroleum from abnormally pressured fluid compartments (1). *AAPG Bulletin*, *74*(1), 1–12.

Jackson, R. B., Vengosh, A., Darrah, T. H., Warner, N. R., Down, A., Poreda, R. J., Osborn, S.G., Zhao, K. & Karr, J. D. (2013). Increased stray gas abundance in a subset of drinking water wells near Marcellus shale gas extraction. *Proceedings of the National Academy of Sciences*, *110*(28), 11250–11255.

Juanes, R., Spiteri, E. J., Orr, F. M., & Blunt, M. J. (2006). Impact of relative permeability hysteresis on geological CO_2 storage. *Water Resources Research*, *42*(12).

Juanes, R., MacMinn, C. W., & Szulczewski, M. L. (2010). The footprint of the CO_2 plume during carbon dioxide storage in saline aquifers: storage efficiency for capillary trapping at the basin scale. *Transport in Porous Media*, *82*(1), 19–30.

Kampbell, D. H., & Vandegrift, S. A. (1998). Analysis of dissolved methane, ethane, and ethylene in ground water by a standard gas chromatographic technique. *Journal of chromatographic science*, *36*(5), 253–256.

Kennedy, B.M., Lynch, M.A., Reynolds, J.H., & Smith, S P. 1985. Intensive sampling of noble gases in fluids at Yellowstone: I. Early overview of the data; regional patterns. *Geochimica et Cosmochimica Acta*, *49*(5), 1251–1261.

Kettel, D. (1996). A method for processing adsorbed methane stable isotope data from the near surface based on fractionation.

Kharaka, Y. K., & Specht, D. J. (1988). The solubility of noble gases in crude oil at 25–100 C. *Applied Geochemistry*, *3(*2), 137–144.

Kim, A. G., and L. J. Douglas, 1972, Hydrocarbon gases produced in a simulated swamp environment: *United States Bureau of Mines Repository Inventory. 7690*, 15 p

Kinnaman, F.S., Valentine, D.L. and Tyler, S.C., 2007. Carbon and hydrogen isotope fractionation associated with the aerobic microbial oxidation of methane, ethane, propane and butane. *Geochimica et Cosmochimica Acta, 71*(2), pp.271–283.

Klusman, R. W. (2003). A geochemical perspective and assessment of leakage potential for a mature carbon dioxideenhanced oil recovery project and as a prototype for carbon dioxide sequestration; Rangely field, Colorado. *AAPG Bulletin, 87*(9), 1485–1507.

Klusman, R.W., 2011. Comparison of surface and near-surface geochemical methods for detection of gas microseepage from carbon dioxide sequestration. *International Journal of Greenhouse Gas Control,* 5, 1369–1392.

Lafleur, P. 2010. Geochemical Soil Gas Survey: A Site Investigation of SW30-5-13-W2M, Weyburn Field, Saskatchewan. *Petro-Find Geochem Ltd*., Saskatoon, SK.

Lafleur, P. 2011. *Geochemical Soil Gas Survey: A Site Investigation of SW30-5-13-W2M, Weyburn Field, Saskatchewan, Monitoring Project Number 2*. Petro-Find Geochem Ltd., Saskatoon, SK.

Laubmeyer, G., 1933, A new geophysical prospecting method: *Zeitschrift fiir Petroleum*, v. 29, no. 18, p. 1–4.

Leifer, I., & Boles, J. (2005). Measurement of marine hydrocarbon seep flow through fractured rock and unconsolidated sediment. *Marine and Petroleum Geology, 22*(4), 551–568.

Leythaeuser, D., Mackenzie, A., Schaefer, R. G., & Bjoroy, M. (1984). A novel approach for recognition and quantification of hydrocarbon migration effects in shale-sandstone sequences. *AAPG Bulletin*, 68(2), 196–219.

Liu, Y., and Whitman, W.B. 2008. Metabolic, phylogenetic, and ecological diversity of the methanogenic archaea. *Annals of the New York Academy of Sciences*, 1125(1), 171–189.

Løseth, H., Wensaas, L., Arntsen, B., & Hovland, M. (2003). Gas and fluid injection triggering shallow mud mobilization in the Hordaland Group, North Sea. *Geological Society, London, Special Publications*, *216*(1), 139–157.

Lower, S. K. (1999). Carbonate equilibria in natural waters. *Simon Fraser University*, *544*.

MacDonald, I. R., Sager, W. W., & Peccini, M. B. (2003). Gas hydrate and chemosynthetic biota in mounded bathymetry at mid-slope hydrocarbon seeps: Northern Gulf of Mexico. *Marine Geology*, *198*(1), 133–158.

Lu, J., Kharaka, Y.K., Thordsen, J.J., Horita, J., Karamalidis, A., Griffith, C., and Hovorka, S.D., 2012. CO_2–rock–brine interactions in Lower Tuscaloosa Formation at Cranfield CO_2 sequestration site, Mississippi, USA. *Chemical Geology* 291, 269–277.

Ma, L., Castro, M. C., & Hall, C. M. (2009). Crustal noble gases in deep brines as natural tracers of vertical transport processes in the Michigan Basin. *Geochemistry, Geophysics, Geosystems*, *10*(6). Q06001, doi:10.1029/2009GC002475.

MacDonald, I. R., Buthman, D. B., Sager, W. W., Peccini, M. B., & Guinasso, N. L. (2000). Pulsed oil discharge from a mud volcano. *Geology*, *28*(10), 907–910.

Mackintosh, S.J., & Ballentine, C.J. 2012. Using $^3He/^4He$ isotope ratios to identify the source of deep reservoir contributions to shallow fluids and soil gas. *Chemical Geology*, 304, 142–150.

Marzec, P., Sechman, H., Kasperska, M., Cichostępski, K., Guzy, P., Pietsch, K., & Porębski, S. J. (2016). Interpretation of a gas chimney in the Polish Carpathian Foredeep based on integrated seismic and geochemical data. *Basin Research*. http://dx.doi.org/10.1111/bre.12216

Meckel, T. A., & Mulcahy, F. J. (2016). Use of novel high-resolution 3D marine seismic technology to evaluate Quaternary fluvial valley development and geologic controls on shallow gas distribution, inner shelf, Gulf of Mexico. *Interpretation*, *4*(1), SC35-SC49.

Moreira, A.C.D.C.A., Landulfo, E., Nakaema, W.M., Marques, M.T., Medeiros, J.A., Musse, A.P.S., & Dobeck, L.M. 2014. The first Brazilian Field Lab fully dedicated to CO_2 MMV experiments: a closer look at atmospheric leakage detection. *Energy Procedia*, 63, 6215–6226.

Mulcahy, F.J. (2015). Use of high resolution 3D seismic data to evaluate Quaternary valley evolution history during transgression, offshore San Luis Pass, Gulf of Mexico. University of Texas at Austin. Master's of Science Thesis.

Nicoll, G. D. (2012). *Evaluation of the Nordland Group overburden as an effective seal for the Sleipner CO2 storage site (offshore Norway) using analytical and stochastic modelling techniques* (Doctoral dissertation, University of Edinburgh).

Nicot, J.P., Oldenburg, C.M., Houseworth, J.E., & Choi, J.W., 2013. Analysis of potential leakage pathways at the Cranfield, MS, USA, CO_2 sequestration site. *International Journal of Greenhouse Gas Control*, 18, 388–400.

O'Leary, M. H. (1988). Carbon isotopes in photosynthesis. *Bioscience*, *38*(5), 328–336.

Osborn, S. G., Vengosh, A., Warner, N. R., & Jackson, R. B. (2011). Methane contamination of drinking water accompanying gas-well drilling and hydraulic fracturing. *proceedings of the National Academy of Sciences*, *108*(20), 8172–8176.

Osmond, J.L. (2016). Fault seal and containment failure analysis of a Lower Miocene structure in the San Luis Pass area, offshore Galveston Island, Texas inner shelf. University of Texas at Austin. Master's of Science Thesis.

Oxburgh, E. R., O'nions, R. K., & Hill, R. I. (1986). Helium isotopes in sedimentary basins. *Nature*, *324*, 632–635.

Ozima, M., & Podosek, F.A. 2002. *Noble Gas Geochemistry*. Cambridge University Press.

Parkhurst D. L. & Appelo C. A. J. 2013. Description of input and examples for PHREEQC version 3—a computer program for speciation, batch-reaction, one-dimensional transport, and inverse geochemical calculations: *U.S. Geological Survey Techniques and Methods*, book 6, chap. A43, 497 p.

Quigley, D. C., Hornafius, J. S., Luyendyk, B. P., Francis, R. D., Clark, J., & Washburn, L. (1999). Decrease in natural marine hydrocarbon seepage near Coal Oil Point, California, associated with offshore oil production. *Geology*, *27*(11), 1047–1050.

Revesz, K., Coplen, T.B., Baedecker, M.J., Glynn, P.D., & Hult, M. 1995. Methane production and consumption monitored by stable H and C isotope ratios at a crude oil spill site, Bemidji, Minnesota. *Applied Geochemistry*, 10(5), 505–516.

Rice, D. D., & Claypool, G. E. (1981). Generation, accumulation, and resource potential of biogenic gas. *AAPG Bulletin*, *65*(1), 5–25.

Richards, L. A., Magnone, D., van Dongen, B.E., Ballentine, C.J., & Polya, D.A. 2015. Use of lithium tracers to quantify drilling fluid contamination for groundwater monitoring in Southeast Asia. *Applied Geochemistry*, *63*, 190–202.

Roberts, H. H., & Carney, R. S. (1997). Evidence of episodic fluid, gas, & sediment venting on the northern Gulf of Mexico continental slope. *Economic Geology, 92*(7–8), 863–879.

Roberts, S. J., & Nunn, J. A. (1995). Episodic fluid expulsion from geopressured sediments. *Marine and Petroleum Geology, 12*(2), 195IN1203-202IN3204.

Romanak, K.D., Smyth, R.C., Yang, C., & Hovorka, S.D. 2009. Modeling shallow groundwater geochemistry and carbon isotopes: test of methodology for CO_2 storage evaluation at an EOR site, West Texas, USA, in *AGU Spring Meeting Abstracts.*

Romanak, K.D., Bennett, P.C., Yang, C., & Hovorka, S.D., 2012. Process-based approach to CO_2 leakage detection by vadose zone gas monitoring at geologic CO_2 storage sites. *Geophysical Research Letters* 39(15). DOI: 10.1029/2012GL052426

Romanak, K., Sherk, G.W., Hovorka, S., & Yang, C., 2013. Assessment of alleged CO_2 leakage at the Kerr farm using a simple process-based soil gas technique: implications for carbon capture, utilization, and storage (CCUS) monitoring. *Energy Proceedings, 37*, 4242–4248.

Romanak, K.D., Wolaver, B., Yang, C., Sherk, G.W., Dale, J., Dobeck, L.M., & Spangler, L.H. 2014. Process-based soil gas leakage assessment at the Kerr Farm: comparison of results to leakage proxies at ZERT and Mt. Etna. *International Journal of Greenhouse Gas Control*, 30, 42–57.

Schoell, M., 1983. Genetic characterization of natural gases. *AAPG Bulletin*, 67(12), 2225–2238.

Scott, A.R., Kaiser, W.R., & Ayers, W.B., Jr. 1994. Thermogenic and secondary biogenic gases, San Juan Basin, Colorado and New Mexico—implications for coalbed gas producibility. *AAPG Bulletin, 78*, 1186–1209.

Shabro, V., Torres-Verdin, C., & Javadpour, F. (2011, January). Numerical simulation of shale-gas production: from pore-scale modeling of slip-flow, Knudsen diffusion, and Langmuir desorption to reservoir modeling of compressible fluid. In *North American Unconventional Gas Conference and Exhibition*. Society of Petroleum Engineers.

Sherk, G.W., Romanak, K.D., Dale, J., Gilfillan, S.M.V., Haszeldine, R.S., Ringler, E.S., & Yang, C. 2011. The Kerr investigation: findings of the investigation into the impact of CO_2 on the Kerr property, final report. *IPAC Res. Inc., Regina, Saskatchewan, Canada*.

Smith, S. P., & Kennedy, B. M. (1983). The solubility of noble gases in water and in NaCl brine. *Geochimica et Cosmochimica Acta, 47*(3), 503–515.

Smith, K.L., Steven, M.D., Jones, D.G., West, J.M., Coombs, P., Green, K.A., & Beaubien, S.E. 2013. Environmental impacts of CO_2 leakage: recent results from the ASGARD facility, UK. *Energy Procedia*, 37, 791–799.

Spangler, L.H., Dobeck, L.M., Repasky, K.S., Nehrir, A.R., Humphries, S.D., Barr, J.L., & Benson, S.M. 2010. A shallow subsurface controlled release facility in Bozeman, Montana, USA, for testing near surface CO_2 detection techniques and transport models. *Environmental Earth Sciences*, 60(2), 227–239.

Spooner, H.V., Jr. 1964. Basal Tuscaloosa sediments, east-central Louisiana. *AAPG Bulletin* 48, 1–21.

Stocker, T. (Ed.). (2014). *Climate change 2013: the physical science basis: Working Group I contribution to the Fifth assessment report of the Intergovernmental Panel on Climate Change*. Cambridge University Press.

Suekane, T., Nobuso, T., Hirai, S., & Kiyota, M. (2008). Geological storage of carbon dioxide by residual gas and solubility trapping. *International Journal of Greenhouse Gas Control*, *2*(1), 58–64.

Tasianas, A., Mahl, L., Darcis, M., Buenz, S., & Class, H. (2016). Simulating seismic chimney structures as potential vertical migration pathways for CO2 in the Snøhvit area, SW Barents Sea: model challenges and outcomes. *Environmental Earth Sciences*, *75*(6), 504.

Templeton, A.S., Chu, K.H., Alvarez-Cohen, L., & Conrad, M.E. 2006. Variable carbon isotope fractionation expressed by aerobic CH_4-oxidizing bacteria. *Geochimica et Cosmochimica Acta*, *70*(7), 1739–1752.

Trevisan, L., Pini, R., Cihan, A., Birkholzer, J. T., Zhou, Q., & Illangasekare, T. H. (2015). Experimental analysis of spatial correlation effects on capillary trapping of supercritical CO_2 at the intermediate laboratory scale in heterogeneous porous media. *Water Resources Research*, *51*(11), 8791–8805.

Trium, 2011. Site Assessment (SW-30-05-13-W2 M), Near Weyburn, Saskatchewan. *Trium Environmental Inc. and Chemistry Matters*, p. 50.

Turnbull, J.C., Keller, E.D., Norris, M.W., & Wilshire, R.M. 2017. Atmospheric monitoring of carbon capture and storage leakage using radiocarbon. *International Journal of Greenhouse Gas Control 56*, 93–101.

Wallace, K. J. (2013) Use of 3-dimensional dynamic modeling of CO_2 injection for comparison to regional static capacity assessments of Miocene sandstone reservoirs in the Texas State Waters, Gulf of Mexico. University of Texas at Austin. Master's of Science Thesis.

Warr, O., Rochelle, C.A., Masters, A. & Ballentine, C.J. (2015) Determining noble gas partitioning within a CO 2 –H 2 O system at elevated temperatures and pressures. *Geochimica et Cosmochimica Acta 159*, 112–125.

Warwick, P.D., Breland, F.C., & Hackley, P.C. 2008. Biogenic origin of coalbed gas in the northern Gulf of Mexico Coastal Plain, USA. *International Journal of Coal Geology 76*.1, 119–137.

Weaver, L.K., & Anderson, K.F., (1966). Cranfield Field, Cranfield Unit, Basal Tuscaloosa reservoir, Adams and Franklin Counties, Mississippi, in Oil Recovery from Gas-Cap Reservoirs: an Engineering Evaluation of Conservation Practices in Six Reservoirs. Interstate Oil Compact Commission, Oklahoma City, pp. 42–58.

Wells, A.W., Diehl, J.R., Strazisar, B.R., Wilson, T.H., & Stanko, D.C., 2013. Atmospheric and soil-gas monitoring for surface leakage at the San Juan Basin CO_2 pilot test site at Pump Canyon New Mexico, using perfluorocarbon tracers, CO_2 soil-gas flux and soil-gas hydrocarbons. *International Journal of Greenhouse Gas Control 14*, 227–238.

Whiticar, M. J. 1999. Carbon and hydrogen isotope systematics of bacterial formation and oxidation of methane. *Chemical Geology*, *161*(1), 291–314.

Wimmer, B.T., Krapac, I.G., Locke, R., & Iranmanesh, A., 2011. Applying monitoring, verification, and accounting techniques to a real-world, enhanced oil recovery operational CO_2 leak. *Energy Proceedings 4*, 3330–3337.

Wolaver, B.D., Hovorka, S.D., & Smyth, R.C. 2013. Greensites and brownsites: implications for CO_2 sequestration characterization, risk assessment, and monitoring. *International Journal of Greenhouse Gas Control, 19*, 49–62.

Wong, C. S., Chin, Y. P., & Gschwend, P. M. (1992). Sorption of radon-222 to natural sediments. *Geochimica et Cosmochimica Acta*, *56*(11), 3923–3932.

Xia, X., & Tang, Y. (2012). Isotope fractionation of methane during natural gas flow with coupled diffusion and adsorption/desorption. *Geochimica et Cosmochimica Acta*, *77*, 489–503.

Yang, C., Romanak, K., Hovorka, S.D., Holt, R.M., Lindner, J., & Trevino, R. 2013. Near-surface monitoring of large-volume CO_2 injection at Cranfield: early field test of SECARB phase III. *SPE Journal, 18*(03), 486–494.

Yang, C., Dai, Z., Romanak, K. D., Hovorka, S. D., & Treviño, R. H. (2014). Inverse modeling of water-rock-CO2 batch experiments: Potential impacts on groundwater resources at carbon sequestration sites. *Environmental science & technology*, *48*(5), 2798–2806.

Yang, C., Hovorka, S.D., Treviño, R.H., and Delgado-Alonso, J. 2015. Integrated framework for assessing impacts of CO_2 leakage on groundwater quality and monitoring-network efficiency: case study at a CO_2 enhanced oil recovery site. *Environmental Science & Technology*, *49*(14), 8887–8898.

Zhang, T., Ellis, G. S., Ruppel, S. C., Milliken, K., & Yang, R. (2012). Effect of organic-matter type and thermal maturity on methane adsorption in shale-gas systems. *Organic Geochemistry*, *47*, 120-131.

Zhou, Z., Ballentine, C. J., Schoell, M., & Stevens, S. H. (2012). Identifying and quantifying natural CO_2 sequestration processes over geological timescales: the Jackson Dome CO_2 Deposit, USA. *Geochimica et Cosmochimica Acta*, *86*, 257-275.